THE INTERFACE BEHAVIOR BETWEEN GRANULAR SOILS AND CONCRETE

by

Egemen Danyıldız

B.S., Civil Engineering, Yıldız Technical University, 2003

Submitted to the Institute for Graduate Studies in
Science and Engineering in partial fulfillment of
the requirements for the degree of
Master of Science
in
Civil Engineering

Graduate Program in Civil Engineering
Boğaziçi University
2007

ACKNOWLEDGMENTS

I would like to express my sincere gratitude to my thesis supervisor, Prof. Dr. Gökhan Baykal for his continuous support, encouragement and for the information he provided throughout the preparation of this thesis. He always enlightened me and I have learnt so much from him. I really am grateful to him for being my thesis supervisor.

I would also like to express my gratitude to members of my thesis committee, Prof. Dr. Erol Güler and Assoc. Prof. İsmail Hakkı Aksoy who devoted their valuable time for reading and commenting on my thesis.

My heartfelt thanks are due to my colleagues, Research Assistants Hakkı Oral Özhan, Öznur Selek and Altuğ Saygılı in Karl-Terzaghi Soil Mechanics Laboratory for sharing all the good and bad moments with me. They are not only my colleagues but also my best friends.

Very special thanks to Süreyya Yorgun, General Manager of Ash Plus Yapı Malz A.Ş who supplied the fly ash used in this study.

Special thanks are due to representatives of Akçansa B. Çekmece Çimento Sanayi A.Ş who supplied the cement used in this study and performed the chemical analyses of fly and cement.

And finally, I owe special thanks to my mother Tülay Danyıldız, my father, Ali Rıza Danyıldız who is also my colleague and my elder sister, Rahşan Danyıldız. They have always supported me and believed in me throughout my whole life.

This thesis is dedicated to my family.

ABSTRACT

THE INTERFACE BEHAVIOR BETWEEN GRANULAR SOILS AND CONCRETE

Interface between construction materials and soils play an important role in many geotechnical systems, including pile foundations, retaining walls and deep foundations. Split samples consisting of concrete block at the bottom half and granular soil at the top half were prepared and direct shear tests were performed.

To be able to control the large number of parameters affecting the interface behavior, granular soil was manufactured using fly ash by cold bonding pelletization technique with predetermined shape, size, grain size distribution, surface roughness, water absorption, unit weight and crushing strength. The pellets which only consists of fly ash was FA group, and the other groups with 10%, %20 cement/fly ash ratios by weight were FAC10 and FAC20 respectively. The physical and mechanical properties of these aggregates were investigated by using conventional soil mechanics tests. Concrete blocks were prepared with only fly ash aggregates (FA) in accordance with ASTM C 33-03 “Standard specifications for concrete aggregates”.

The comparison of direct shear and interface tests indicated that the angles of internal friction of granular soils are approximately 10% higher than soil to concrete interface friction angles but the contact efficiencies remain almost constant for all groups. Under low normal stress, FA group aggregates have the advantage of angular shapes and rough surfaces relative to others. FAC10 and FAC20 group aggregates exhibited higher performance due to their resistance to crushing under high normal stresses of 100 kPa and 200 kPa and attained interface friction angles of 33 and 34 degrees respectively.

Surface roughness of concrete blocks was scanned with a 3D scanner and a relationship between concrete surface and maximum interface stress was established.

ÖZET

GRANÜLER ZEMİNLER İLE BETON ARASINDAKİ ARAYÜZEY ETKİLEŞİMİ

Yapı malzemeleri ile zemin arasındaki arayüzeyin özellikleri, kazık temeller, istinat duvarları ve derin temeller gibi birçok geoteknik sistemde önemli bir rol oynar. Alt yarısı beton ve üst yarısı granüler zemin olmak üzere iki parçadan oluşan numuneler hazırlanarak kesme kutusu deneyleri yapılmıştır.

Arayüzey etkileşini etkileyen birçok parametreyi kontrol altında tutabilmek için, peletleme yöntemi ile önceden belirlenmiş büyüklük, dane çapı dağılımı, su emme kapasitesi, birim hacim ağırlığı ve ezilme dayanımında granüler zemin malzemeleri üretilmiştir. Sadece kül ile üretilen peletler FA grubu, ağırlıkça çimento/kül oranı 10%, 20% olan peletler ise sırasıyla FAC10 ve FAC20 grubu olarak gösterilmiştir. Bu agregaların mekanik ve fiziksel özellikleri geleneksel zemin mekaniği deneyleri yapılarak araştırılmıştır. FA grubu hafif agregalar kullanılarak ASTM C33-03 standartlarında beton bloklar üretilmiştir.

Kesme kutusu ve arayüzey deneylerinin karşılaştırılması danelerin içsel sürtünme açılarının arayüzey sürtünme açılarından yaklaşık olarak 10% oranında daha yüksek olduğunu bununla birlikte arayüzey verimliliğinin tüm gruplarda yaklaşık olarak aynı kaldığını göstermiştir. Sadece kül ile üretilen FA grubu agregalar düşük normal yüklerde(50 kPa), daha köşeli şekilleri ve daha pürüzlü yüzeyleri sayesinde diğer gruplara oranla daha yüksek performans göstermiştir. FAC10 ve FAC20 grubu agregalar yüksek normal yükler altında (100 kPa, 200 kPa) ezilmeye karşı dayanımlarından dolayı iyi bir performans göstererek sırasıyla 33 ve 34 derece arayüzey sürtünme açılarına ulaşmışlardır.

Beton blokların yüzey pürüzlülükleri üç boyutlu tarayıcı ile taranarak beton yüzeyleri ile testlerde ulaşılan en yüksek arayüzey gerilmeleri arasında bağlantı kurulmuştur.

TABLE OF CONTENTS

LIST OF FIGURES

LIST OF TABLES

LIST OF SYMBOLS / ABBREVIATIONS

c	Cohesion
D	Pelletization disc diameter
D_{50}	Mean grain size
d_m	Mean diameter of particle
F_c	Maximum force attained in crushing tests of pellets
F_t	Load at failure
h	Height of liquid column
k	Constant for the soil
k_c	Capillary constant
k_n	The normal stiffness
k_s	Interface shear stiffness
L	Profile length (mean grain size)
n_{cr}	Critical revolutions per minute
P	Frictional or tangential force required to induce relative displacement
P_c	Pressure at the point of contact
R_{max}	Vertical distance between the highest peak and the lowest trough
R_n	Relative interface roughness
$\overline{R_n}$	Average of normalized roughness along a line
$\overline{R}_{n3d}$	Three dimensional surface roughness parameter
$\overline{R}_{n2d}$	Two dimensional surface roughness parameter
r	Radius of the capillary
s_0	Maximum displacement due to failure
s	Displacement
Q	Normal load between two materials
q_u	Unconfined compressive strength
α	Dilation angle of soil
δ	Interface friction angle between soil and structure
Δ_{actual}	Actual sliding displacement between the soil particles

Δ_{dis}	Deformation of soil particles
Δ_{meas}	Measured sliding displacement
Δ_n	Displacement normal to the interface
Δ_s	Displacement along the interface
ϕ	Internal friction angle
ϕ_f	Corrected friction angle corrected for the contribution of dilation
ϕ_v	Deformation at constant volume
μ	Coefficient of friction
σ	Normal stress
σ_c	Crushing strength of a single particle
σ_f	Normal stress at failure
σ_n	Normal stress acting on the interface or soil
τ	Shear stress
τ_f	Shear stress at failure
τ_s	Interface shear stress

ASTM	American Society for Testing and Materials
DSB	Direct shear box
DSS	Direct simple shear
GICT	Geotextile-soil interface cylindrical test
LDSB	Large size direct shear box
OD	Oven dry
SSD	Saturated surface dry
WA	Water absorption (%)

1. INTRODUCTION

Friction has been the subject of intensive study since the early investigation of da Vinci, Amontos, Coulomb and Euler. At the molecular level, even smooth, solid surfaces have valleys and ridges or asperities, and at a given instant some of these asperities will be touching. The response of these asperities to each other when sliding depends on their respective material deformation properties.

Coulomb's law of friction is broadly used in geotechnical engineering. It means that if a material, such as soil is in contact with another material like a concrete block, the frictional force can be obtained by;

$$P = \mu * Q \tag{1.1}$$

where P is the frictional or tangential force required to induce relative displacement at the contact surface, μ is the coefficient of friction, and Q is the normal load between the two materials as given in Figure 1.1a.

By dividing the normal load and shear force by the contact surface area to convert them to normal stress and shear stress and considering the adhesion c between the two materials, then the Mohr-Coulomb failure criterion is obtained as follows,

$$\tau_f = c + \sigma_f \tan(\delta) \tag{1.2}$$

where τ_f and σ_f are the shear stress and normal stress at failure along the contact surface and δ is the angle of interface friction respectively.

Fig.1.1b defines a failure envelope for the friction between the two materials where δ is the slope of the failure envelope and c is its intercept with the axis, τ_f and σn are obtained from interface stress-displacement relation curves.

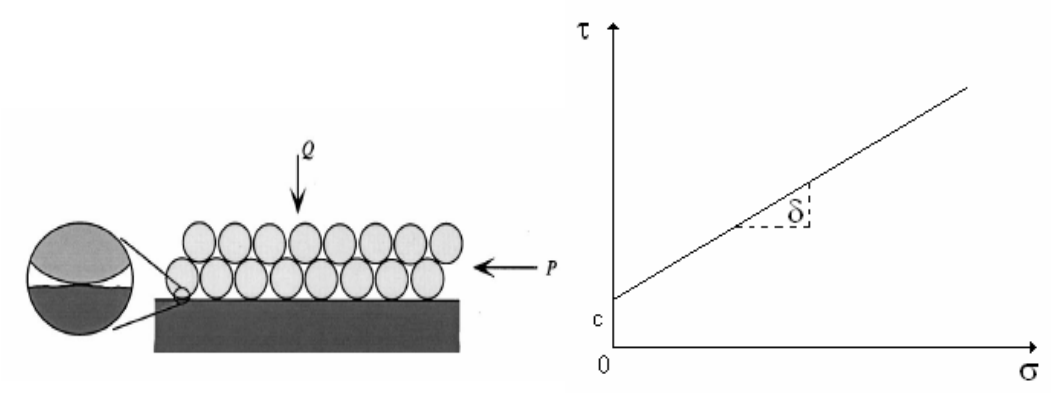

(a) (b)

Figure 1.1. a) Schematic illustration of nondilative interface system, b) Coulomb failure criterion

In geotechnical engineering, there are many situations where soils interact with structural materials. The contact zone between the soil and a structural material is referred to as "interface". The interface is a thin layer of material through which stress is transferred from one medium to the other. For dense granular soils, around a peak stress, the deformation suddenly localizes into narrow bands (called shear bands), and the stress drops sharply down to a residual stress state. Understanding this behavior is of great importance to solve engineering problems related to soil-structure interface.

The response of soil-structure systems subjected to static or dynamic loading is influenced significantly by the nature of mechanical behavior of interfaces. Development of design methods for interfaces between granular soils and civil construction materials depends on understanding how particulate strength and volume change behavior is influenced by the geometry of rigid counter faces. This mutual effect of soils and structures in the transmission of forces from the one to the other through the contact surface is called skin friction.

The skin resistance could not be higher than the ultimate shearing strength of soil, and it is important to find out the ratio between soil strength and skin resistance. Since the development of skin friction due to displacement, the stress-strain curves can be obtained

from the experimental results. For granular soils, the experimental stress-strain relation was expressed in a mathematical term by Kézdi (1959) and applied to determine the earth pressure and pile resistance. In the case of skin friction, the stress-strain curve was expressed as an exponential function of displacement [1]:

$$\frac{\tau}{\sigma} = \tan\delta\left[1 - \exp\left(-k\frac{s}{s_0 - s}\right)\right] \tag{1.3}$$

where τ = shearing stress which produces a displacement of "s"

σ = normal stress

δ = angle of skin friction

s = displacement

s_0 = maximum displacement due to failure

k = constant for the soil.

The description of the mechanical behavior of interfaces requires information on the strength characteristics and load-displacement relation. The behavior of interfaces is very complex. Many geotechnical problems involve estimation of stresses transferred along the interface between soils and solid surfaces. Furthermore, no consideration was given to the surface roughness of different construction materials. Subsequently, engineers started to conduct laboratory investigations on the behavior of soil-structural material interfaces as the need for reliable estimates of soil-structure interface behavior has increased.

In engineering applications, laboratory experiments are carried out to determine the shear strength parameters and stress-displacement relations of interfaces. Since Potyondy, 1961 first performed a comprehensive series of direct shear type interface tests to determine the skin friction between different types of soils and construction materials, more and more investigations regarding soil-structure interface behavior have been done using various interface testing devices [2].

The mechanical behavior of granular materials is dependent on the properties of grains of which they are constituted. Hence, it is natural to search for correlations between the parameters of the constitutive model of a supposedly continuous medium and the properties of grains (form, size, granulometry…) [3].

The physical properties and mechanical properties of granular soils undergo significant change if the particles are broken into smaller pieces due to the application of an external force. For this reason, the significant particle breakage phenomenon is sited as of the major importance in the soil mechanics field in conjunction with the practical problems such as the bearing capacity of piles and stability of earth structures [4].

Particle crushing occurs when the force acting on a grain exceeds its crushing strength even if the breakage of the grain is in a soil matrix. The relationship between single particle and collective crushing behaviors is not straightforward because the loading of a particle in the matrix can not be exactly modeled by single grain [5].

A single particle crushing strength σ_f defined as;

$$\sigma_f = \frac{F_t}{d_0^{\,2}} \tag{1.4}$$

where d_0 is the average diameter of the particle and F_t is the load at failure.

In this study, synthetic lightweight aggregates were manufactured with desired dimensions and different crushing strengths by pelletization process. The effect of crushing, surface geometry and particle shape of aggregates on the interface behavior was investigated. The effect of surface roughness of concrete on the interface behavior between granular soils and concrete was also investigated by performing interface tests on specially designed concrete blocks which consist of fly ash aggregates and have different surface roughness parameters.

2. LITERATURE REVIEW

Interface Tests

The interface between granular materials (e.g. soils, grains) and continuum surfaces (e.g. steel, concrete, geosynthetics, wood) is critical to the performance of a variety of systems including grain hoppers and chutes as well as deep foundations, microtunneling technologies, and earth retention structures. Many researchers have studied interface friction between soil and other construction materials (e.g. Potyondy, 1961, Tsubakihara and Kishida, 1993, Tsubakihara, Kishida and Nishiyama, 1993, Fakharian and Evgin, 1996) using a variety of equipment including simple shear (Kishida and Uesagi, 1987), direct shear (Potyondy, 1961), torsion (Yoshimi and Kishida, 1981) or annular shear devices (Brumund and Leonards, 1973). For example, Fakharian and Evgin, 1996 have described three dimensional monotonic and cyclic testing of interfaces for examining the influence of relative density on interface behavior. Baykal and Akkol, 1997 developed a cylindrical test device and performed geotextile to soil interface tests. Others have studied the influence of overconsolidation ratio (Subba Rao et al., 2000), and surface roughness (Tsubakihara, Kishida and Nishiyama, 1993) on interface behavior.

2.1.1 Direct Shear Box (DSB) Devices

Several studies have been published regarding laboratory interface testing. Most often, interface tests were performed to determine the soil-to-structure friction angle for design of geotechnical structures, such as retaining walls, buried culverts, piles, geosynthetics etc., and, in some cases, for the determination of parameters for constitutive modeling of interface response.

Early systematic efforts to find out the behavior of soil-to-structure interfaces were carried out by Potyondy, 1961, Clough and Duncan, 1971, and Peterson et al., 1976, among others. Interface tests were performed using a slightly modified Direct Shear Box (DSB) in which a concrete specimen occupied one of the halves of the shear box as shown in Figure 2.1.

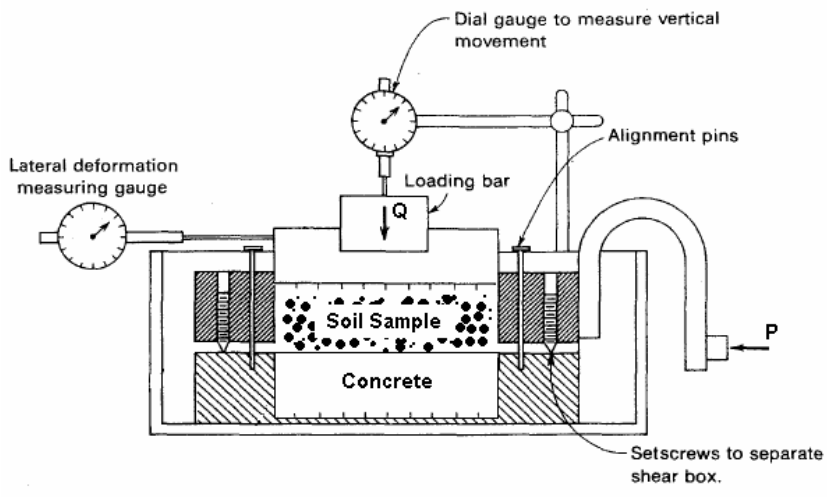

Figure 2.1. Illustration of Modified Direct Shear Box

Potyondy, 1961 proposed to express the skin friction resistance in a similar form to Equation 1.2 as a sum of the adhesion and the normal stress dependent component. He performed series of direct shear tests on different types of soils such as clay and sand under constant normal load to determine the skin friction between soil and construction materials for both strain controlled and stress controlled conditions. In addition to this, he developed a database of interface friction parameter values for interfaces between sand and concrete of varying roughness and concluded that the interface strength was influenced by the moisture content, soil composition, surface roughness, and normal load [2].

Brumund and Leonards, 1973 concentrated on the surface roughness, observing that as the surface roughness increased, the interface friction angle increased until it became equal to the internal friction angle of the soil, resulting in failure within the contacting soil and not at the interface. They also observed the influence of size, angularity, and surface texture of sand grains on interface friction [6].

Peterson et al., 1976 studied the fundamental factors that influence the interface behavior using a 102- by 102-mm (4- by 4 in.) DSB. They performed a large number of sand-to-concrete interface tests, under drained conditions and constant normal load, to a maximum displacement of 12.5 mm. They analyzed the influence of normal stress, interface roughness, and soil characteristics on interface behavior, and developed a

database of sand-to-concrete interface friction angles [7].

Acar et al., 1982 conducted direct shear testing on interfaces between sand and structural materials such as steel, wood and concrete, and came to a conclusion that relative density of sand and normal stress obviously influenced the angle of friction. This evidence showed that the influence of relative density of sand and normal stress level on the interface behavior were also given by others, such as Desai et al., 1984, Fakharian and Evgin, 1996 [8, 9, 10].

A computer-controlled direct shear device providing constant normal stiffness condition was developed by Leichnitz, 1985 to study the behavior of rock discontinuities. Afterwards Ooi and Carter, 1987 developed another constant normal stiffness direct shear device capable of applying static and cyclic shear loading to a specimen containing one of a variety of possible interfaces.

Boulon and Plytas, 1986 developed a direct shear test apparatus capable of testing soil-construction material interfaces under constant normal stress, constant volume and constant normal stiffness conditions.

Kishida and Uesugi, 1987, Fakharian and Evgin, 1995, Evgin and Fakharian, 1996 have defined that the actual sliding displacement Δ_{actual} between the soil particles and the concrete cannot be directly measured in the DSB, as illustrated in Figure 2.2a. The displacement Δ_{meas} measured between soil box and the concrete specimen includes the sliding displacement at the interface, as well as the deformation Δ_{dis} of the sand mass due to distortion under the applied shear stresses [11, 12, 13].

Shibaya, Mitachi and Tamate, 1997 showed that proper procedures enable the direct shear box test to provide strength and large-strain dilatancy characteristics that are similar to those measured in a simple shear test. They have given an optimum configuration of the shear box apparatus for measuring the strength and dilatancy characteristics in direct shear. Important aspects of the procedure include measuring the vertical load in the lower half of the box, and maintaining the size of the opening between the two halves of the shear box at a fixed value of approximately 10-20 times the mean

particle diameter of the test specimen.

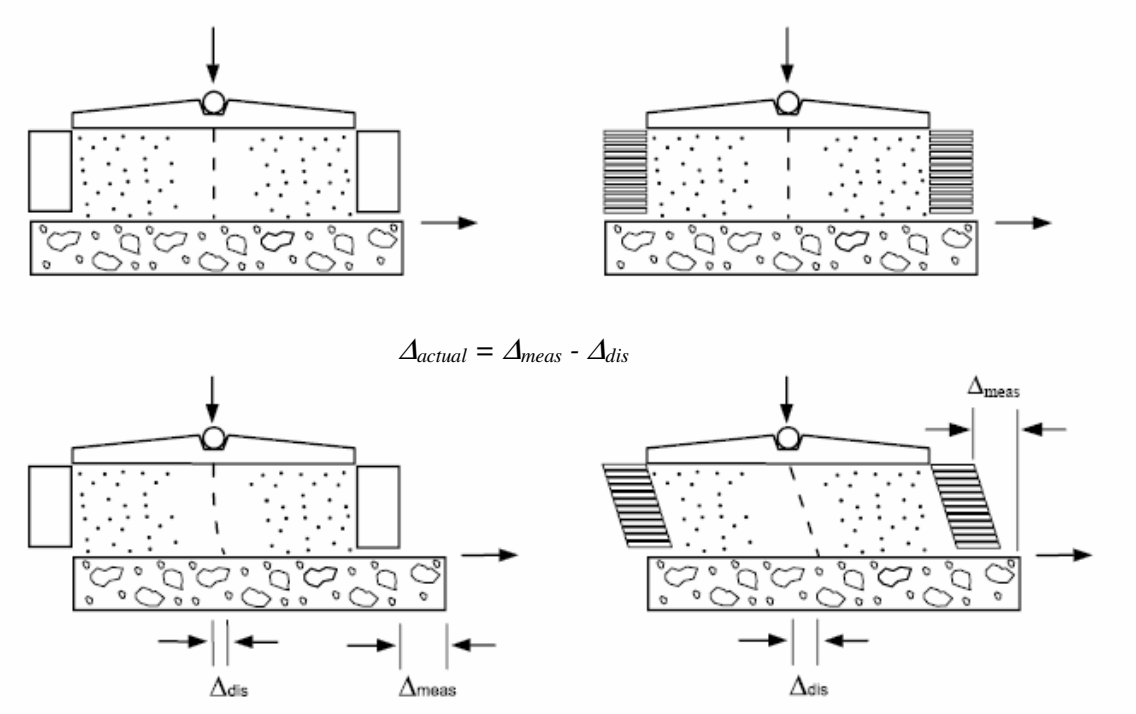

a) Direct Shear Box (DSB) b) Direct Simple Shear Box (DSS)

Figure 2.2. Distortion of the sand mass during interface tests in the DSB and DSS devices.

The direct shear device for soil testing is available in most of geotechnical laboratories, which can easily be employed for interface testing with simple modifications. Consequently, it has been the common choice for interface testing in research and practice. Other applications of the DSB include testing interfaces such as soil to geomembrane, soil to geotextile, and geomembrane to geotextile. Large size direct shear devices have been developed for interface areas of up to 305 by 305 mm and they can be used for soil-to-concrete testing.

Conventional DSB devices present several limitations due to insufficient amount of relative displacements which leads to difficulties in determination of interface residual

strength. The direct-shear test was formerly quite popular. Then, as the state of the art advanced, it tended to become less popular for several reasons:

- The area of the sample changes as the test progresses but the change may not be very significant, as most samples "fail" at low deformations.
- The actual failure 'surface is not plane, as is assumed or as was intended from the way the shear box was constructed, nor is the shearing stress uniformly distributed over the "failure" surface, as is also assumed.
- Test uses a small sample, with the result that preparation errors can become relatively important.
- The size of the sample precludes much investigation into pore-water conditions during the test.
- Values of modulus of elasticity E_s and Poisson's ratio ν cannot be determined [14].
- Principal stress planes rotate during the test.

Table 2.1 summarizes some of the previous work on interface behavior in which testing was performed in DSB apparatuses.

Table 2.1. Previous works on direct shear testing of sand-to-concrete and sand-to-steel interfaces

Source	Type of Interface and Dimensions	Type of Loading	Summary
Potyondy (1961)	Sand to concrete Sand to steel	Monotonic under constant normal stress	* Developed a database of interface friction parameter values for interfaces between sand and concrete of varying roughness.
Clough and Duncan (1971)	Sand to concrete	Monotonic shear under constant normal stress	*Developed a hyperbolic formulation for modeling interface response.
Peterson et al. (1976) and Kulhawy Peterson (1979)	Sand to concrete 102 mm x 102 mm	Monotonic shear and shear reversal under constant normal stress	* Analyzed the relationship between the interface response and the interface roughness, soil type, and soil density and gradation. * Added important contributions to the database of parameters for the Clough and Duncan (1971) hyperbolic formulation.
Acar, Durgunoglu, and Tumay (1982)	Sand to concrete Sand to steel	Monotonic shear under constant normal stress	* Studied the relationship between void ratio of the sand and interface friction angle. * Presented a relationship between void ratio and hyperbolic parameter values for Clough and Duncan (1971) formulation for the materials used in their tests.
Desai, Drumm, and Zaman (1985)	Sand to concrete 305 mm x 305 mm	Cyclic shear under constant normal stress	* Developed the Cyclic Multi-Degree-of-Freedom (CYMDOF) device for interface testing. * Studied the influence on interface response of the following factors: displacement and shear stress amplitude, number of loading cycles, and initial density of the sand.
Bosscher and Ortiz (1987)	Sand to concrete Sand to rock	Cyclic shear under constant normal stress	* Studied the relationship between interface roughness and interface friction angle. * Assessed the effect of roughness on damping ratio of the interface.
Lee et al. (1989)	Sand to concrete 100 mm x 100 mm	Monotonic shear under constant normal stress	* Developed of a set of hyperbolic parameter values for the response of the interfaces used in their tests.
Hryciw and Irsyam (1993)	Sand to ribbed Steel 267 mm x 76 mm	Monotonic and cyclic shear under constant normal stress	* Studied the mechanisms of dilation and shear band formation at the interface. * Studied the influence of rib geometry and spacing, and soil density on the interface response

2.1.2. Direct Simple Shear (DSS) Devices

Uesugi and Kishida, 1986a developed a simple shear type device which was capable of measuring both sliding displacement between steel and soil as well as shear deformation of soil mass. The contact surface between steel and sand was originally 400 mm in length and 100 mm in width. The area of friction surface remained constant during a test even if sliding occurred, since the steel plate was longer than the friction surface. Normal and tangential loads were applied by the vertical and horizontal hydraulic actuators. The surface of each plate was lubricated to allow the container to follow the shearing deformation of sand with minimum friction resistance. They established the bi-linear relationship between the structure surface roughness and the measured interface friction. An increase in the surface roughness of the continuum surface (e.g. steel) will result in a proportional increase in the interface friction up to a critical surface roughness. Above the critical roughness the interface friction is equal to the sand friction reflecting that the failure zone has moved away from the interface into the adjacent soil. The effect of an increase in surface roughness alone has been shown to increase the interface friction by more than 100% [15].

Uesugi and Kishida, 1986b also used another simple shear type apparatus in which the sample had a smaller contact surface of 100 mm x 40 mm. This apparatus was used for one-way and two-way repeated loading of interfaces between sand-steel and sand-concrete (Uesugi et al., 1989, 1990). In these two devices, normal load was measured by a strain gage type transducer and kept constant. Tangential load was measured by the same type of transducer, and was applied to keep the tangential displacement in control. Later, they (1986b) concluded that the relative density of the sand only makes the upper-bound of the coefficient of friction different, and that the mean grain size (D_{50}) also has a significant influence on the coefficient of friction at yield [16].

Evgin et al., 1996, Boulon and Nova, 1990 showed that in constant volume interface tests, the magnitude of the normal stress would reduce to zero during shearing. They concluded that the peak stress ratio is dependent on the magnitude of the normal stress measured at the time when the stress ratio is at its peak, and shear stress behavior is largely affected by the magnitude of the normal stiffness in 2-D tests under constant normal

stiffness condition [13].

Besides having the advantages of the direct shear type apparatus, the simple shear type apparatus has solved the problem of separation between sliding displacement and shear deformation of soi1 sample. But it still has the disadvantage of stress concentration at the ends. This type of device can be extended to operate in three-dimensional space.

Direct Simple Shear (DSS) devices have been intensively employed for interface testing during the last two decades, primarily on sand-to-steel and clay-to-steel interfaces. Sand-to-steel tests have yielded interesting results regarding the general behavior of interfaces. Many of these results are applicable to sand to-concrete interfaces as well. Table 2.2 summarizes some of the previous work on interface behavior in which testing was performed in DSS apparatuses.

One of the main advantages of DSS devices is the ability to measure separately the total interface displacements Δ_{meas} and the soil distortion Δ_{dis} as illustrated in Figure 2.2b.

According to Uesugi and Kishida, 1986b, the horizontal deformation due to distortion of the sand mass is an important component of the total displacement measured in the DSS device.

DSS devices have important limitations for interface testing:

- Nonuniform distribution of stresses at the interface.
- Complicated sample preparation.
- Limited maximum total displacement, which does not exceed 25.4mm [16].

Table 2.2 summarizes some of the previous work on interface behavior in which testing was performed in DSS apparatuses.

Table 2.2. Previous works on direct simple shear testing of sand-to-concrete and sand-to-steel interfaces

Source	Type of Interface and Dimensions	Type of Loading	Summary
Uesugi and Kishida (1986a and 1986b)	Sand to steel 100 mm x 40 mm	Monotonic under constant normal stress	* Concluded that distortion of the sand sample is an important component of the total displacement.
Kishida and Uesugi (1987)	Sand to steel 400 mm x 100 mm	Monotonic shear under constant normal stress	* Found direct relationship between steel roughness and interface friction coefficient was found.
Uesugi, Kishida and Tsubakihara (1988)	Sand to steel 400 mm x 100 mm	Monotonic shear and shear reversal under constant normal stress	* Found that slippage and rolling of sand particles occurs during shear, on rough steel surface. * Found that only slippage occurs on smooth steel surface. * Found that large volume changes of sand occur near the contact with the steel surface. * Reported shear band formation on rough surfaces, not on smooth surfaces.
Uesugi, Kishida and Tsubakihara (1989)	Sand to steel 100 mm x 40 mm	Cyclic shear under constant normal stress	* Confirmed observations on shear band formation by Uesugi, Kishida and Tsubakihara (1988).
Uesugi, Kishida and Uchikawa (1990)	Sand to concrete 100 mm x 40 mm	Cyclic shear under constant normal stress	* Observed similar behavior as in sand-to steel interfaces. * Found that large volume changes of the sand occur in the vicinity of the concrete surface. * Observed shear band formation. * Reported that actual sliding displacement between sand particles and concrete is small. * Found a direct relationship between concrete roughness and friction coefficient.
Evgin and Fakharian (1996)	Sand to steel 100 mm x 100 mm	Monotonic shear under constant normal stiffness	* Developed the Cyclic 3-D Simple Shear Interface (C3DSSI), from a previous DSB version by Fakharian and Evgin (1996), capable of applying shear stresses in two orthogonal directions.
Fakharian and Evgin (1997)	Sand to steel 100 mm x 100 mm	Cyclic shear with constant normal stiffness	* Studied the interface shear strength degradation during cyclic shear under constant normal stiffness.
Desai and Rigby (1997)	Clay to steel and clay to rock 165-mm diameter	Cyclic shear under constant normal stress	* Presented the CYMDOF-P device, with pore pressure measurement capabilities, which is still under development.

2.1.3. Large Size Direct Shear Box (LDSB) Devices

Shallenberger and Filz, 1996 developed a Large Displacement Shear Box (LDSB) especially designed for interface testing. The LDSB is essentially a DSB-type device with the capability to handle interfaces as large as 711 by 406 mm. Shallenberger and Filz, 1996 pointed out the advantages of the LDSB over conventional devices:

- The maximum displacement of 305mm (12 in.) allows the determination of the interface.
- No eccentric normal loads are generated during shear.
- End effects are negligible [17].

The main disadvantage of this apparatus is that sample preparation is a time-consuming process due to the large size of the interface. Furthermore, the distortion deformations of the soil sample cannot be measured; therefore, the actual interface displacements are not known.

Several modifications were implemented in the device to conduct sand-to-concrete interfaces and perform tests that included unloading-reloading and shear reversals. The main reasons for large size direct shear boxes use are the large displacement capabilities of the LDSB which permit staged tests with several steps of normal pressure increments, and its reduced end effects.

2.1.4. Annular Torsion Type Devices

Several investigators have developed special devices in order to overcome the limitations of the conventional apparatuses for interface testing.

Brummund and Leonards, 1973 developed an annular device in which a cylindrical specimen of the structural material is embedded in sand. During testing, the specimen of structural material is pulled along its axis to failure under a confining pressure applied on the boundary of the sand sample. The sample preparation for this type of test is complicated, and the normal stresses at the interface are difficult to control and depend on

the relative stiffness between the structural specimen and the sand [6].

Huck et al., 1973, Huck and Saxena, 1981 performed experimental investigation on soil to concrete interface phenomena under static and dynamic shear loading conditions. A ring simple shear apparatus was used, where the soil sample confined by standard triaxial membranes was in contact with the lower and upper concrete rings which were held by steel holders [18].

A picture of ring-shear device and the specimen chamber of the ring-shear device are given in Figure 2.3.

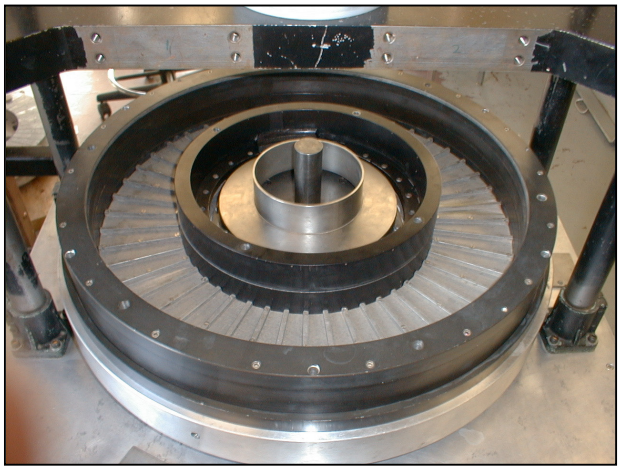

Figure 2.3. A picture of Ring Shear Device

Yoshimi and Kishida, 1981 have reached to the conclusion that the coefficient of friction is essentially governed by the surface roughness of the structural material. They rained dry sand into an annular container lined with 0.3 mm thick rubber membrane, and the top surface of the sand was leveled with a suction device. A static torque was applied to shear the interface under either constant normal stress or constant volume conditions. Circumferential and vertical displacements of the metal ring, the deformation of the sand and slippage at the soil-metal contact were measured in some tests using x-ray radiography. They have concluded that the relative density of the sand and the type of structural material play a negligible role on the value of coefficient of friction. The type of sand also has little influence on the coefficient of friction if the surface roughness *R*,

(L = 2.5 mm) exceeds about 20 μm [19].

According to Stark, Williamson, and Eid, 1996, ring shear devices have the following advantages:

- Unlimited interface displacements, making possible the determination of residual interface shear strengths.
- Shearing along the same interface throughout the test.
- No eccentric loading during shear.

The principal disadvantages of the ring shear device are as follows:

- Complicated sample preparation procedures, especially for sand-to-concrete interfaces.
- Relatively narrow soil samples, which may induce scale effects in some interface tests.
- Nonuniform radial distribution of shear stresses.
- Unknown actual sliding displacements at the interface in the case of rigid ring shear devices [20].

2.1.5. Geotextile-Soil Interface Cylindrical Test (GICT) Device

Akkol, 1997 performed Geotextile-soil interface tests on sands and developed a new interface testing device. The geotextile was glued around a cylindrical block and rotated in a soil sample where the normal load was applied radially. The device has many advantages such as:

- Unlimited interface displacements, making possible to reach critical state.
- Constant shear area during the tests.
- Possibility to change dimensions of shear samples.
- Minimized machine friction and load eccentricity.
- Minimized boundary effects.

Akkol, 1997 compared the results of interface tests performed on fixed shear tests to GCIT and concluded that the results obtained from GICT are less than those obtained in fixed shear tests [21].

2.1.6. Interface Modeling

The mechanical characteristics of interfaces between structural and geological materials and accurate modeling are very important if numerical methods are to be used in predicting soil to structure interaction. Several kinds of interface elements have been developed to model the behavior of the interface under certain loading conditions. A constitutive model for interfaces must be adequate for the problem to be analyzed, and therefore it must be able to capture the characteristic behavior of a discontinuity under the specific loading/flow conditions under consideration.

Interface elements were first introduced by Goodman, Taylor [21]. The adoption of interface elements represented a significant improvement over previous methods, which assumed either of two conditions: a perfectly rough interface with no slip between soil and structure, or a perfectly smooth interface with no shear stresses developed (Clough and Duncan, 1971).

The element developed by Goodman, Taylor, and Brekke, 1968 is commonly referred to as joint element or zero-thickness interface element. It is a four-node element of zero thickness as illustrated in Figure 2.4. In their derivation of the joint element stiffness matrix, they used a very simple constitutive law consisting of constant values for both the shear stiffness and the normal stiffness:

$$k_n \,.\, \Delta_n = \sigma_n \tag{2.1}$$

$$k_s \,.\, \Delta_s = \tau_s \tag{2.2}$$

where k_n = the normal stiffness.

Δ_n = displacement normal to the interface

σ_n = normal stress acting on the interface

k_s = interface shear stiffness

Δ_s = displacement along the interface

τ_s = interface shear stress.

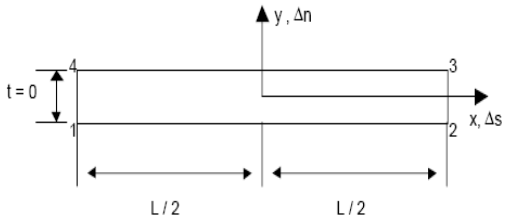

$$K = \frac{1}{6}\begin{pmatrix} 2ks & 0 & ks & 0 & -ks & 0 & -2ks & 0 \\ 0 & 2kn & 0 & kn & 0 & -kn & 0 & -2kn \\ ks & 0 & 2ks & 0 & -2ks & 0 & -ks & 0 \\ 0 & kn & 0 & 2kn & 0 & -2kn & 0 & -kn \\ -ks & 0 & -2ks & 0 & 2ks & 0 & ks & 0 \\ 0 & -kn & 0 & -2kn & 0 & 2kn & 0 & kn \\ -2ks & 0 & -ks & 0 & ks & 0 & 2ks & 0 \\ 0 & -2kn & 0 & -kn & 0 & kn & 0 & 2kn \end{pmatrix}$$

Figure 2.4. Zero thickness interface element and corresponding element stiffness matrix (Goodman, Taylor, and Brekke, 1968)

Clough and Duncan, 1971 observed that compressive stresses normal to the interface would induce overlapping among soil and structural elements adjacent to the interface. To minimize this effect, they proposed assigning a high value of normal stiffness to the joint element under compression. Similarly, for interface elements under tension, they proposed assigning a small value of normal stiffness to minimize the development of tensile stresses at the interface [23].

Morrison, 1995 also presented a comprehensive review of previous investigations of interface elements. Many of the studies he reviewed described numerical integration problems arising from the use of interface elements of high normal stiffness adjacent to softer soil elements. He studied an interface element formulation with relative degrees of freedom proposed by Wilson, 1975 to minimize such numerical problems. Morrison, 1995 showed that the Wilson formulation is not necessary if Newton-Raphson iteration is used to find the interface displacements resulting from each load increment [24].

In nonlinear models, the interface shear stress-displacement relationship is represented by a mathematical function of higher degree. The interface shear stiffness changes during shear, depending on the magnitude of the displacement and any other factor included in the model. Nonlinear models have been used by Clough and Duncan, 1971; Zaman, Desai, and Drumm, 1984; Desai, Drumm, and Zaman, 1985 among others [25].

Clough and Duncan, 1971 developed the hyperbolic model for interfaces. This model has been used extensively in SSI analyses and design of geotechnical structures, including analyses of lock wall [23].

Desai, Drumm, and Zaman, 1985 presented a modified Ramberg-Osgood model for interfaces under cyclic loading. The model accounts for shear stress reversals, hardening or degradation effects with number of load cycles, normal stress, relative density of the sand, and maximum displacement amplitude [25].

Uesugi and Kishida, 1985 observed that the modified Ramberg-Osgood model yields inconsistent results for shear stresses close to failure. In all the interface models described previously, the interface yield stress is determined by the Mohr-Coulomb.

2.1.7. Interpretation of Interface Tests Results

Observations of the soil-structure interface friction test results indicate that interface behaves nonlinearly from the viewpoint of stress development accompanying relative sliding displacement. Both the surface roughness and the soil density are found to have a considerable effect on the interface behavior. The stress-displacement curves for dense sand along a rough surface show a clear peak with a pronounced strain softening. After an initial contraction stage, the volume change is strongly dilatant and finally stagnates at a certain stage of displacement. Both the stress ratio and the volume change increase with increasing roughness. But the shear deformation of sand mass is not affected by the surface roughness.

The static coefficient of friction is affected by sand type (i.e., soi1 composition considering the size distribution, angularity, and surface texture of the sand grains), regardless of the nature of the surface against which slip is occurring. When the sliding surface is rough in comparison to the grain size of the sand, the angle of interface friction exceeds the angle of shearing resistance of the sand and sand / sand slip occurs. In static tests, shearing rate has no effect on coefficient of friction for dry sand. It has been observed that the apparatus type and the sample dimension have minor effects on the maximum coefficient of friction in some tests.

The shear strength and the tendency for dilation of a granular medium increases as the particle angularity increases due to increased interlocking. Recently Lee and Frost, 2002 demonstrated the effect of increased particle angularity on interface behavior. An increase in particle angularity results in increased interface friction due to a higher degree of interlocking with the continuum surface.

Table 2.3 summarizes a number of different factors have been identified to contribute to granular-continuum interface performance as factors of primary importance include the particle angularity, density, continuum surface roughness and hardness, and normal conditions. The other factors are considered to have a second order effect in most interface conditions.

Table 2.3. Factors affecting granular-continuum interfaces [26]

Type	**Factor**	**Significance**
Granular Material	Particle Angularity	High
	Density	High
	Initial Soil Structure	Low
	Mean Grain Size(D_{50})	Medium
	Surface Roughness	Low
	Uniformity Coefficient(C_u)	Low
Solid Surface	Surface Hardness	High
	Surface Roughness	High
Testing Conditions	Normal Confinement Condition	High
	Test Method	Low
	Strain Rate	Low

A number of studies have shown that surface topography is important in the behavior of soil-structure interfaces. Frost et al., 1999 studied the evolution of the structure of sand adjacent to the geomembrane, and found that it was directly influenced by the surface roughness. The roughness of contact surface is determined in a certain gauge length for which the particle size must be taken into account. It is found that the maximum coefficient of friction is mainly dependent on the surface roughness of solid material and mean particle diameter. The effects of these two factors can be combined into the influence of so-called normalized roughness.

Frost et al., 2002 performed interface tests to determine the peak and residual interface friction angles of the different materials when sheared against sands. Additionally, direct shear tests were performed on sands to assess the strength of the sand. The internal friction values for both sands provide the upper bound of possible interface friction angle values for continuum materials sheared against these sands since for very rough surfaces, the failure zone would move away from the interface and into the soil mass. For the Ottawa sands, the peak and residual internal friction angles were 39°and 28° respectively. Figure 2.5 shows shear stress – horizontal displacement curves for interface friction of Ottawa sand and three different materials [27].

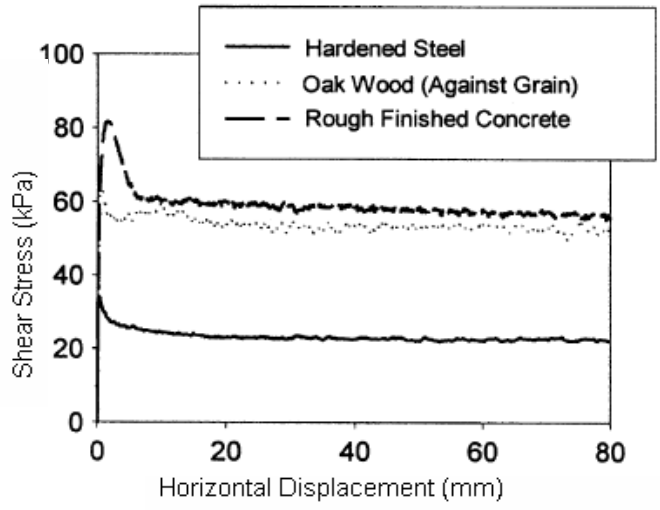

Figure 2.5. Shear stress–horizontal displacement curves from Ottawa sand sheared against hardened steel, oak wood (against grain), and rough finished concrete (normal load 100 kPa) [27]

Figure 2.6 shows the results of interface tests conducted by Acar, Durgunoglu, and Tumay, 1982. The tests were conducted with a quartz sand and concrete, wood, and steel as foundation materials with a normal stress of 100 kPa in order to obtain the variation of δ and ϕ between quartz sand and the same foundation materials as a function of normal stress(σ).

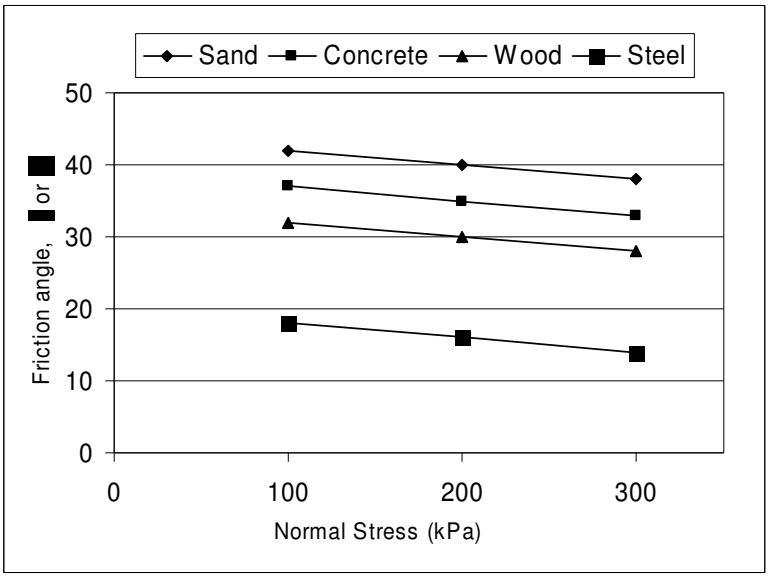

Figure 2.6 Variation of ϕ and δ with normal stress [8]

The test results conducted by Potyondy on dry sands with a stress strain controlled direct shear box are given in Table 2.4. Potyondy indicated that, when the normal load was increased from 48.88 kPa to 143.64 kPa, the angle of internal friction decreased from 44°30′ to 43°30′. For rough and smooth concrete, the angle of interface friction was very close to angle of internal friction for sands [2].

Table 2.4 Stress and strain controlled shear box results of skin friction for sand [2]

Normal Load	48.88 kPa		143.64 kPa	
Material	ϕ	δ	ϕ	δ
Smooth Steel	44°30′	24°10′	43°30′	24°00′
Rough Steel	44°30′	34°00′	43°30′	33°40′
Wood par. To grain	44°30′	35°00′	43°30′	33°20′
Wood at right angles to grain	44°30′	39°00′	43°30′	38°30′
Smooth concrete	44°30′	39°30′	43°30′	38°30′
Rough Concrete	44°30′	44°00′	43°30′	42°30′

The quantification of surface roughness in terms relative interface roughness R_n (Equation 2.3), as reported by Uesugi and Kishida, 1986b, was defined by measuring R_{max} (vertical distance between the highest peak and the lowest trough) along a profile length L equal to the mean grain size D_{50} and then normalizing it by D_{50} as shown in Figure 2.7.

$$R_n=R_{max}(L=D_{50})/D_{50} \tag{2.3}$$

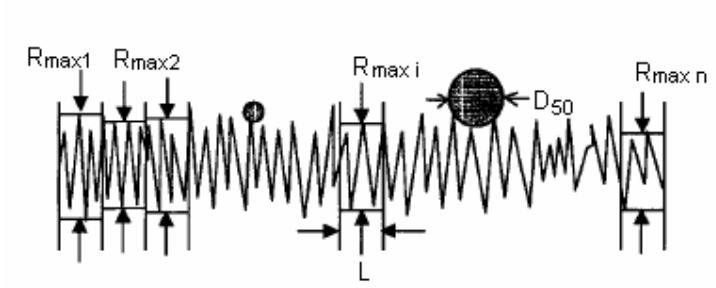

Figure 2.7. Illustration of R_{max} [15].

Alternative definition, relative roughness (R_a /D_{av}) , introduced by Subba Rao et al., 1998 where R_a is the average roughness and D_{av} is the weighted average particle size of the sand [28].

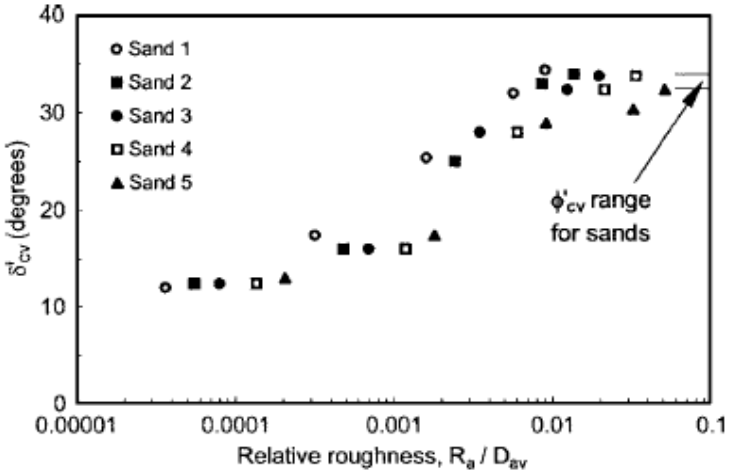

Figure 2.8. Influence of relative roughness on interface strength after peak [28]

The interface is a thin shear zone along the contact surface between soil and construction material. The interface soil undergoes very large structural changes and grains crush during the localized shear. The interface thickness is usually within the range of two to eight times the mean grain size. The lower density of sand in the shear zone results in the lower maximum shear stress ratio. Therefore the upper limit to the coefficient of friction decreases because of the shear zone formation.

Lok-Man Chu and Jian-Hua Yin, 2004 stated that the behavior of shear stress–displacement curves in the soil–grout interface direct shear tests is similar to those from the soil–soil direct shear tests using a direct shear box. The shear stress–normal stress envelopes for the soil–soil direct shear tests, soil–grout interface shear tests with zero roughness angle and regular surface nail pullout tests are shown in Fig. 2.9.

Huabei Liu, Erxiang, Song and Hoe I. Ling, 2006 used the critical state theory which has been successfully used in the modeling of soil behavior to develop a constitutive model for soil-structure interface in the framework of generalized plasticity. The model was capable of modeling strain hardening, softening, normal dilatancy and stress-path dependency of interface between sandy soil and structures during shearing. They verified the performance of the model various experimental results. Figure 2.10 shows the comparison of interface test results with data obtained from model and previous experimental studies.

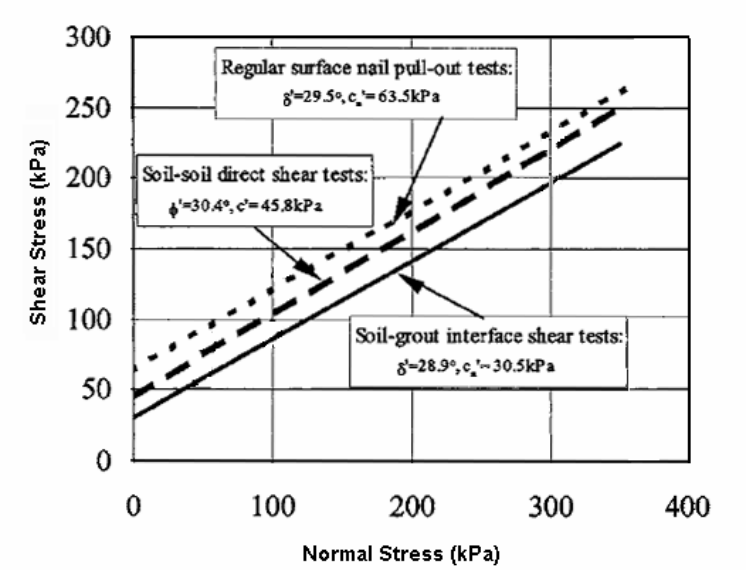

Figure 2.9. Comparison of shear strength parameters among soil–soil direct shear tests, soil–grout interface shear tests (zero roughness angle), regular surface nail pullout tests at peak shear strength [29]

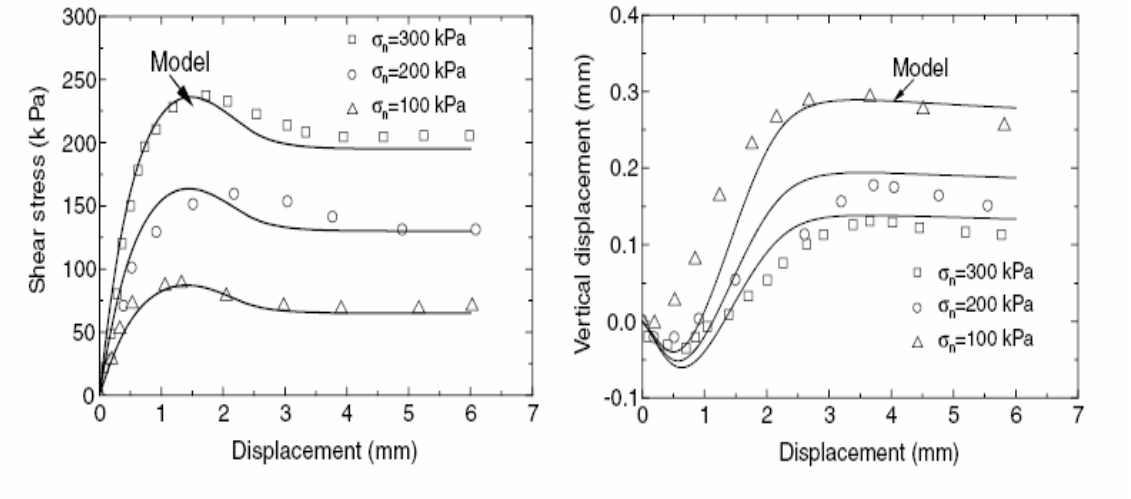

Figure 2.10. Comparison of model prediction and experimental results: interface tests with different normal stress levels [30, 31]

2.2. Mechanical Behavior and Crushing of Granular Materials

Granular materials are constituted of an assembly of particles. In spite of the simplicity of this assembly, its mechanical behavior is complex. The mechanical behavior of granular materials is dependent on the properties of the grains of which they are constituted. Hence, it is natural to search for correlations between the parameters of the constitutive model of a supposedly continuous medium and the properties of the grains (form, size, granulometry...) [32].

Granular materials forming part of the base of pavements and railroads, embankments, and pile foundations are subjected during their engineering lives to either static or dynamic loads. As a result of these loads these materials can break. The breakage of these materials will change their original mechanical properties. These original mechanical properties were used for the design of the civil engineering structures that were placed on the granular materials. A change of the granular materials' original mechanical properties could be detrimental to the safety of the structures that rest on them.

The strength of a granular soil mass is developed through frictional forces of interlocking soil particles as they are pressed together by gravity. The rougher and more angular the particles, the more tightly they cling to one another, resisting sliding and shear failure.

Grain breakage is an important subject in Soil Mechanics. Fukumoto, 1992 qualified it as a subject of major importance as the soil undergoes significant changes due to this phenomenon. There are many practical problems related to grain breakage such as the stability of earth dams, the bearing capacity of piles [4].

Grain rupture may be classified according to three modes as in Figure 2.11:

- Fracture: a grain breaks into smaller grains of similar sizes.
- Attrition: a grain breaks into one grain of a slightly smaller size and several much smaller ones.
- Abrasion: the result is that the granulometry remains almost constant but with a

production of fine particles [33].

The mechanical resistance of grains may be linked, on one hand, to its mineralogical nature and on the other hand to its state of alteration. It therefore depends on the history of how the natural deposits were formed, the history of its fabrication (crushing. . .) for the artificial mixtures. The influence of the shape may be linked to the preceding point in that the statistical distribution of faults (grain joints, fissures. . .) depends on the shape of the particles, the smallest being more resistant than the large ones (scale effect).

Figure 2.11. Different modes of grain breakage

Taylor, followed later by Bishop and others, divided the shear resistance of granular soils into two components [34, 35].

- The internal, frictional component between particles, which is a combination of rolling and sliding friction, and
- The additional component arising from shearing against interlocked particles.

In a plane strain test, a dense granular soil is first deformed homogeneously. Around a peak stress, however, the deformation suddenly localizes into narrow bands (called the shear bands) and the stress drops sharply down to a residual stress state. Oda observed the microstructure of shear bands developed in several natural sands, by means of X-ray application and an optical method using a microscope and thin sections [36].

The two results are;

- very large voids are generated inside a shear band, while shear strain is being concentrated, and as a result of this, the void ratio can exceed the corresponding maximum one determined by a standard method and
- particles rotate extensively in the shear band so that a high particle rotation gradient is generated along the boundaries.

It was proposed by Rowe that the peak friction angle ϕ_μ has three components: the sliding resistance at contacts, particle rearrangements and dilation where the effect of crushing is neglected. The general interrelationships among the strength contributing factors were represented by Oda and M. Kazama, 1998. (Figure 2.12)

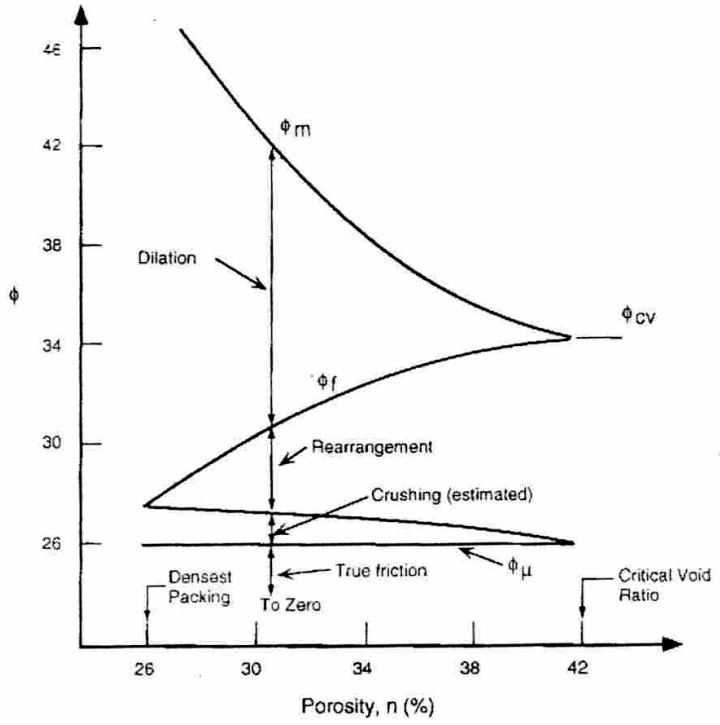

Figure 2.12. Contributions to shear strength of granular materials [32]

where ϕ_f = corrected friction angle corrected for the contribution of dilation and

ϕ_v = deformation at constant volume.

The parameters that affect the shear strength of granular materials can be separated into two main groups. The first group is the constant parameters, independent of the arrangement and the other is the variable parameters, describing the arrangement geometry as shown Figure 2.13.

The relationship between single particle and collective crushing behaviors is not straightforward because the loading of a particle in a matrix cannot be exactly modeled by single particle crushing and the relationship between macroscopic and microscopic stresses is complex. The mechanical behavior of a soil in the context of the crushing characteristics of individual particles must be discussed in order to understand the effects of particle crushing on the mechanical behavior of soils [38].

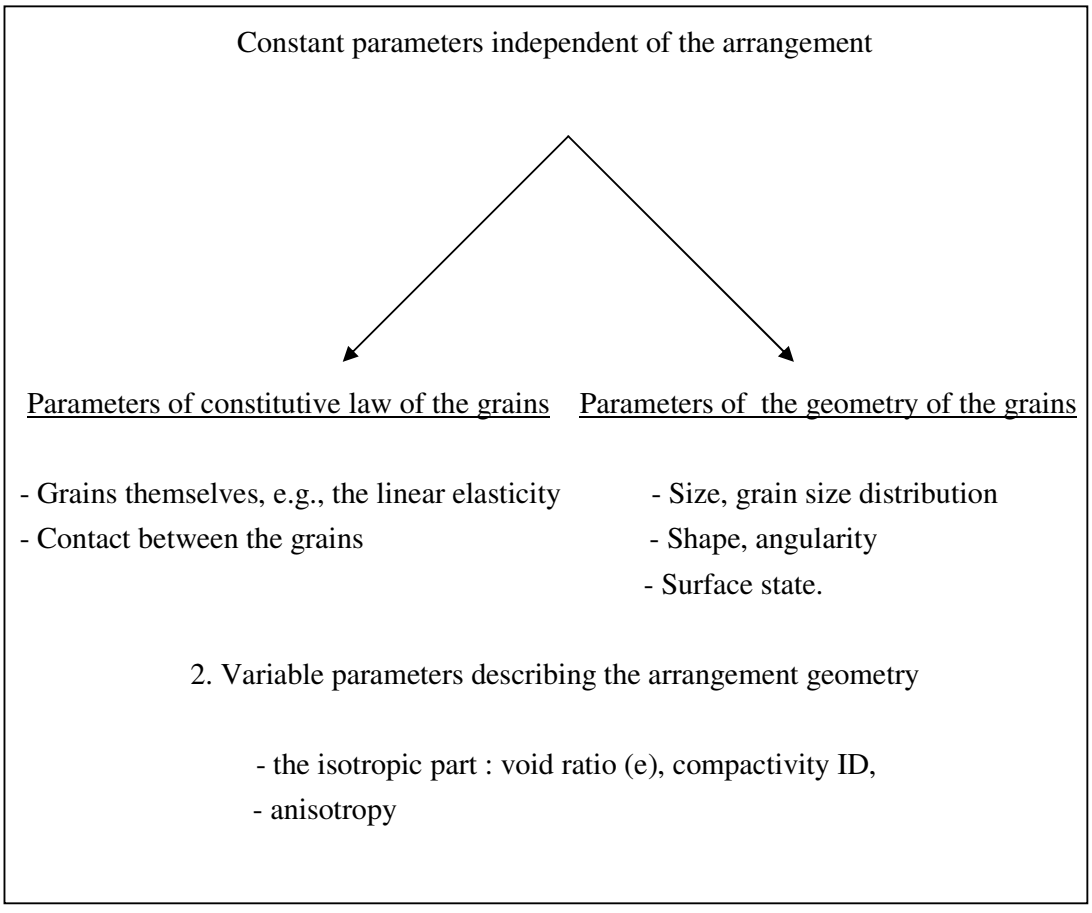

Figure 2.13 Parameters affecting shear strength of sands and gravels [37]

2.3. Fly Ash

According to the American Concrete Institute (ACI) Committee 116R, fly ash is defined as 'the finely divided residue that results from the combustion of ground or powdered coal and that is transported by flue gasses from the combustion zone to the particle removal system' (ACI Committee 232 2004).

Fly ash is a major by product of coal burning in thermal power plants. The disposal of such fly ash is creating a serious problem because of its storage space and cost involved in its storage. At the same time there is a lot of pollution of the environment due to the fineness of the fly ash. The effects for its utilization for many gainful purposes have been made since late sixties of this century by various research institutions and public enterprises. Some researchers have investigated methods to beneficiate high-carbon fly-ash into a marketable product. High percentage of fly ash is utilized in developed countries. The majority of the fly-ash produced every year is not being used; nearly 80% of the fly-ash produced is still land filled.

Fly ash consists of inorganic matter present in the coal that has been fused during coal combustion. This material is solidified while suspended in the exhaust gases and is collected from the exhaust gases by electrostatic precipitators. Fly ash is made up of fine, spherical particles with a diameter range of 0.074 to 0.005mm. These hard and round particles are so small that in laboratory tests for fineness. Under a microscope, fly ash particles look like tiny ball bearings. A SEM of typical fly ash particles is given in Figure 2.14.

Silica is the primary compound in fly ash. Fly ash is a pozzolan. A pozzolan is primarily a siliceous or siliceous and aluminous material, in a finely divided form and in the presence of water, chemically reacts with calcium hydroxide at ordinary temperatures to form compounds possessing cementitious properties.

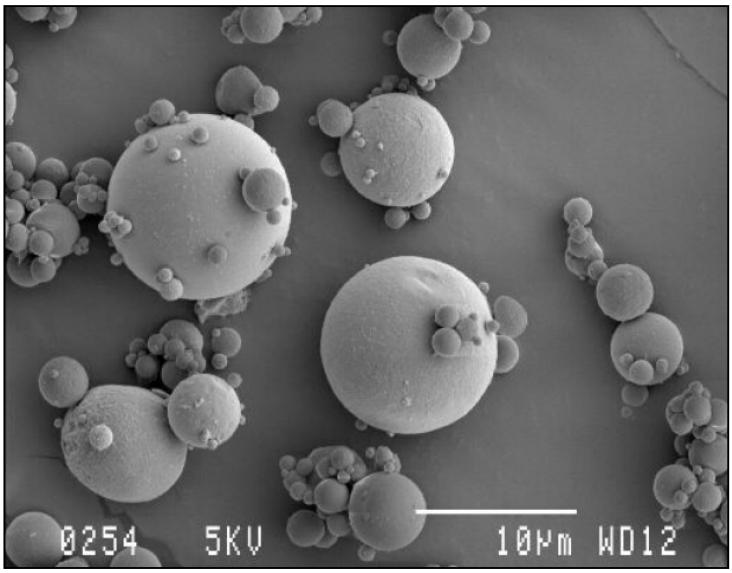

Figure 2.14. SEM of typical fly ash particles.

Formation of cementitious material by the reaction of free lime (CaO) with the pozzolans (AlO_3, SiO_2, Fe_2O_3) in the presence of water is known as hydration. For class C fly ash, the calcium oxide (lime) of the fly ash can react with the siliceous and aluminous materials (pozzolans) of the fly ash itself. Since the lime content of class F fly ash is relatively low, addition of lime is necessary for hydration reaction with the pozzolans of the fly ash. For lime stabilization of soils, pozzolanic reactions depend on the siliceous and aluminous materials provided by the soil. The pozzolanic reactions are as follows:

$$Ca(OH)_2 \Rightarrow Ca^{++} + 2[OH]^-$$

$$Ca^{++} + 2[OH]^- + SiO_2 \Rightarrow CSH$$

(Silica) (gel)

$$Ca^{++} + 2[OH]^- + Al_2O_3 \Rightarrow CAH$$

(Alumina) (gel)

Hydration of tricalcium aluminate in the ash provides one of the primary cementitious products in many ashes. The rapid rate at which hydration of the tricalcium aluminate occurs results in the rapid set of these materials, and is the reason why delays in compaction result in lower strengths of the stabilized materials. The hydration chemistry of fly ash is very complex in nature. So the stabilization application must be based on the physical properties of the ash treated stabilized soil and cannot be predicted based on the chemical composition of the fly ash.

Fly ash has been classified into two classes, F and C, based on the chemical composition of the fly ash. According to ASTM C 618, the chemical requirements to classify any fly ash are shown in Table 2.5.

Table 2.5. Chemical requirements for fly ash classification.

Properties	Fly Ash Class	
	Class F	Class C
Silicon dioxide (SiO_2) plus aluminum oxide (Al_2O_3) plus iron oxide (Fe_2O_3), min, %	70.0	50.0
Sulfur trioxide (SO_3), max, %	5.0	5.0
Moisture Content, max, %	3.0	3.0
Loss on ignition, max, %	6.0*	6.0
* The use of class F fly ash containing up to 12% loss of ignition may be approved by the user if acceptable performance results are available.		

Fly ash can be used in various developmental and construction activities. Some of the prominent uses of fly ash are given as under:

- For development of various value added products, fly ash based bricks, blocks, mosaic tiles, glazed floor, wall tiles, partition boards, concrete products, cellular light weight concrete blocks etc.
- For reclamation of waste land/filling of low lying areas, soil amendment.
- As mine fills in open cast mines and the underground mines can be stowed with ash.

- Production of cement
- For use in concrete as lightweight aggregate.
- In construction of embankments, dykes, road sub-base and base course.
- In agriculture as a source of micronutrient for improvement of soil condition.
- Road-building applications

2.4. Pelletization Process

Artificial lightweight aggregates which consist primarily of fly ash, fine and/or coarse aggregates and a small amount of Portland cement are being used increasingly in the construction industry. Pelletization is a promising process for making artificial aggregates from fine-grained materials like fly ash, which facilitates its high volume utilization as lightweight aggregate in concrete.

2.4.1. Definition and Objectives of Pelletization

Anderson, 1912 was the first to put the idea of pelletization process. Brackbelserg revised process with the addition of binder to the fines being pelletized and the pellets would be strengthened at elevated temperatures during production [39].

Two basic steps have to be performed to produce an aggregate from fly ash: bonding of the material in the pellets by firing, hydrothermal processing, and cold bonding which gives the pellets strength and other properties necessary to meet the criteria for a lightweight aggregate, and agglomeration of the fine fly ash particles to form aggregate-size pellets [40].

Agglomeration (also called "pelletization') can be performed by two distinct methods. One is by agitation, where fly ash particles are introduced onto an inclined rotating disk along with a wetting agent and an appropriate binder. Balling of the material occurs by the formation of 'seeds' which ultimately grow into pellets of a certain maximum size. The product obtained at the end of the process is termed as “fresh pellet”. The crushing strength of the fresh pellet must be adequate for hauling and stockpiling purposes [39].

The other method is the pressure or extrusion method where agglomeration is accomplished by using a continuous piston-type press where more or less rectangular or cylindrical pellets are formed. The extrusion process generally results in a product having a higher density than the spherical pellets produced by agitation [40].

Regardless of which manufacturing process is used, pellets have to meet the following requirements [41]:

- They should be near spherical and have a smooth surface; both considered optimum characteristics for subsequent film coating.
- The particle size range should be as narrow as possible. The optimum size of pellets for pharmaceutical use is considered to be between 600 and 1000μm.
- The pellets should contain as much as possible of the active ingredient to keep the size of the final dosage form within reasonable limits.

The pellets may also be sintered during a specified interval of time after production depending on concerns like properties of the fines used in pelletization process, the purpose of use and the rate of increment in engineering performance of pellets. Beside that, several advantages of cold bonding process based on experiences to date show that:

- Cold bonded process plants tend to have lower capital costs than sintering/rotary kiln firing plants.
- Cold bonded processes tend to have lower operating costs than sintering/rotary kiln firing.
- Cold bonded process plants have less environmental impact than sintering/rotary kiln firing plants (no exhaust gases). Both processes require particulate emission controls and may have waste water streams.
- Finished material costs tend to be lower for cold bonded material than for sintered material.

2.4.2. The Theory of Pelletization

Pelletization depends on the size of particles and their distribution, moisture content, along with the process related parameters. Only limited studies have been reported on the pelletization of fly ash aggregates. The previous studies showed that the performance of pelletization process is a function of;

(i) speed of revolution of pelletizer disc,
(ii) angle of pelletizer disc,
(iii) moisture content, and
(iv) duration of pelletization.

When a fine grained material is moisturized, there forms a thin liquid film on the surface of the grains, which forms meniscus between the grains (Fig. 2.15a). In case the particles are rotated in a balling drum or disc, then there forms ball shape structures with enhanced bonding forces between grains due centrifugal and gravitational forces (Fig. 2.15b, c) [39].

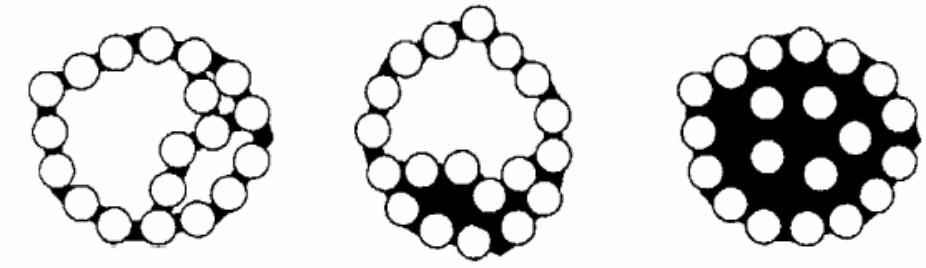

(a) (b) (c)

Figure 2.15. Mechanism of pellet formation [40]

As described in Figure 2.15 the initial bonding between particles is a meniscus formed due to water film, however it does not provide sufficient cohesion between particles to hold them together. As the amount of water increases, the particles begin to coalesce due to increased surface tension formed by increased liquid column. There are also voids in the structure formed.

The primary structure forms the nucleus of the pellet and the pellet gradually grows in size as more moisturized particles are coated on the nucleus. When these structures are rotated in the balling drum or disc, the pellets are compacted in denser state under the mechanical forces developed by the balls bumping against each other and against the walls of the balling device as well as centrifugal gravitational forces. At this stage of process, the forces developed on pellets expel the air that fills the free space between the individual particles, leaving the gaps to particles and water. As the particles get closer, the structure becomes denser, and the height of capillary rise increases, which improves the structure coherence and makes the fresh pellets have sufficient strength for handling and stockpiling conditions. As the particles get denser, the engineering performance of the fresh pellets is improved as well as their performance for the rest of their service life [39].

The strength of the pellets depends on the pelletization process parameters, and finally the resultant magnitude of pressure being exerted on the pellets. Moreover, the capillary forces (surface tension generated by the height of liquid column) play a greater role in the magnitude of the coherence of the pellets. The coherence of the structure is directly proportional to the mechanical and capillary forces exerted on the pellets. In this respect, the capillary force theory was developed by Sastry, 1995 [42];

$$h = \frac{2 * \sigma_s * \cos \delta_c}{r * \rho * g} \quad \text{(cm)} \tag{2.4}$$

where h is the height of the liquid column (cm), σ_s is the surface tension of the liquid (N cm^{-1}), δ_c is the angle of contact between the liquid and the solid phase (°), ρ is the density of the liquid (g/cm^{-3}), r is the radius of capillary (cm), g is the acceleration of gravity (cm s^{-2}).

As defined in the formula above, the cohesiveness of the structure and, consequently, the strength of the pellet are directly proportional to the capillary rise and inversely proportional to the radius of capillaries. The minimization of void ratio of the final product and the radius of capillary during pelletization process may be provided by a wider range of granulometric distribution as well as process efficiency.

If the liquid used in the pelletization process is assumed to be water and assumed that all fines are uniformly wetted with water, then;

$$\delta_c = 0, \qquad \cos\delta_c = 1, \qquad \rho = 1 gr/cm^3 \quad (20°C) \tag{2.5}$$

$$k_c = \frac{2 * \sigma_s * \cos\delta_c}{\rho * g} \tag{2.6}$$

the capillary constant k_c can be defined as in the formula above. When the values in Equation 2.5 are substituted in Equation 2.6, then the equation simplifies into;

$$k_c = 0.15 \tag{2.7}$$

and

$$h = 0.15/r \tag{2.8}$$

The radius of capillary (r) that takes place in equations is found by the help of the specific surface area and the specific gravity of the material. Then the height of the liquid column, h is found by substituting the value of radius of capillary, r, in Eq. 2.8.

The experimental studies showed that the strength of fresh pellets is directly proportional to the height of liquid column found out by the help of above equations. At this stage, it is obvious that the maximum strength (the strength of fresh pellets and, consequently, the strength of cured pellets) may only be reached if all the capillaries are filled with water during production. The lack of sufficient water causes air voids to be entrapped inside the structure, which restricts the capillary action. On the other hand, excessive water causes a water film on the surface of the ball, which destroys the capillary forces resulting in particle cohesiveness limited to the magnitude of the surface tension water. Sastry, 1995 defined pelletization process in three steps depending on the degree to which the inter-granular spaces are filled with water [42].

According to Sastry, 1995, the pelletization process may be analyzed in three steps depending on the degree to which the intergranular spaces are filled with water :

(a) The pendular state: The water is present at only the point of contacts of grains.

(b) The funicular state: In this state, in addition to the conditions present in pendular state, some of the pores are completely filled with water.

(c) The capillary state: In this state, all inter-granular spaces are completely filled with water and no water film exits on the surface of the pellet [42].

The force being exerted on the particles can be expressed in terms of equation below;

$$P_c = \frac{2 * \pi * d * \sigma_s}{\tan \beta / 2} \tag{2.10}$$

where P_c = pressure at the point of contact,

σ_s = surface tension of the liquid,

β = central angle of the meniscus and

d = diameter of the spherical particle.

There are two factors determining the strength of the ‘‘fresh pellet’’:

(a) The magnitude of cohesive force acting on the particles during the process,

(b) The interlocking effects.

The strength of the ‘‘fresh pellet’’ is equivalent to the superposition of the strength gained by these two factors. The magnitude of the cohesive force is determined by the void ratio of the structure, whereas the strength gained due to interlocking effect is a function on the surface texture of the fresh particles. However, for the ideal condition of fully rounded particles, the strength of the fresh pellet may be assumed to be equal to the cohesive force that is formed during process [42].

H. Rumpf, introduced the following assumptions and simplifications, formulized the capillary and cohesive forces being exerted on the particles;

1. all particles are spherical and have uniform diameters;
2. the bonding pattern is uniform throughout the ball section;
3. the particles in the ball are evenly distributed;
4. effective bonding forces fluctuate around the average value.

Then, according to the above assumptions, following equation may be derived for cohesive forces in the capillary state;

$$P_c = 8 * \frac{(1-\varepsilon) * \sigma_s}{\varepsilon * d} \tag{2.11}$$

where σ is the surface tension of the liquid, P_c is the cohesive force exerted on the structure in capillary state, ε is the ball porosity and d is the diameter of the spherical particle.

Schematic views for ball formation are given in Figures 2.16 and 2.17. In Figure 2.16 the mechanism of ball formation is sketched for the moisture content less than the optimum state. In this state, the moisturized particles move closer, become connected with water bridges. As more particles join the structure, the formation tightens under mechanical forces. The degree of saturation increases by decreasing volume of voids, since the air is expelled leaving the pore spaces to particles and water. In this state, if the structure is fed with additional moisture, then the capillary bonding occurs [37].

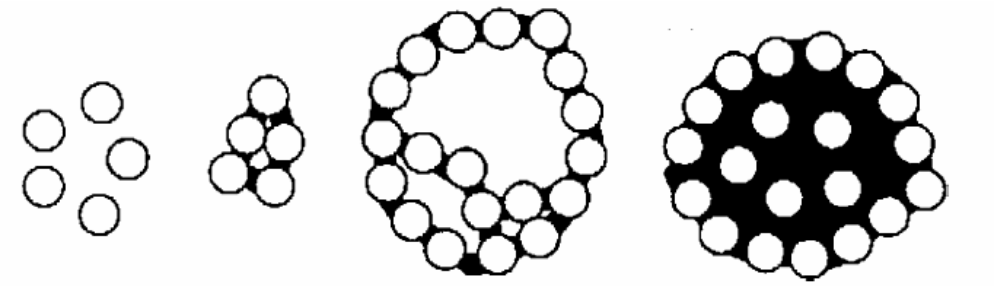

Figure 2.16. Mechanism of ball nuclei formation (water content below optimum state)

When the water content is above optimum state as in Figure 2.17, the particles are wetted excessively to form the nucleus by means of the surface tension of water. The formation is weaker than capillary force diminished. The formations are also random sized, and they may easily degrade upon mechanical forces created in balling drum disc. This methodology has disadvantages, since the granulometric distribution of pellets can not be controlled during pelletization process [37].

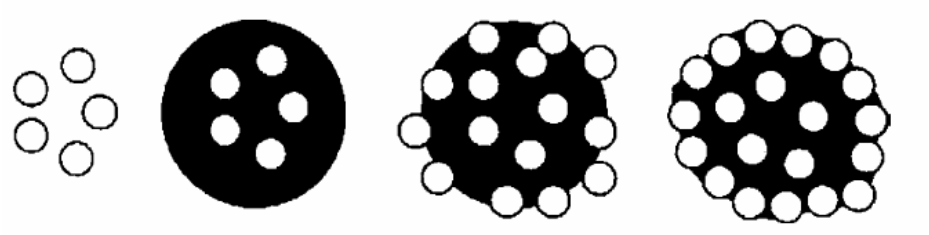

Figure 2.17. Mechanism of ball nuclei formation (water content above optimum state)

The variations of movements of pellets in the pelletization disc with respect to the revolution speed are given in Figure 2.18. As described in figure as well, for low revolution speed the movement of pellets is governed by gravitational force, and for high speeds the movement is governed by centrifugal force. If one of these forces becomes dominant on the movement, then either pellet formation is ceased or the pellets formed have loose structure. Especially if the dominant force is centrifugal force, the pellet formation is almost ceased since all the particles will stick to the sidewall of the disc by means of adherence created by moisture [43].

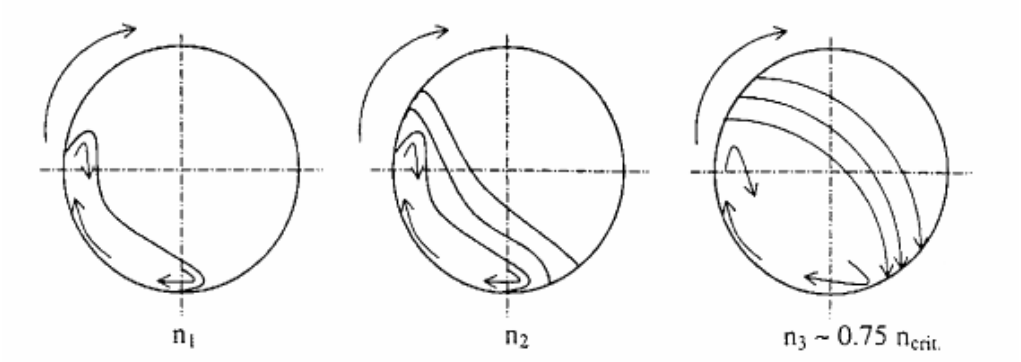

Figure 2.18. Motion of material in disc pelletizer revolving at various speeds [43]

The optimization studies of Baykal and Doven (1999) showed that the 'critical revolutions per minute is [43];

$$n_{cr} = \frac{43.2}{\sqrt{D}} \sqrt{\sin \alpha_i} \tag{2.12}$$

where n_{cr} = critical revolutions per minute (rpm),

D = disc diameter (m),

α_i = angle of disc inclination in degrees.

2.4.3. Factors Affecting the Pelletized Product Quality

The amount of water used in pellet production is of extreme importance since the formation and structure of pellet is dependant on moisture content regardless of other mechanical factors of the process. The effect of moisture content on pellet formation, diameter and structure are described in Figure 2.19.

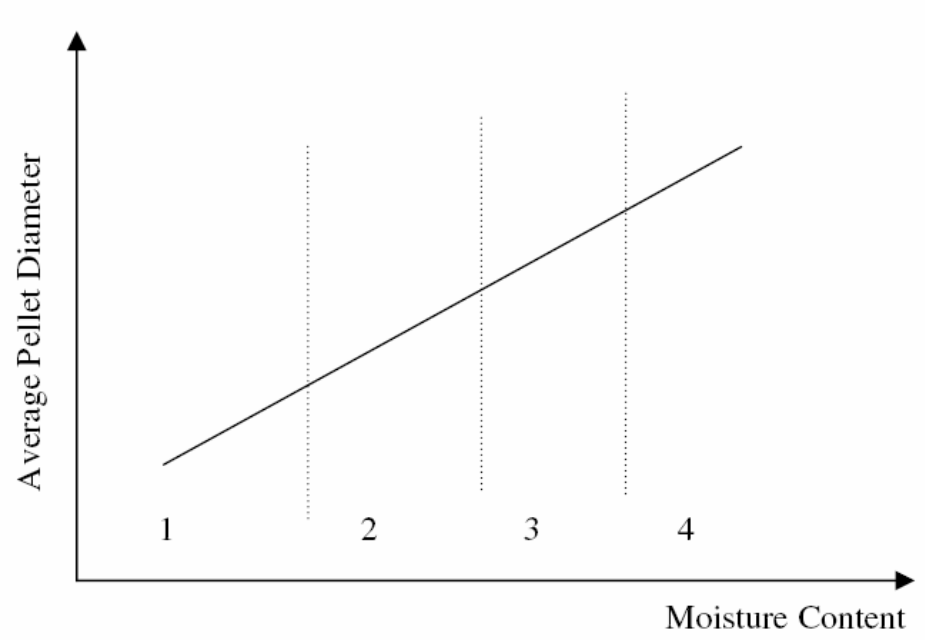

Figure 2.19. The effect of moisture content on pellet formation, diameter, and structure [39]

The moisture content used for pelletization process affects the residence of time of pellets in the pan and the rate of production besides the size of pellets. The general relationship is shown in Figure 2.20. The diagonal lines represent the moisture content (f_i) increasing from lower right to upper left.

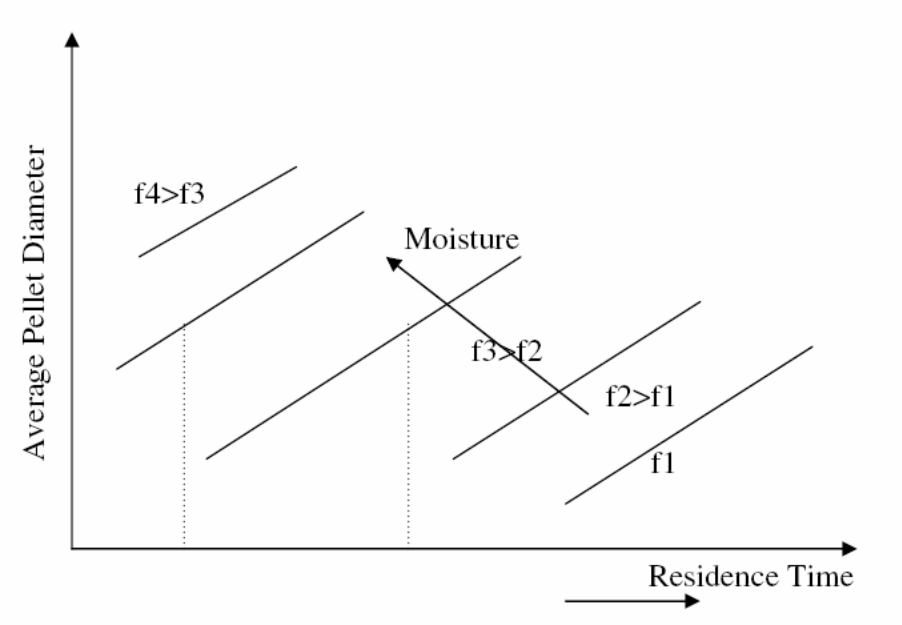

Figure 2.20. The effect of moisture on the duration time of fresh pellet [39]

3. METHODOLOGY

Synthetic lightweight aggregates with various fly ash / cement ratios (FA, FAC10, FAC20) produced by pelletization process were tested for grain size distributions (before and after tests), specific gravity, water absorption, crushing strength, internal friction and interface friction between the aggregates and concrete made with lightweight aggregates.

A commercially available direct shear device was used to perform both direct shear and interface tests. Interface and internal friction tests under 50, 100 and 200 kPa normal stresses for soil to soil and soil to concrete were performed for comparison of interface friction angles to internal friction angles by first increasing the normal pressure to a desired value, then shearing the interface under constant normal stress. The effects of grain crushing, particle shape and roughness of interface surface were also investigated.

3.1. Materials

The Portland cement used in this study was provided from Akçansa B. Çekmece cement plant which supplies 8% of Turkey's cement requirement with its products that comply with global quality standards. Cements produced by the plant and their properties are shown in Table 3.1.

Table 3.1. Cements produced by Akçansa B. Çekmece plant and their properties

Akçansa B. Çekmece cement plant			Strength (N/mm^2)		Setting Time (h)		Blaine Specific Surface Area cm^2/g
			7 days	28 days	Initial Set	Final Set	
PC 42,5	Portland Cement	TS EN 197-1 Standard	40	51	02:28	03:08	3550
PCC 32,5	Portland Composite Cement	TS EN 197-1 Standard	23	36	02:50	03:15	4200
SRC 32,5	Sulphate Res. Cement	TS 10157 Standard	35	47	02:40	03:17	3075

Coal is one of the major sources of energy and its consumption is about 31.9% in thermal plants in Turkey. This is predicted to increase in the future in order to meet the continuous demand for electric power generation.

The utilization of fly ash in Turkey is limited mainly as a substitute of clinker in cement production. Thus, the use of lignite in the power plants has led to increasing environmental problems associated not only with gaseous emissions but also with the disposal of ash residues, because not paying the necessary attention to effectively create disposal sites and techniques to deposit wastes before and during the construction of the power plants.

Although the mineralogical properties of fly ash obtained from different power plants maybe somehow similar, the physical and chemical properties may vary depending on the operational conditions. The chemical analyses of fly ashes from various power plants in Turkey are given in Table 3.2.

Table 3.2. Chemical analysis tests results of samples obtained from various thermal plants in Turkey [39]

	Soma	**Yeniköy**	**Kangal**	**Afşin**	**Tunçbilek**
ASTM Classification	Type C	-	Type C	Type C	Type C
SiO_2 (%)	49,00	17,54	38,67	30,78	53,00
Al_2O_3 (%)	24,22	9,94	16,63	10,41	19,63
Fe_2O_3 (%)	7,78	0,37	6,41	10,81	10,74
CaO (%)	11,60	33,10	23,63	32,59	12,02
MgO (%)	0,49	2,46	3,90	4,06	2,04
SO_3 (%)	4,35	33,75	6,00	12,23	0,57
Loss on Ignition (%)	2,08	0,45	2,54	0,27	1,15

The fly ash used in this study is obtained from Soma Thermal Plant located 2 km out of Soma, Manisa. The plant is made of eight units 1034 MW energy capacity, consumes low–quality lignite reserves of Soma Basin. At the Soma thermal power plant, approximately 30,000 tons of coal is burnt and approximately 12.000 tons of fly ash is produced per day.

The physical and chemical properties of fly ash used in this study were obtained in Akçansa cement factory laboratories in Büyükçekmece, Istanbul. All the equipment was certificated by Turkish Standards Institute and was recently calibrated. The chemical analyses on cement and fly ash used in this study are given in Table 3.3.

Table 3.3. Chemical analysis tests results of cement and fly ash used in this study

	Cement	**Fly Ash**
Insoluble Residue (%)	0,47	---
SiO_2 (%)	21,08	43,42
Al_2O_3 (%)	4,77	19,66
Fe_2O_3 (%)	3,23	5,60
CaO (%)	63,61	23,66
MgO (%)	1,15	1,32
SO_3 (%)	2,49	3,60
Cl^-	0,0251	0,0007
Na_2O	0,20	0,54
K_2O	0,94	1,33
Loss on Ignition (%)	1,78	0,13

Portland cement 42.5 and type C fly ash are materials used in this study. The physical properties of cement and fly such as specific gravity, specific surface fineness (Blaine fineness) obtained from laboratory tests are given in Table 3.4. Additionally, the strength activity index of fly ash was investigated in accordance with European Standard EN 450 “Fly ash for concrete” as ratio (in percent) of the compressive strength of standard mortar bars, prepared with 75 % reference cement plus 25 % fly ash by mass, to the compressive strength of standard mortar bars prepared with reference cement alone, when tested at the same age. Compressive strengths of cement, cement fly ash mortar, mixture proportions and the activity index of fly ash are given in Table 3.5.

Table 3.4. Specific gravity and surface fineness of cement and fly ash

	Cement	**Fly Ash**
	PC 42,5	Type C
Specific Gravity (gr/cm^3)	3,18	2,35
Blaine Fineness (cm^2/gr)	3600	3490

Table 3.5. Compressive strengths of mortars and activity index of fly ash

	Standard Mortar	**Sample**	**Activity Index (%)**
Cement (gr)	450	337,5	93,54
Fly Ash (gr)	-	112,5	
Sand (gr)	1350	1350	
Water (gr)	225	210	
28 Days Compressive Strength (N/mm^2)	52,6	49,2	

The average grain size of fly ash and cement was 22.91μm, 19.95μm respectively. The grain size distribution of fly ash and cement are presented in Figure 3.1.

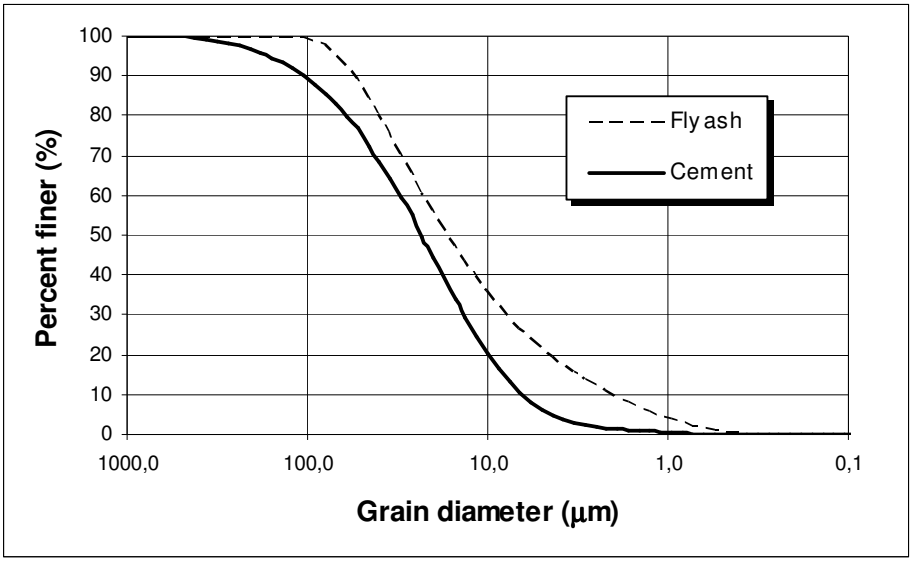

Figure 3.1. Grain size distribution of fly ash and cement

3.2. Experimental Study

3.2.1. Pelletization Process

The details of the pelletization disc are given in Figure 3.2 and Figure 3.3. The pelletization disc is a combination of five main units; a pelletizing disc with a diameter of 40 cm, a motor reduction unit, a divisor table with 1/30 degree sensitivity to adjust the normal of disc, a carrying frame and a speed controller unit which is capable of changing revolution speed of the disc between 0 and 7 with 0.15 rpm sensitivity.

Scraping blades are placed from centre to one edge of the disc with 6 cm intervals. (Figure 3.3) The properties of the blades are:

- to remove any mix that sticks to the bottom and walls of the disc,
- to create an energy barrier before either free or radial rotating balled material to compact them more and,
- to let different grain size of balled material move in different path for ease in screening the grain size distribution (coarse size material in interior path, and fine size in outer path) [39].

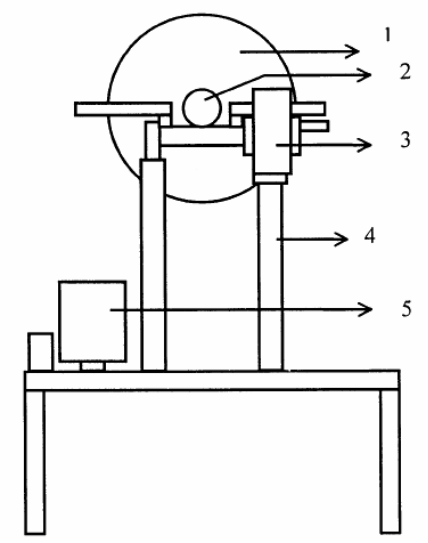

Pelletization Disc Elements

1. Pelletizing Disc
2. Motor Reduction Unit Group
3. Divisor Table
4. Carrying Frame
5. Speed Controller Unit

Figure 3.2. Sketch of pelletization disc unit (back view)

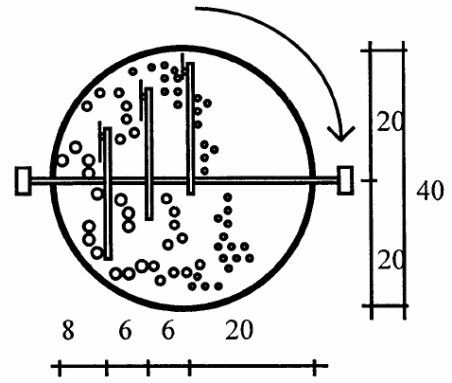

Figure 3.3. Sketch of scraping blades positioning (plan view / units in cm)

Three groups of mixtures were used during the pelletization process to investigate the behavioral changes in short and long term engineering performance of pellets. The objective of addition of cement to the mixture with different ratios is to provide enough strength to final products against crushing. The proportions and codes are given below;

FA : Fly ash only group
FAC10 : %10 cement blended fly ash group (%10 by weight of fly ash)
FAC20 : %20 cement blended fly ash group (%20 by weight of fly ash)

Trial pellet production was done by observing of pellet formation stages, the shape and apparent strength of pellets with changing the angle and the revolution speed of the pelletizing disc. During the optimization, firstly, the angle and revolution speed parameters were tried to be determined for the desired pelletization process. A simple method was used for the determination of apparent strength of fresh pellets to investigate if they have adequate strength for hauling and stockpiling conditions in which the pellets are let to fall from a 115 cm. height.

The result of optimization study was in accordance with Doven (1998). The execution of theoretical equations with defined parameters and observations on 'fresh pellet' formation and strength showed that operation angle should change between 35 and 50° and revolution speed between 35 and 55rpm [39].

For FAC10 and FAC20 groups, the blending of fly ash with mineral additives was done prior to pelletization process. After placing the materials in the disc, the disc was rotated at suitable speeds to ensure that homogeneity in mixture was provided. The water was sprayed on the material with a spray gun. The amount of water to be used in process was determined prior to the production according to the data obtained in trial productions. The amount of water of the FA, FAC10 and FAC30 groups were %24, %24.5 and %25 respectively.

The formation of pellets occurred between 6 and 9 minutes. The total pelletization time was about 20 minutes, since it was found that under the mechanical and capillary forces, the saturation point in volume compression was reached around this time. Avoiding

water film on the surface of the pellets was of extreme care during production. The pellets were kept in plastic bags in the curing room in which the temperature and relative humidity were 21°C and 70% respectively.

3.2.2. Lightweight Concrete Specimens

Synthetic lightweight aggregates which consist primarily of fly ash, fine and/or coarse aggregates and a small amount of Portland cement are being used increasingly in the construction industry. For direct shear box, 100x100x20 mm concrete samples consist of only fly ash lightweight aggregates were produced in order to obtain interface properties between granular materials and concrete.(Figure 3.4a) Additionally, 50x50x50mm cubic lightweight concrete specimens were produced and were left for curing for 7 and 28 days in the curing room to investigate the physical (unit weight) and mechanical properties (compressive strength) of concrete made with synthetic fly ash aggregates (Figure 3.4b). A general view of concrete specimens is given in Figure 3.4.

(a) (b)

Figure 3.4. (a) Block concrete sample, (b) Cubic sample made with lightweight aggregates

Only fly ash (FA) group aggregates were used in concrete specimens. The main reason using FA group aggregates was to achieve more information on economical benefits of lightweight aggregates by means of their strength, interface properties and their contribution to decrease in unit weight of concrete. The design water to cement ratio was

chosen as 0.6. The grain size distribution of pellets used in concrete was in accordance with fine aggregates in concrete division in ASTM C 33-03 “Standard specifications for concrete aggregates”. The mix proportions with respect to mass percentage of components of concrete specimens are presented in Figure 3.5.

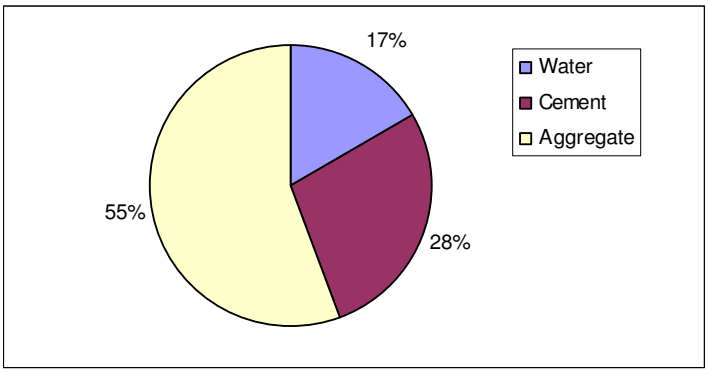

Figure 3.5. Mass percentages of components used in concrete samples

3.2.3. Cylindrical Specimens

According to the ASTM D-2166 standard, the unconfined compressive strength (*qu*) is defined as the compressive stress at which an unconfined cylindrical specimen of soil will fail in a simple compression test. In this test method, the unconfined compressive strength is taken as the maximum load attained per unit area, or the load per unit area at 15% axial strain, whichever occurs first during the performance of a test.

The primary purpose of this test is to determine the unconfined compressive strength of cylindrical specimens made with same mixture proportions of FA, FAC10 and FAC20 group pellets, which is then used to compare with crushing strength of pellets for 7 and 28 days. For all groups of specimens, optimum water contents were obtained in accordance with ASTM D-698. The optimum water contents of FA, FAC10 and FAC20 group specimens were %19.5, %20 and % 20.5 respectively.

The specimens were kept in humidity room in plastic bags for curing until the test day. Prior to test, top and bottom surfaces of the specimens were trimmed in order to have smooth surfaces. The exact diameter and length of the specimens were measured at three

locations and average measurements were recorded. The weight of specimens was recorded to obtain the unit weights of before the compression test.(Figure 3.6a) The specimens were carefully placed in the compression device and centered between bottom and top plates and loaded at a strain rate of 1 mm/min (Figure 3.6b).

(a)

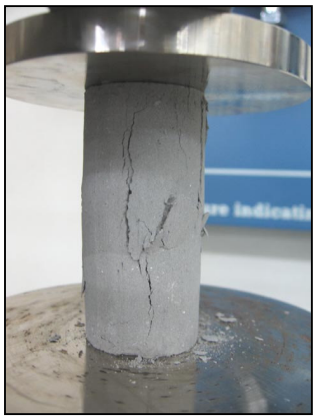

(b)

Figure 3.6. Cylindrical specimens (a) before, and (b) after unconfined compression test

3.2.4. Specific Gravity and Water Absorption

For all three groups of pellets (FA, FAC10 and FAC20), bulk specific gravity, bulk specific gravity at saturated surface, apparent specific gravity, and water absorption values were obtained with respect to ASTM C127-04.

Relative density (bulk specific gravity) is the characteristic generally used for calculation of the volume occupied by the aggregate in various mixtures containing aggregate, including portland cement concrete, bituminous concrete, and other mixtures that are proportioned or analyzed on an absolute volume basis.

Relative density (bulk specific gravity) (SSD) is used if the aggregate is wet, that is, if its absorption has been satisfied. Conversely, the relative density (bulk specific gravity) (OD) is used for computations when the aggregate is dry or assumed to be dry. Apparent density and apparent relative density (apparent specific gravity) pertain to the solid

material making up the constituent particles not including the pore space within the particles which is accessible to water.

Water absorption values are used to calculate the change in the mass of an aggregate due to water absorbed in the pore spaces within the constituent particles, compared to the dry condition, when it is deemed that the aggregate has been in contact with water long enough to satisfy most of the absorption potential. The definitions of the terms are given below;

Bulk Specific Gravity (Oven Dry, OD)	=	A / (B-C)
Bulk Specific Gravity (Saturated Surface Dry, SSD)	=	B / (B-C)
Apparent Specific Gravity (Apparent Relative Density)	=	A / (A-C)
Water Absorption (%)	=	((B-A) / A) x 100

where A is the weight of the oven-dry specimen in air, gr,

B is the weight of saturated surface dry specimen in air, gr,

C is the weight of saturated specimen in water, gr.

3.2.5. Crushing Strengths of Pellets

Single particle crushing tests have been conducted by several researchers: for example, Lee, Kwag et al. and Kato et al. Single crushing tests were performed on all three groups of pellets to obtain crushing strengths of pellets. The pellets used in crushing tests were selected randomly. The sizes of the pellets varied between 9.5-14 mm and were close to the specifications in ASTM E 389 standard (9.5-12.5 mm). Although the mean diameters of pellets used in direct shear tests were smaller than 4.75 mm, the results of crushing tests of single grains gave interpretable results in order to understand the effect of crushing on the interface and internal friction angles of granular soils.

A triaxial compression test apparatus was equipped with a 2 kN load ring in order to have adequate sensitivity. A displacement transducer with an accuracy of 0.01 mm measured the displacements. A spacer made of steel was used on the bottom plate of compression apparatus for applicability (Figure 3.7).

The compressive plates were installed in parallel planes. The surface of the plates that are in contact with the sample was made of surface-hardened steel. A single pellet of the sample was placed in approximate center of the surface-hardened portion of the spacer. The load was applied with a constant rate of 0.01 mm/sec over the entire test period.

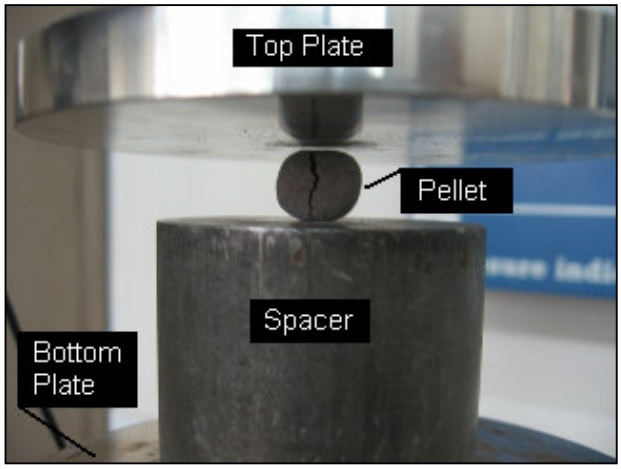

Figure 3.7. A close view of single pellet crushing setup

Assuming the shape of a particle is approximately spherical, the crushing strength of a single aggregate can be defined as follows:

$$\sigma_c = \frac{F_c}{A_m} = \frac{F_c}{\left(\frac{\pi}{4} d_m^{\,2}\right)} \tag{3.1}$$

$$d_m = \frac{d_1 + d_2 + d_3}{3} \tag{3.2}$$

where σ_c is the crushing strength of single particle, F_c is the maximum force attained in crushing test, A_m is the mean area of the particle, d_1, d_2, d_3 are the measured diameters of the particle at three locations and d_m is the mean diameter of particle.

3.2.6. Direct Shear Tests

In principle, the shear box test is an angle of friction test, in which one portion of soil is made to slide along another by the action of a steadily increasing horizontal shearing force, while a constant load is applied normal to the plane of relative movement. These conditions are achieved by placing the soil in a rigid metal box, square in plan, consisting of two halves. The lower half of the box can slide relative to the upper half when pushed (or pulled) by a motorized drive unit, while a yoke supporting a load hanger provides the normal pressure [44].

The direct shear test is simple to perform, but it has some inherent shortcomings. The reliability of the results may be questioned because the soil is not allowed to fail along the weakest plane but is forced to fail along the plane of split of the shear box. Also, the shear stress distribution over the shear surface of the specimen is not uniform.

In terms of stress, Coulomb's law of friction can be expressed as:

$$\tau_f = \sigma_n \tan(\phi) \tag{3.3}$$

The geometry of soil grains and structural arrangement of soil fabrics are complex. In soils, the particles are randomly distributed and often irregular. Shearing of a given volume of soil would cause impending slip of some particles to occur up the plane while others occur down the plane. Actually, the total frictional resistance to shear is the sum of intergranular friction, friction between the particles and interface, and dilation of the soil as shown in Equation 3.4. The dilation angle α is the instantaneous change of soil sample height over an increment of horizontal displacement. The shear strength of a cohesionless granular material can be given as:

$$\tau_f = \sigma_n \tan(\phi \pm \alpha) \tag{3.4}$$

where ϕ = internal friction angle of soil,

τ_f = frictional resistance to shear,

σn = normal stress on the soil and

α = dilation angle of soil.

Digital direct shear apparatus EL26-2112 equipped with a 100x100x42 mm direct shear box was used in this study. (Figure 3.8) The device was fully capable of providing variable speeds between 0.00001 to 9.99999 mm/min. The speed of displacement was chosen 1 mm/min which resulted in the failure occur in approximately 10 minutes.

Minimum three specimens of all groups of aggregates were tested under 50 kPa, 100 kPa and 200 kPa to investigate the relationship between normal stress and shear stress parameters of manufactured aggregates. According to ASTM D 3080, the minimum specimen width for square specimen shall be 50 mm or not less than ten times the maximum particle size diameter, the minimum initial specimen thickness shall be 12 mm, but not less than six times the maximum particle diameter, and minimum specimen width to thickness ratio shall be 2:1. Therefore, according to ASTM D 3080, 100x100 mm square box was used in the test because the maximum diameter of the aggregates is 4.75 mm, and the height of the box is 42 mm that is bigger than six times of the maximum particle size.

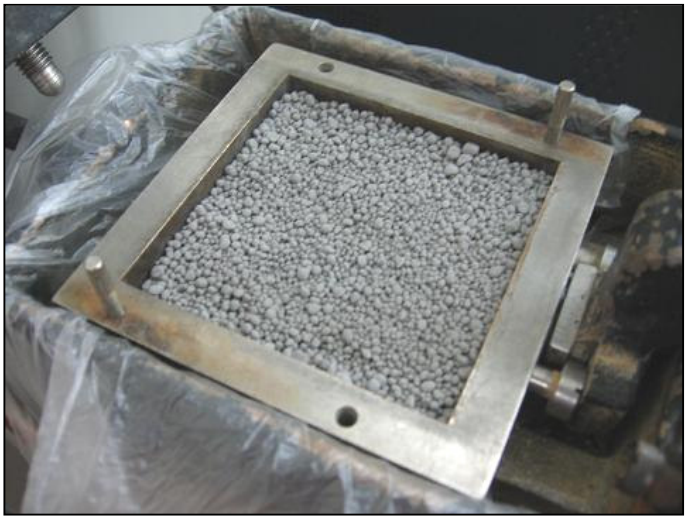

Figure 3.8. Direct shear box with dimensions of 100x100x42 mm

The data recorded for each test were the horizontal displacements, horizontal forces, vertical displacements, and the constant vertical force under which the test is conducted. For measuring vertical and horizontal displacement of the specimen, digital dial indicators with an accuracy of 0.001 mm were used.

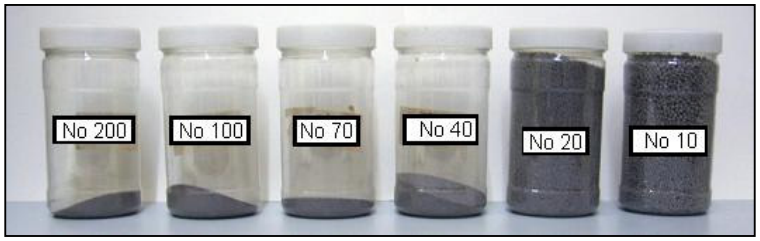

Figure 3.9. Different sizes of grains retained on sieves

A load ring with a 3 kN capacity was used for measurement of shear loads. A maximum displacement of 10 mm was chosen because of the limitations of the direct shear device.

Previous studies in the literature indicate that the grain size distribution has a considerable effect on shear strength of soils. The particle size distributions of samples have great importance in this study; therefore the crushing ratio of grains was obtained by comparing the grain size distributions before and after the tests according to ASTM D 421 – ASTM D 422. In order to avoid the effects related to the contribution of particle size distribution, all the samples were prepared in the same granulometry by separating the grains with respect to their sizes and mixing them again in same proportions for all samples used in the test (Figure 3.9). The grains were separated and kept in plastic containers before the tests. In order to avoid loosing of particles during the direct shear test, a thin nylon plastic bag was placed under the box as shown in Figure 3.8.

The tests were conducted in dense condition. The relative density of the grains used in the tests was 68%. The density was obtained by pouring the grains very slowly into the shear box from a constant height of 50 mm and tamping the granular to reach desired density level. The target normal pressure was achieved by applying vertical loads on the beam hanger that transfer loads to the load cap by 1:10 ratio.

3.2.7. Interface Tests.

The direct shear testing of interfaces is approximately similar to the direct shear testing of soils. Normal load is applied to the top of the soil sample by a loading cap, and then a horizontal load is applied to shear the interface between the soil and the construction material.

Figure 3.10 shows the relationships should exist between interface strength behavior and asperity height (h), asperity spacing, asperity angle, spatial distribution of asperity geometry (texture pattern), grain and surface hardness, initial particulate material void ratio, normal stress, grain shape, and grain roughness.

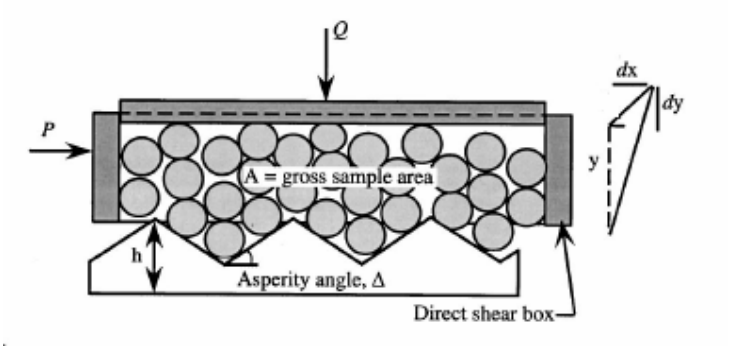

Figure 3.10. Idealized granular dilative system

The shear strength along the surface of contact of the soil and the foundation for a cohesionless granular material can be given as;

$$\tau_f = \sigma_n \tan(\delta \pm \alpha) \tag{3.5}$$

where δ = interface friction angle between soil and structure,

τ_f = frictional resistance to shear,

σ_n = normal Stress on the soil and

α = interface dilation angle (d_x/d_y)

The tests were performed as in the same manner of direct shear tests under 50, 100 and 200 kPa. Differently, the half of the direct shear boxes were replaced with concrete blocks in order to obtain interface friction angles between concrete and granular media as given in Figure 3.11. The displacement rate was 1 mm/min which resulted in the failure occur approximately in 10 minutes. Sieve analysis tests were performed before and after test to investigate the crushing of particles under shear.

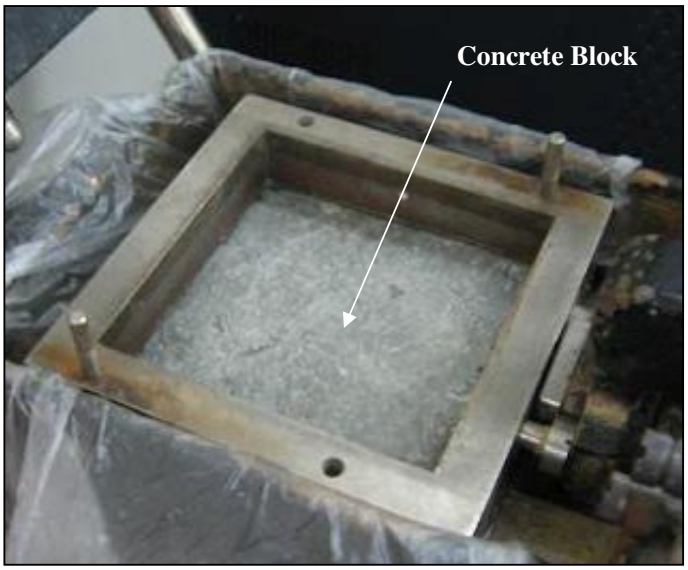

Figure 3.11. The setup of interface tests

For each test horizontal displacements, horizontal forces, vertical displacements, and the constant vertical force under which the test is conducted were recorded. The tests were conducted in dense condition with a relative density of 68% as in the same manner of direct shear tests. The grain size distributions of the samples were also same with those used in direct shear tests.

3.2.8. Surface Topography

The importance of surface topography, and the degree of surface roughness in interface behavior and soil-structure interaction response, has been noted by many investigators. In this study, the effect of surface roughness on the maximum interface stress was investigated by conducting interface tests between concrete blocks with various

surface roughness parameters and granular soils manufactured by pelletization process.

The interface tests were performed with FAC20 group pellets which consist of 20% cement and 80% fly ash in order to refrain from the effect of grain crushing under normal stress. Since the grain size distribution has considerable effect on interface stresses, only pellets that retained between No4 (4.75 mm) and No10 (2.00 mm) were used in interface tests. The average diameter of pellets was assumed as 3.00 mm and the normal stress was chosen as 50 kPa.

Four types of concrete blocks were selected according to their surface roughness and named as C1, C2, C3 and C4 blocks. After a curing period of 28 days, concrete blocks were left for drying in order to have dry surfaces. The dimensions of the concrete blocks were 100x100x20 mm, which were same with the ones used in the prior interface tests.

The C1 and C2 concrete blocks were the ones with a smoother surface relative to the others. The concrete block with an average surface roughness was C3, and C4 was the one which has the roughest surface. Each block was marked on the bottom surface in order to be distinguished from each other.

The surface roughness of each concrete block investigated was measured and digitized with a commercially available compact size 3D scanning and milling device Roland Modela MDX-20. A picture of the scanner used in this study is shown in Figure 3.12.

Figure 3.12. A picture of Roland Modela MDX-20 3D scanning and milling device

The MDX-20 3D scanner is connected to the computer with an RS-232C cable. The scanner is capable of scanning objects at four to 15 mm per second with a resolution of up to 0.05 mm by contacting, mesh-point height-sensing. The scanning pitch was selected as 0.5 mm in order to have high resolution data which results in more accurate information about concrete surfaces.

The 3D scanning software Dr. Picza was used in scanning process. The scanning area was selected and each concrete block (C1, C2, C3 and C4) placed on the table of the scanner and were scanned one by one. The scanning process took approximately five hours for each block.

Elevations on the surfaces were recorded in three dimensions which provided more accurate results differently from other approaches where roughness characteristics are calculated from a set of intersecting or parallel 2D line segments. The obtained data were recorded as point cloud format which are the combination of coordinates (x, y and z) in three dimensional space.

An algorithm was developed to measure the normalized surface roughness parameter R_{n3d} of each concrete block in three dimensions. The main function (R_n) was identical with the one reported by Kishida and Uesugi, 1987 [11]. R_n can be defined by measuring R_{max} (vertical distance between the highest peak and the lowest trough) along a profile length L equal to the mean grain size D_{50} and then normalizing it by D_{50} as mentioned before. The average of normalized surface roughness parameter R_n along a profile in 2 dimensions can be given as;

$$\overline{R_n} = \frac{\sum_1^n \frac{R_{\max n}}{L}}{n} \tag{3.6}$$

where $\overline{R_n}$ = average of normalized surface roughness along a line,

$R_{\max n}$ = vertical distance between the highest peak and the lowest trough,

n = number of sections along the profile

L = mean grain size D_{50}

Actually, the above equation represents a two dimensional approach where the other dimension is neglected. Since the data recorded in scanning process were in three dimensions, there was a need of a three dimensional approach which can take into account the other direction. The addition of y dimension to the equation above, turns the profile into a three dimensional surface which is a more representative. The illustration of the three dimensional approach and the three dimensional surface roughness parameter R_{n3d} are given in Figure 3.13 and Equation 3.7.

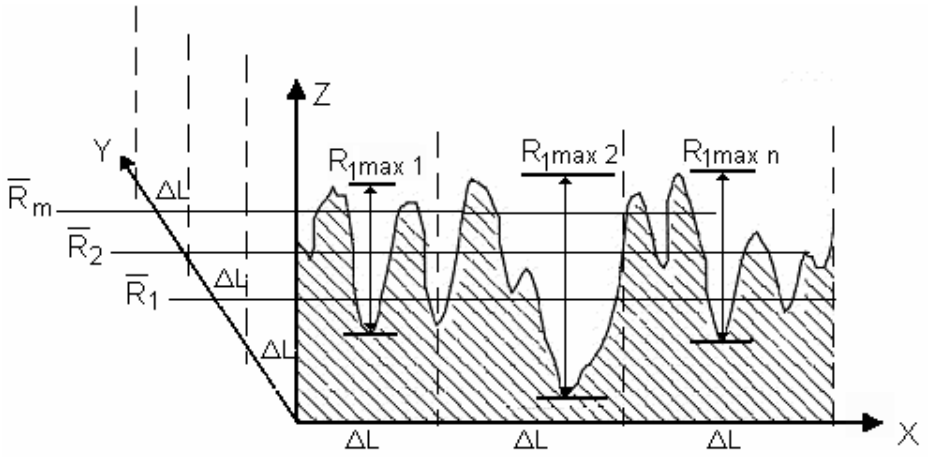

Figure 3.13. Illustration of three dimensional surface roughness

$$\overline{R}_{n3d} = \frac{\sum_{n=1}^{m} \overline{R}_n}{m} \tag{3.7}$$

$\overline{R}_{n3d}$ = average of normalized surface roughness along the surface,

$\overline{R_n}$ = average of normalized surface along n line,

m = number of sections along the y axis

A user friendly stand alone application was developed in order to evaluate the surface characteristics of individual concrete blocks in three dimensions. The software is capable of previewing the surface roughness and magnifying z axis on the screen which allows being aware of surface texture prior to calculation of $\overline{R}_{n3d}$. The supported format of the software is point cloud format which is very common in industry.

The three dimensional normalized surface roughness parameters ($\overline{R}_{n3d}$) of C1, C2, C3 and C4 were computed by the algorithm. Interface tests were performed and the results were compared in order to establish a relationship between $\overline{R}_{n3d}$ and the maximum interface stresses between pellets and concrete blocks. Sieve analyses tests were also conducted before and after tests to understand if grain crushing occurred. Screen shot of the developed software is given in Figure 3.14.

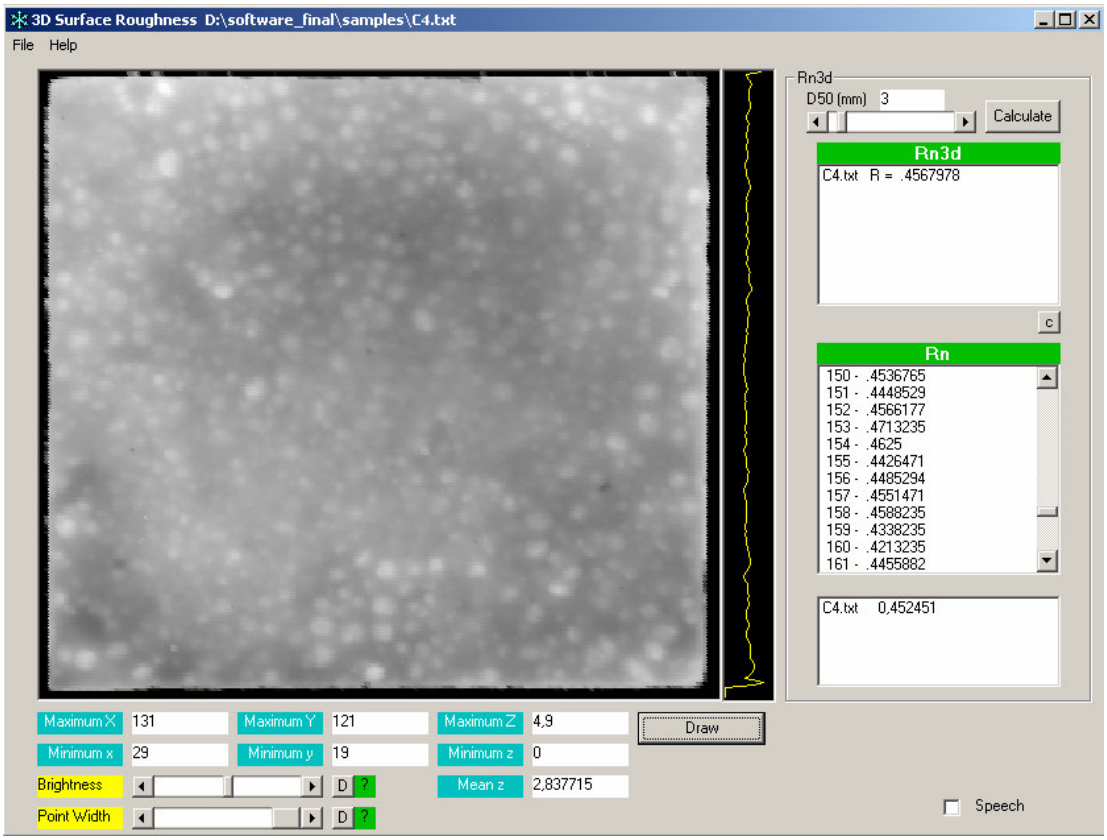

Figure 3.14. Screen shot of the developed software

4. RESULTS and DISCUSSION

4.1. Crushing Strengths of Pellets

Crushing strength tests were performed on 7, 14 and 28 days cured pellets by applying load on individual aggregates. For each group of pellets (FA, FAC10, FAC20), 15 aggregates were selected randomly in order to have representative results. The load ring used in the test was capable of measuring up to 2 kN and sensitive enough for the loading conditions. The load was applied with a constant rate of 0.01 mm/sec over the entire test period. Each group of pellets was kept in plastic bags until the test day in humidity room at 21°C with a relative humidity of 70%. The results of crushing tests for each group of pellets for 7, 14, 28 days for are given in Table 4.1.

Table 4.1. Crushing strength tests results of FA, FAC10 and FAC20 groups pellets

	Day	**$F_{average}$ (N)**	**$d_{average}$ (cm)**	**$\sigma_{average}$ (N/cm^2)**
FA	7	15.18	1.27	11.83
	14	65.55	1.29	49.88
	28	246.10	1.24	201.62
FAC10	7	63.11	1.23	52.81
	14	150.51	1.22	126.72
	28	320.53	1.21	278.15
FAC20	7	123.37	1.21	107.40
	14	269.19	1.16	254.20
	28	393.85	1.21	341.29

The results clearly show that, after 7 days, FA group pellets were the weakest and have a crushing strength of 11.83 N/cm^2. The addition of cement to the mixture resulted in an increase in the crushing strength of FAC10 and FAC20 groups of pellets.

The crushing performances FA, FAC10 and FAC20 groups of pellets are given in Figure 4.1a, b, c respectively.

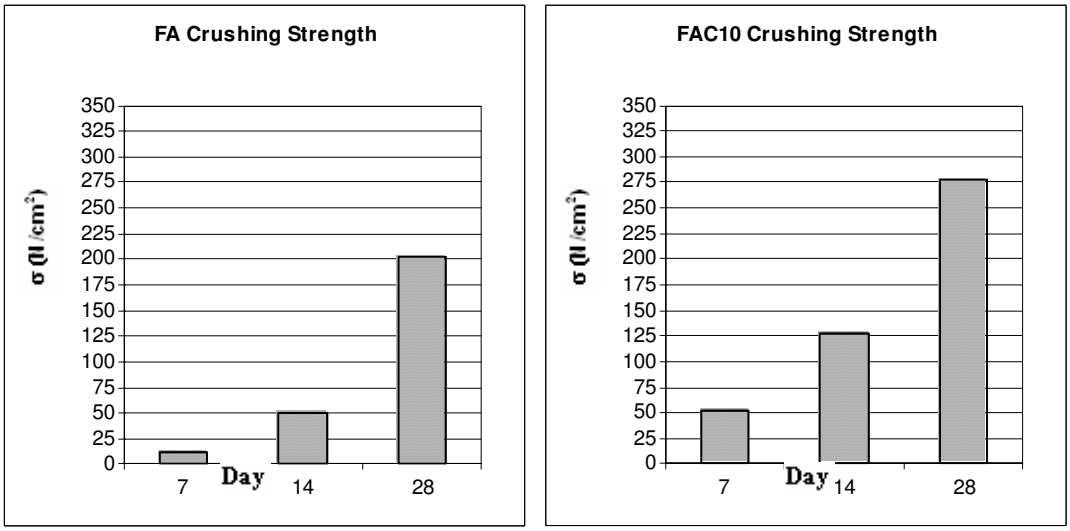

(a) (b)

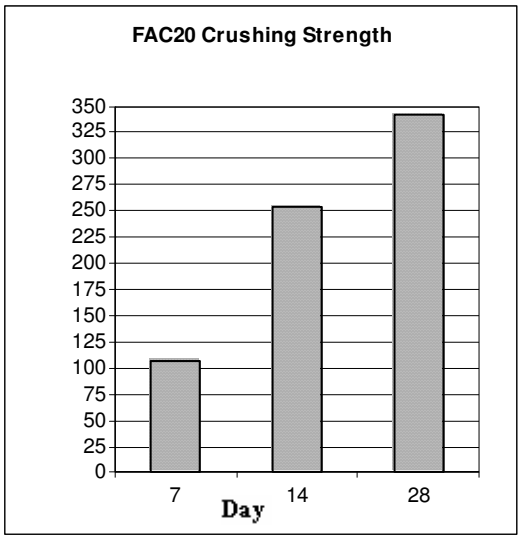

(c)

Figure 4.1. The crushing performances of pellets a) FA group b) FAC10 group c) FAC20 group

The crushing strengths of FAC10 and FAC20 group pellets for 7 days were 52.81 and 107.40 N/cm^2. For 14 days, the crushing strengths of FA, FAC10 and FAC20 group pellets were 49.88, 126.72 and 254.20 N/cm^2 respectively. The crushing strengths of pellets continued to increase for all groups, FA and FAC10 group pellets reached to 201.62 and 278.15 N/cm^2 after 28 days from production (pelletization). FAC20 group pellets attained

341.29 N/cm^2 crushing strength after 28 days which was the maximum crushing strength obtained for all of the groups.

For both 7, 14 and 28 days FAC20 group pellets were the strongest while FA group pellets, which only consist of fly ash, were the weakest. The performance of FAC10 group pellets was average as expected. The overall performance of pellets is represented in Figure 4.2. The addition of cement obviously increased the crushing strength of pellets in the short term (28 days), but from Figure 4.2, it can be concluded that, as the proportion of cement increases in the mixture, the slope of crushing strength lines flatten. The crushing strengths of individual pellets can be found in appendix A.

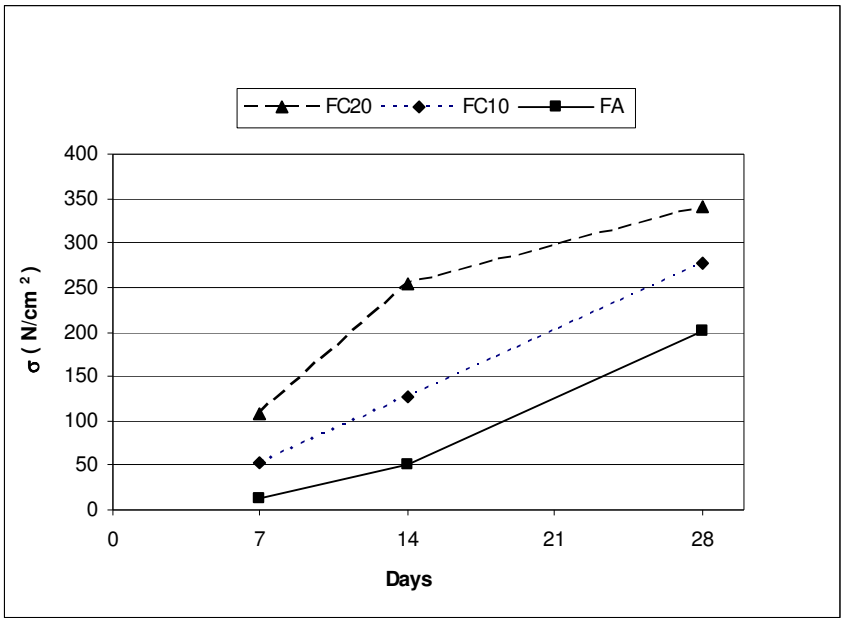

Figure 4.2. The overall performance of FA, FAC10 and FAC20 groups pellets

4.2. Unconfined Compressive Strengths of Cylindrical Specimens

Unconfined compression tests on cylindrical specimens were conducted on 7th and 28th days for each group of mixtures (FA, FAC10 and FAC20). The load ring used in the test for 7 days was capable of measuring up to 4.5 kN and for 28 days, the compression device was equipped with a different load ring which has a maximum capacity of 28 kN.

The load was applied with a constant rate of 0.5 mm/min over the entire test period. Each group of specimen kept in plastic bags until the test day in humidity room.

The physical properties and unconfined compression strengths (q_u) of the specimens are given in Table 4.2. The stress-strain relationships of each group of pellets for 7 and 28 days are given in Figure 4.3, Figure 4.4 and Figure 4.5 respectively.

Table 4.2. Physical properties and maximum unconfined compression strengths of cylindrical samples

	Day	**Weight (N)**	**Height (cm)**	**Diameter (cm)**	**γ (kN/m^3)**	**q_u (kPa)**
FA	7	0,934	7,42	3,51	13,00	395,70
	28	0,948	7,52	3,51	13,03	2375,87
FAC10	7	0,976	7,53	3,46	13,78	1396,50
	28	0,968	7,50	3,46	13,73	4398,85
FAC20	7	1,065	7,38	3,43	15,62	7188,70
	28	1,063	7,37	3,43	15,60	10661,78

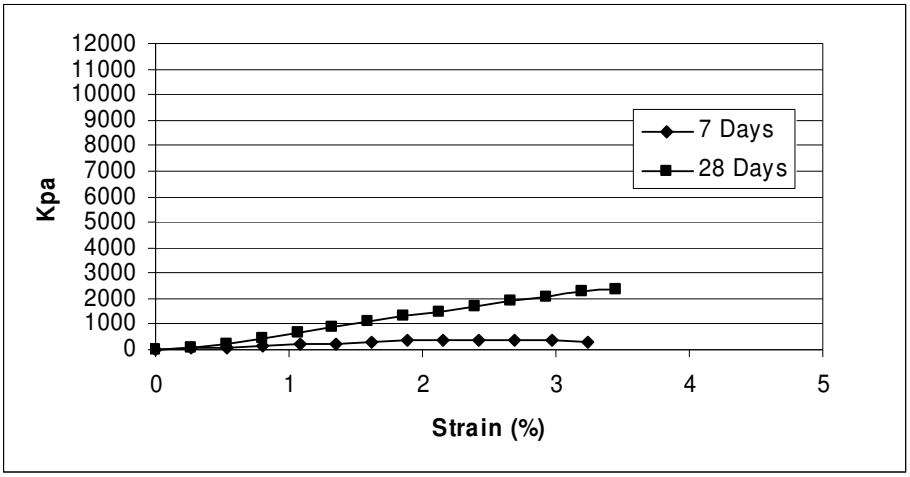

Figure 4.3. Stress-strain relationship of FA group cylindrical specimens

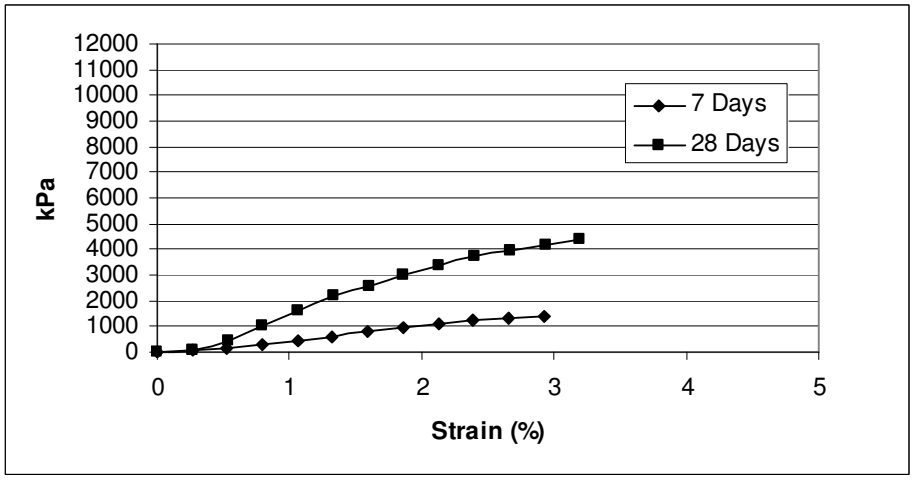

Figure 4.4. Stress-strain relationship of FAC10 group cylindrical specimens

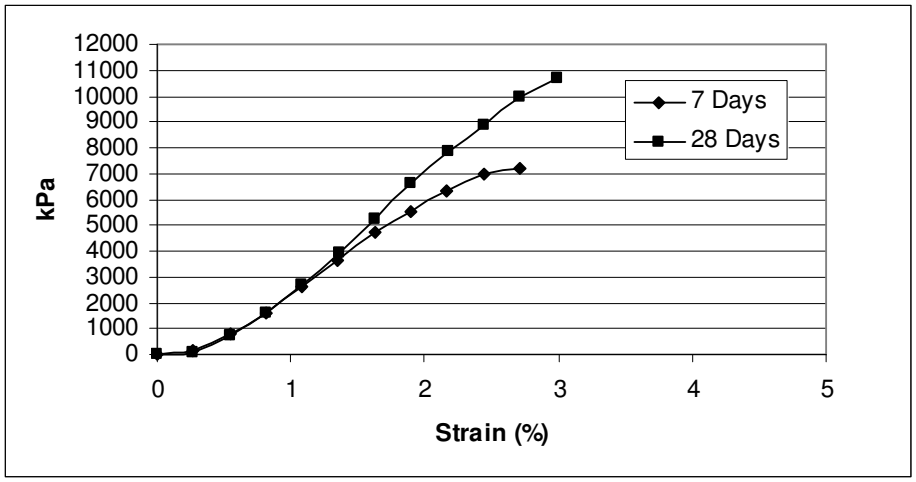

Figure 4.5. Stress-strain relationship of FAC20 group cylindrical specimens

The results indicate that FAC20 group cylindrical specimens were the strongest for both 7, and 28 days in the same manner as crushing strengths of pellets. The addition of cement highly increased the unconfined compressive strengths of specimens but resulted in a more brittle behavior.

The FA group specimens reached to 3.46% strain at the end of 28 days unconfined crushing strength test which was the maximum strain level obtained in all groups. The

maximum compressive strength obtained in unconfined compression tests was 10662 kPa for FAC20 group specimens on 28th day and this was approximately three times greater than the one obtained for FAC20 group pellets crushing test.

The minimum unconfined compressive strength was 396 kPa for FA group specimens and this is about 3 times greater than the one obtained for crushing strength tests of pellets in the same manner as FAC20 group. Figure 4.6 represents the increase of unconfined compressive strengths of FA, FAC10 and FAC20 group cylindrical specimens with respect to curing period of specimens.

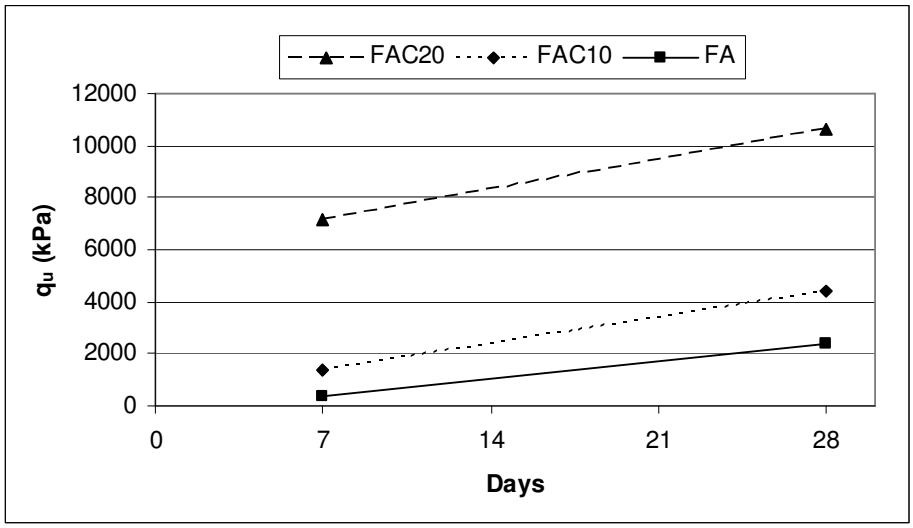

Figure 4.6. Maximum unconfined compression strengths of FA, FAC10 and FAC20 group cylindrical specimens for 7 and 28 days

4.3. Specific Gravity and Water Absorption

Oven dried bulk specific gravity (OD), saturated surface dry bulk specific gravity (SSD), apparent relative density (ARD) and water absorption (WA) values of FA, FAC10, FAC20 groups of pellets are given in Table 4.3.

The results indicate that the addition of cement to the mixture increased both oven dried and saturated surface dry bulk specific gravities while resulting in a decrease in the capacity of water absorption.

Table 4.3. Specific gravity and water absorption values of FA, FAC10 and FAC20 group pellets

	A (gr)	B (gr)	C (gr)	OD	SSD	ARD	WA (%)
FA	106,5	144,6	55,1	1,19	1,67	2,07	35,74
FAC10	126,5	164,1	68,4	1,32	1,71	2,18	29,78
FAC20	119,5	145,5	68,3	1,55	1,88	2,33	21,81

4.4. Shear Strengths of Pellets

Both horizontal displacement versus interface stress and horizontal to vertical displacement data were recorded for FA, FAC10 and FAC20 groups of pellets by conducting direct shear tests on pellets under 50, 100 and 200 kPa normal stresses. The results of the tests for FA, FAC10 and FAC20 groups of pellets are given in Figure 4.7 to Figure 4.15 respectively.

Additionally, sieve analysis tests were performed both before and after direct shear tests in order to obtain grain size distributions and the effect of crushing on the internal frictions of pellets. The grain size distribution has considerable effect on the shear strength of granular materials, so the grain size distributions of all groups were identical as mentioned before.

For FA group pellets, under 100 kPa normal stress, the maximum shear stress obtained was 78.23 kPa and under 50 kPa normal stress, the shear stress reached to 42.94 kPa. The FA group pellets attained a maximum shear stress of 131.13 kPa under 200 kPa normal stress where the strain level was approximately 6%. The horizontal displacement-shear stress curves of FA group pellets are given in Figure 4.7.

The vertical-horizontal displacement curves indicate that under 50 and 100 kPa normal stresses FA group pellets initially showed a contractive behavior then dilation occurred. The dilation angle was about zero after a 10% strain which means that FA group pellets reached to the critical state both under 50, 100 and 200 kPa normal stresses. The behavior of FA group pellets was a total contraction under 200 kPa normal stress. The

vertical-horizontal displacement curves of FA group pellets under various normal stresses are given in Figure 4.8.

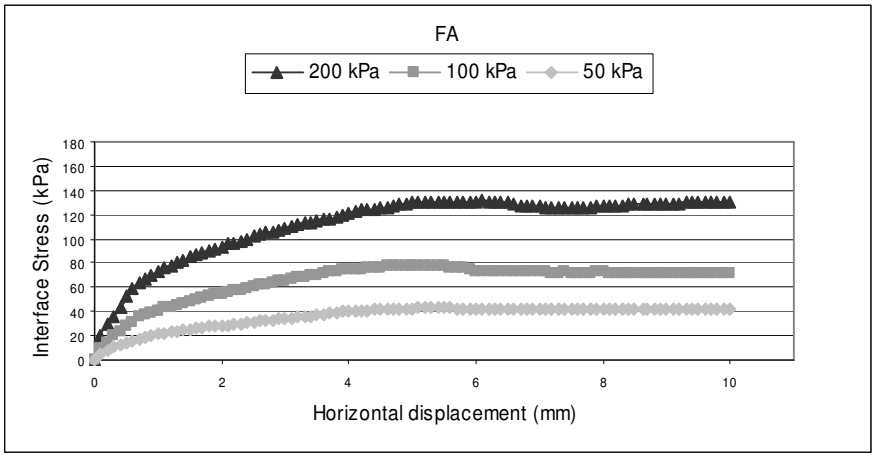

Figure 4.7. The shear stress-horizontal displacement curves of FA group pellets under 50,100 and 200 kPa normal stresses

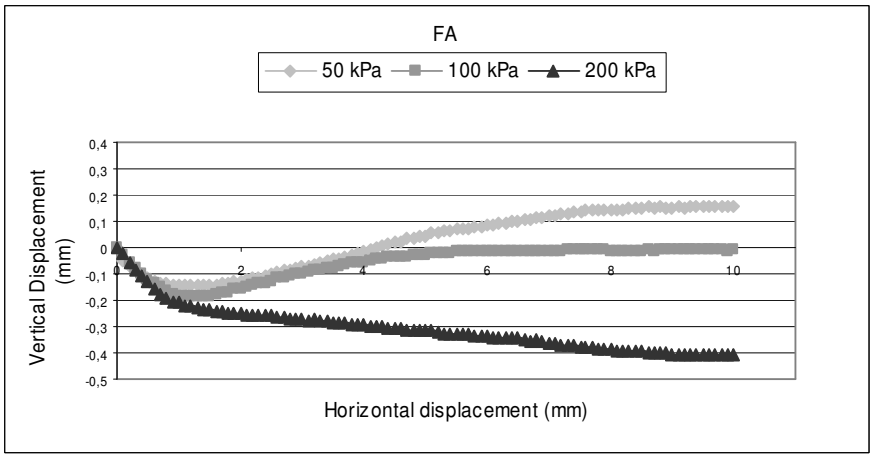

Figure 4.8. The vertical-horizontal displacement curves of FA group pellets under 50,100 and 200 kPa normal stresses

Figure 4.9 shows the relationship between shear stress and normal stress for FA group pellets. The internal friction angle of FA group pellets at peak shear stress was found as 30.09° which was the lowest internal friction angle in direct shear tests conducted for FA, FAC10 and FAC20 groups.

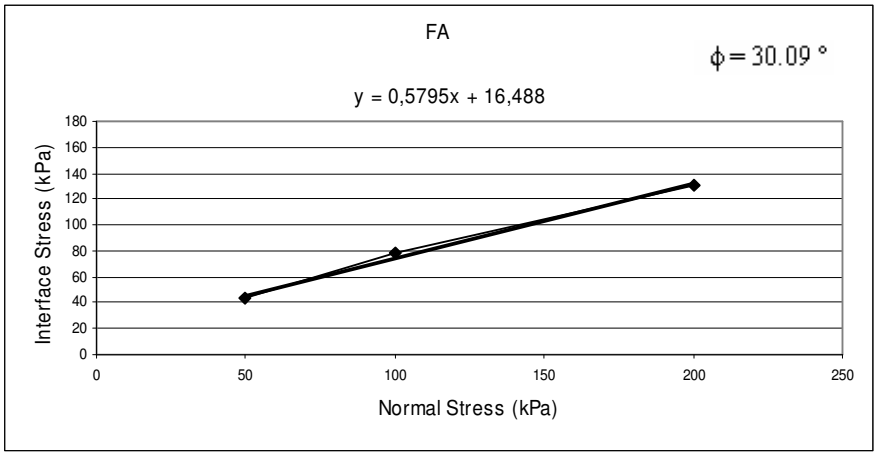

Figure 4.9. The internal friction angle of FA group pellets (ϕ_{FA})

The maximum shear stress obtained under 50 kPa normal stress for FAC10 group pellets was 39,08 kPa. This was followed by 79.98 kPa under 100 kPa normal stress. The FAC10 group pellets attained a maximum shear stress of 151.02 kPa under 200 kPa normal stress at a strain rate of 4.5% which is lower than the one for FA group pellets. The horizontal displacement-shear stress curves of FAC10 group pellets are given in Figure 4.10.

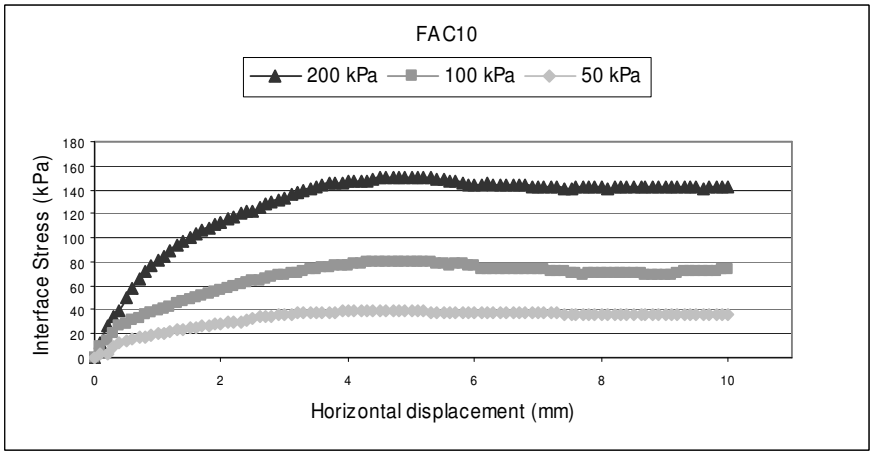

Figure 4.10. The shear stress-horizontal displacement curves of FAC10 group pellets under 50,100 and 200 kPa normal stresses

Figure 4.11 indicates that under 50, 100 and 200 kPa normal stresses, FAC10 group pellets initially had a contraction then dilation occurred. The FAC10 group pellets reached to critical state under 100 and 200 kPa normal stress values. Conversely, the dilation angle was not zero under 50 kPa normal stress; the expansion was still increasing even at the end of the test, consequently the pellets couldn't reach to critical state.

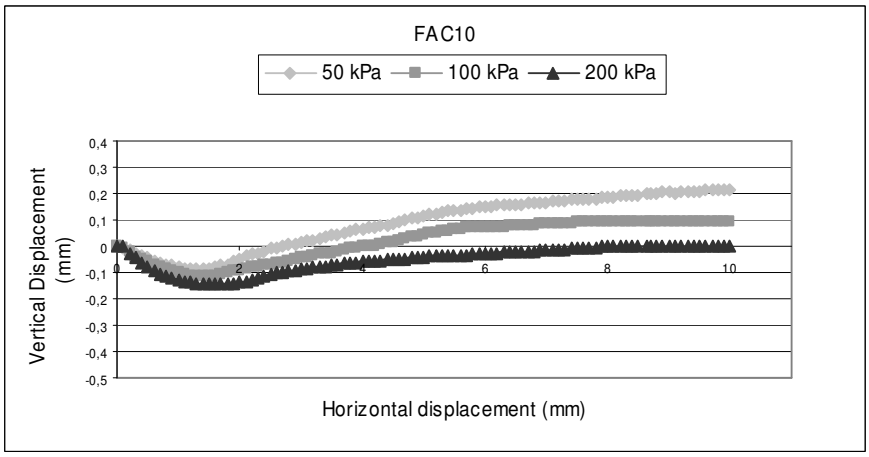

Figure 4.11. The vertical-horizontal displacement curves of FAC10 group pellets under 50,100 and 200 kPa normal stresses

The FAC10 group pellets exhibited considerable performance. The angle of internal friction angle of FAC10 group pellets (ϕ_{FAC10}) at peak shear stress was 36.55° which is very close to the one obtained for FAC20 group pellets. Figure 4.12 represents the relationship between shear stress and normal stress of FAC10 group pellets.

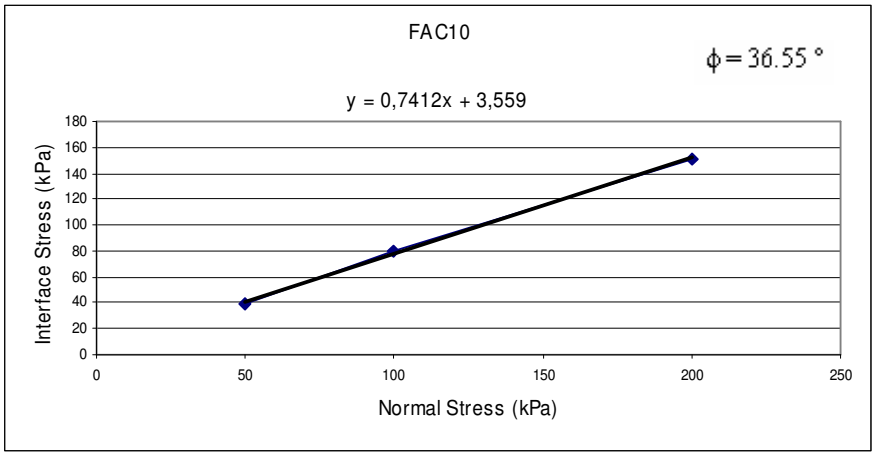

Figure 4.12. The internal friction angle of FAC10 group pellets (ϕ_{FAC10})

The FAC20 group pellets were the strongest among all groups and attained a maximum shear stress of 155.83 kPa under 200 kPa normal stress. Under 50 kPa normal stress, the maximum shear stress was 37.86 kPa which is the lowest value obtained in all groups. The FAC20 group pellets had a higher shear stress under 100 kPa with respect to other groups. The horizontal displacement-shear stress curves of FAC20 group pellets are represented in Figure 4.13.

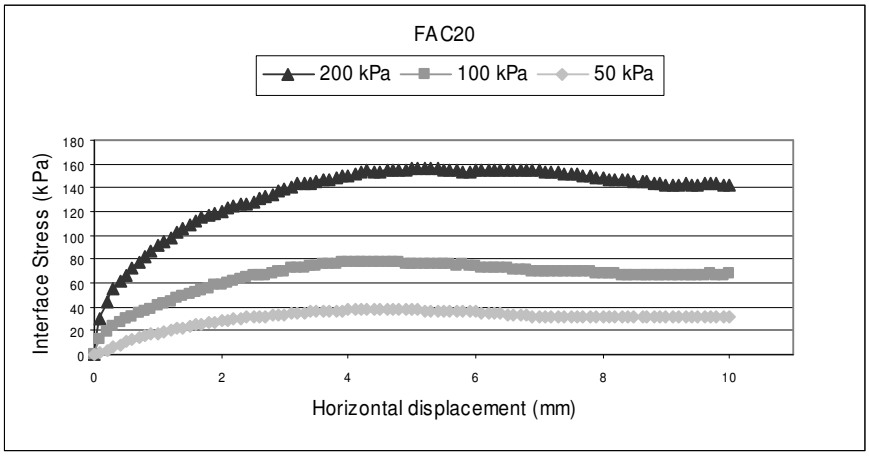

Figure 4.13. The shear stress-horizontal displacement curves of FAC20 group pellets under 50,100 and 200 kPa normal stresses

The FAC20 group pellets showed similar volume chance behavior under 50, 100 and 200 kPa but differently from other groups, the maximum contraction was lower and the expansion was higher as expected.

The FAC20 group pellets reached to critical state only under 200 kPa normal stress because of their relatively high resistance to crushing. The vertical-horizontal displacement curves of FAC20 group pellets under 50,100 and 100 kPa normal stresses are given in Figure 4.14.

Figure 4.15 shows the relationship between shear stress and normal stress for FAC20 group pellets. The internal friction angle of FAC20 group pellets (ϕ_{FAC20}) at peak shear stress was found as 37.98° which is higher than the ones obtained for FA and FAC10 groups.

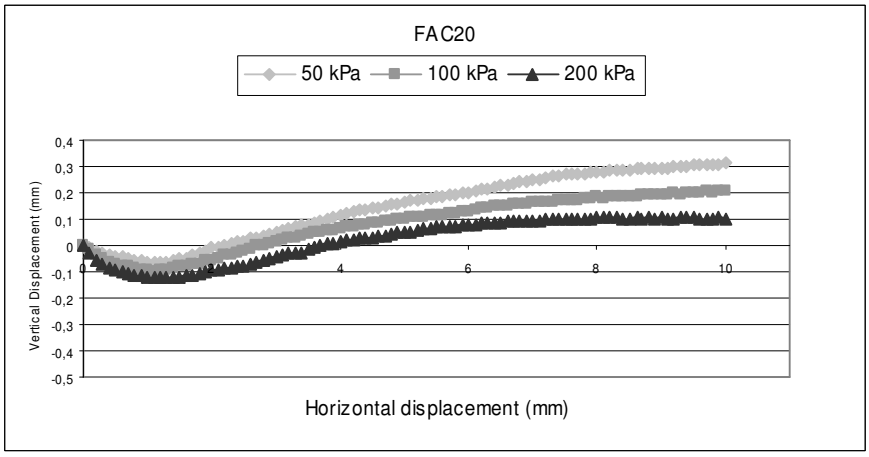

Figure 4.14. The vertical-horizontal displacement curves of FAC20 group pellets under 50,100 and 200 kPa normal stresses

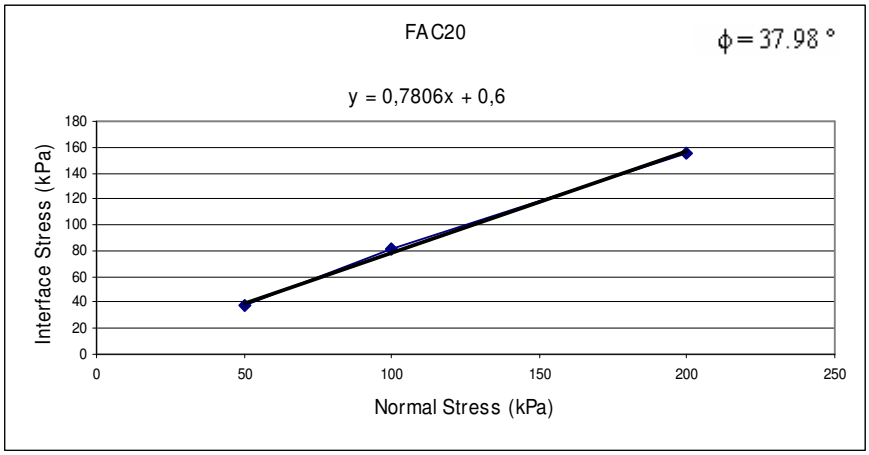

Figure 4.15. The internal friction angle of FAC20 group pellets (ϕ_{FAC20}).

With the increase of normal stress the dilation of pellets were suppressed and the dominant mechanism turned into particle crushing which mostly affected the FA group pellets because of their vulnerable structure to crushing. The volume change behavior of the pellets was first contraction and then dilation under 50 and 100 kPa normal stresses. Consequently a total contractive behavior appeared in the tests performed on FA group pellets under 200 kPa normal stress.

The grain size distributions of FA group pellets under various normal stresses for both before and after direct shear tests are given in Figure 4.16.

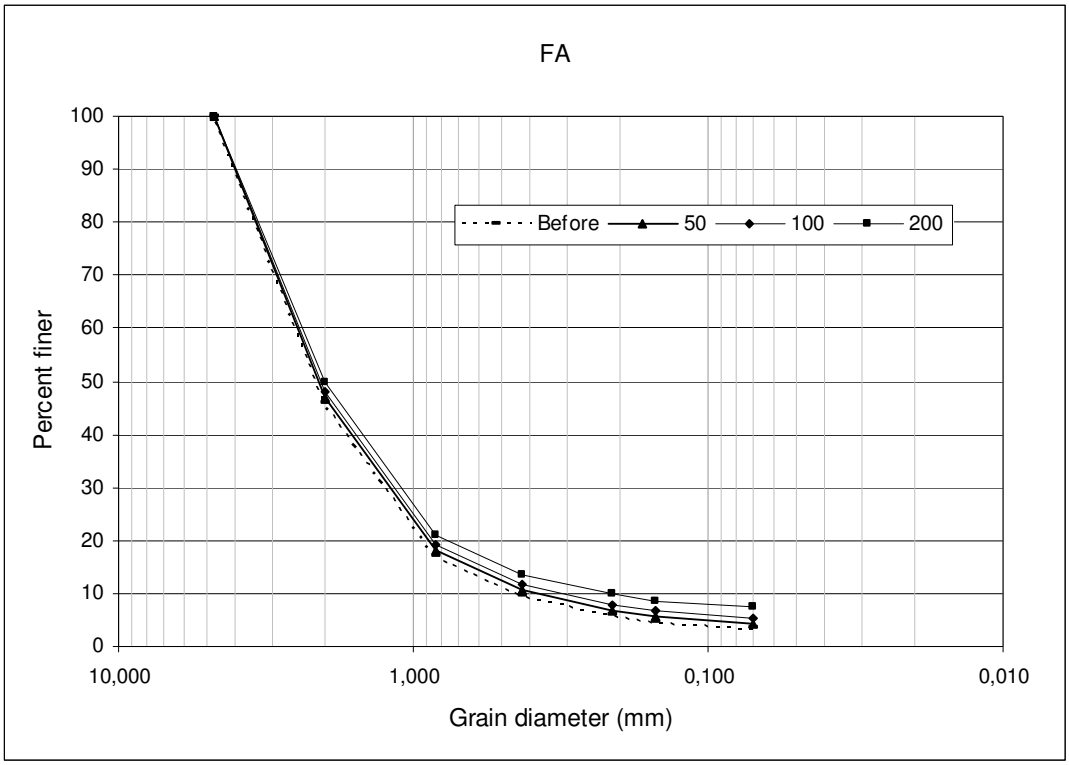

Figure 4.16. The sieve analysis test results of FA group pellets before and after direct shear tests, under 50 kPa, 100 kPa and 200 kPa normal stresses

The FAC10 and FAC20 group pellets were relatively more resistant to crushing in comparison with FA group pellets. The FAC10 group pellets have been slightly affected by grain crushing under 50 kPa normal stress. The effect of crushing was noticeable under 100 and 200 kPa normal stresses. The grain size distributions of FAC10 group pellets before and after direct shear tests are given in Figure 4.17a.

The FAC20 group pellets grain size distribution remained the same even under 200 kPa normal stress because of the high amount of cement in their structure. Hence, there was no crushing observed in FAC20 group pellets after the tests. The grain size distributions of FAC20 group pellets before and after tests direct shear tests under various normal stresses are given in Figure 4.17b.

The results of individual sieve analysis tests for all groups of pellets before and after direct shear tests can be found in appendix B.

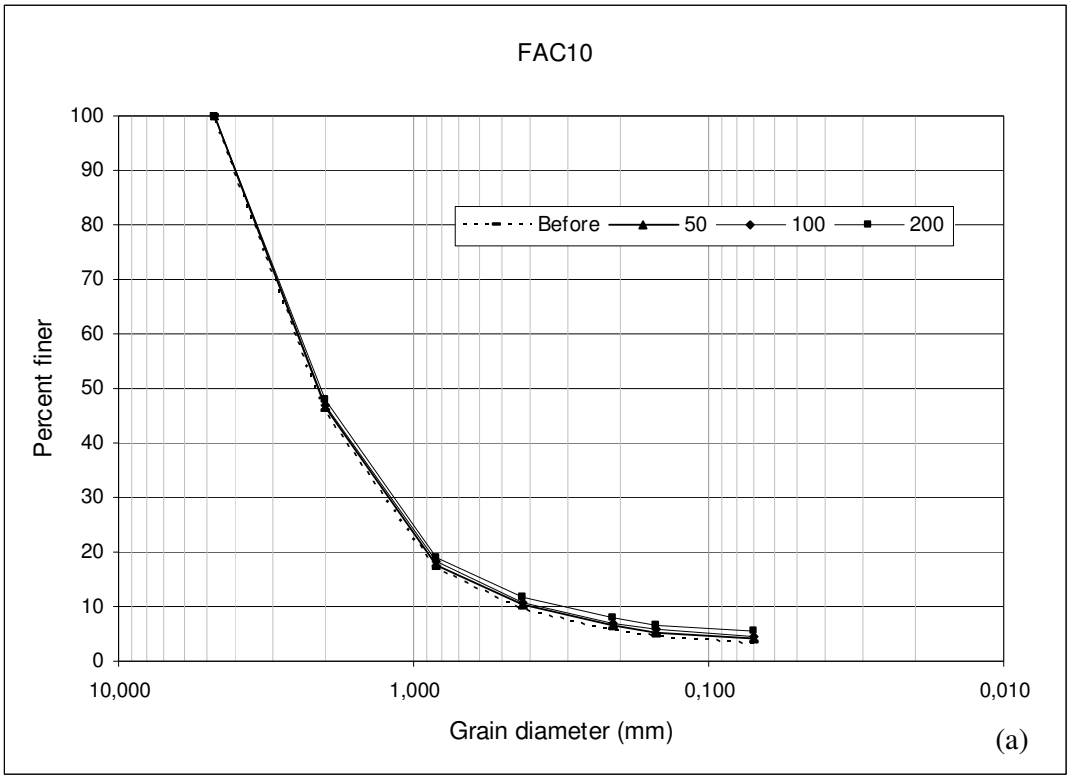

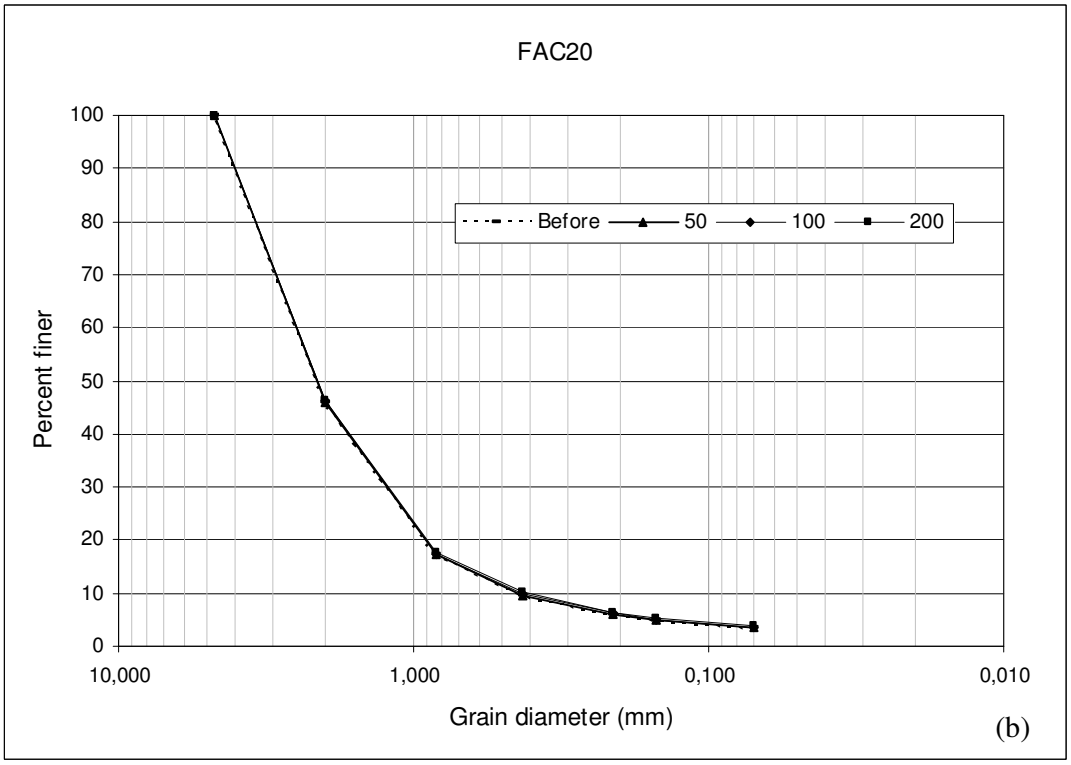

Figure 4.17. The sieve analysis test results of a) FAC10, b) FAC20 group pellets before and after direct shear tests under 50 kPa, 100 kPa and 200 kPa normal stresses

4.5. Interface Frictions Between Pellets and Concrete Blocks

Pellets to concrete interface tests performed under 50,100 and 200 kPa normal stresses with concrete blocks which consist of only lightweight aggregates. The tests were conducted in the same manner as direct shear tests but differently placing the concrete blocks in the bottom half of the direct shear box.

Sieve analysis tests were performed both before and after direct shear tests in order to obtain grain size distribution and the effect of crushing on the interface friction angles of pellets.

The FA group pellets attained a maximum interface stress of 109.1 kPa under 200 kPa normal stress where the strain level was approximately 8%. The maximum interface stress under 50 kPa normal stress was 30.5 kPa which is the highest interface stress obtained in interface tests under 50 kPa normal stress. Under 100 kPa normal stress, the interface stress was 58.3 kPa. The horizontal displacement-interface stress curves of FA group pellets under 50, 100 and 200 kPa normal stress are given in Figure 4.18.

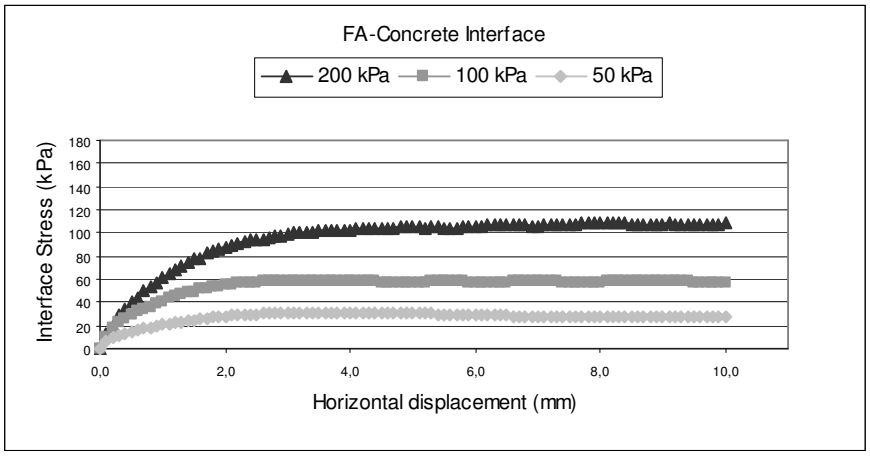

Figure 4.18. The interface stress-horizontal displacement curves of FA group pellets under 50,100 and 200 kPa normal stresses

Since the direct shear device has limitations, the tests were conducted only up to a strain rate of 10% in the same manner as direct shear tests. The vertical-horizontal

displacement curves indicate that under 50 kPa normal stress, FA group pellets couldn't reach to critical state because the dilation angle (α) was not zero even at the end of the test. With the increase of normal stress, FA group pellets reached to critical state under 100 and 200 kPa normal stresses. The pellets initially exhibited a contractive behavior following by dilation under 50 and 100 kPa normal stresses. Under 200 kPa normal stress FA group pellets couldn't dilate because of the high normal stress. The vertical-horizontal displacement curves of FA group pellets are given in Figure 4.19.

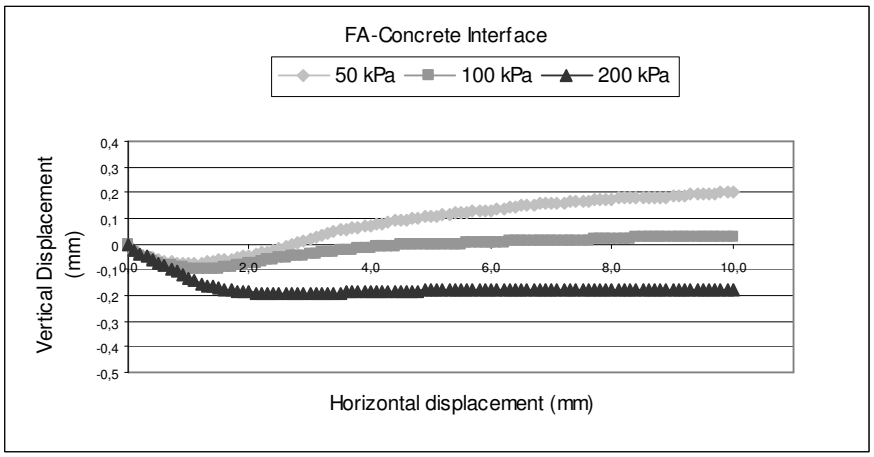

Figure 4.19. The vertical-horizontal displacement curves of FA group pellets under 50,100 and 200 kPa normal stresses

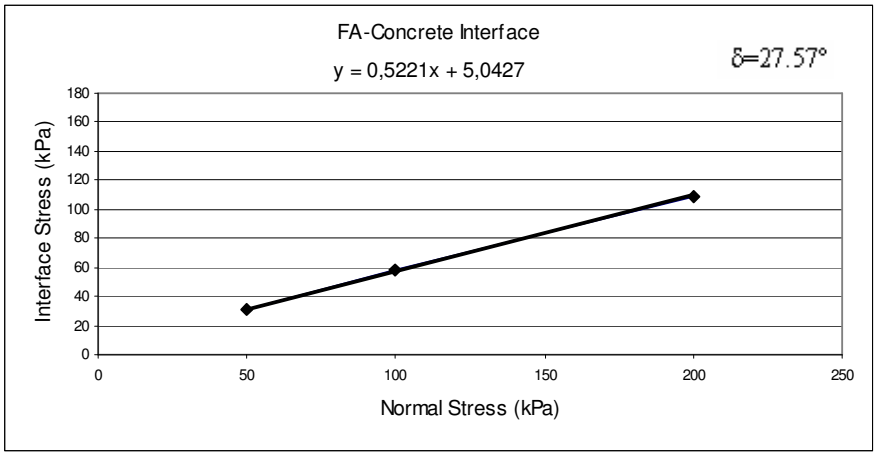

Figure 4.20. The interface friction angle of FA group pellets (δ_{FA})

Figure 4.20 represents the relationship between interface stress and normal stress for FA group pellets. The interface friction angle of FA group pellets between concrete blocks (δ_{FA}) at peak interface stress was found as 27.57° which was the lowest interface friction angle obtained in interface tests.

The results of interface tests obtained from FAC10 group pellets were close to the ones obtained from FAC20 group pellets. FAC10 group pellets were designed to be the average group between FA and FAC20 but somehow exhibited a great performance even under 200 kPa normal stress. The horizontal displacement-interface stress curves of FAC10 group pellets under 50, 100 and 200 kPa normal stress are given in Figure 4.21.

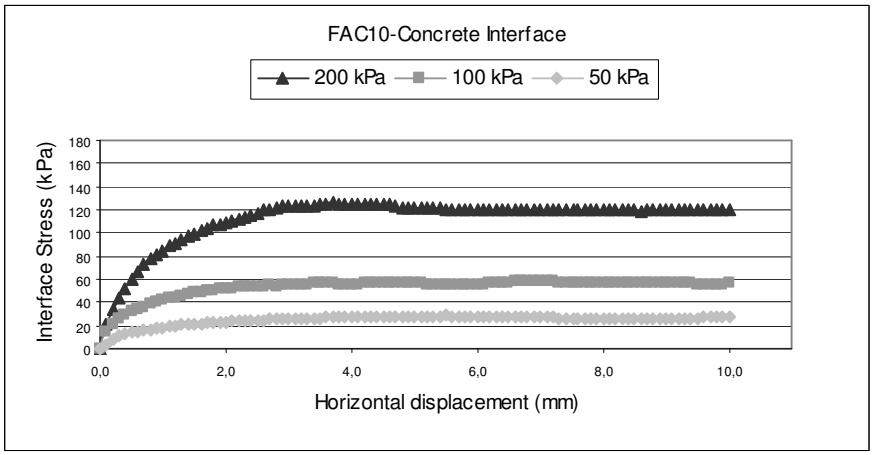

Figure 4.21. The interface stress-horizontal displacement curves of FAC10 group pellets under 50,100 and 200 kPa normal stresses

The FAC10 group pellets attained a maximum interface stress of 125.9 kPa under 200 kPa normal stress where the strain level was approximately 4.5%. The maximum interface stress under 50 kPa normal stress was 28.42 kPa, and under 100 kPa normal stress, the interface stress was 58.67 kPa which is almost similar with the one obtained for FA group pellets to concrete interface.

The FAC10 group pellets couldn't reach to critical state under 50 and 100 kPa normal stresses because the dilation angle (α) was not zero at a strain rate of 10%. The contraction of samples increased as the normal stress increased and resulted in a decrease

in dilation under 100 and 200 kPa normal stresses. The FAC10 group pellets reached to critical state only under 200 kPa normal stress at a strain rate of 8%. The vertical-horizontal displacement curves of FAC10 group pellets are given in Figure 4.22.

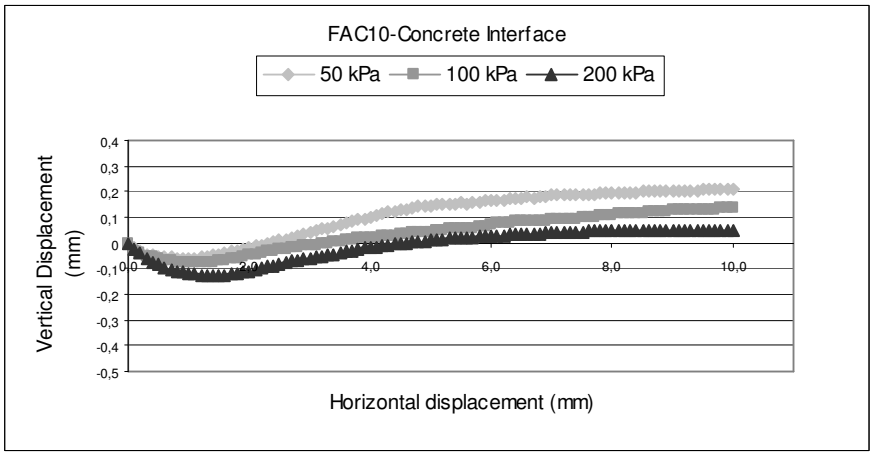

Figure 4.22. The vertical-horizontal displacement curves of FAC10 group pellets under 50,100 and 200 kPa normal stresses

The interface friction angle of FAC10 group pellets between concrete blocks at peak interface stress is represented in Figure 4.23. The interface friction angle for FAC10 group pellets (δ_{FAC10}) was 33.15° which is higher than the one obtained for fly ash only (FA) group pellets but almost similar with the one obtained for FAC20 group pellets.

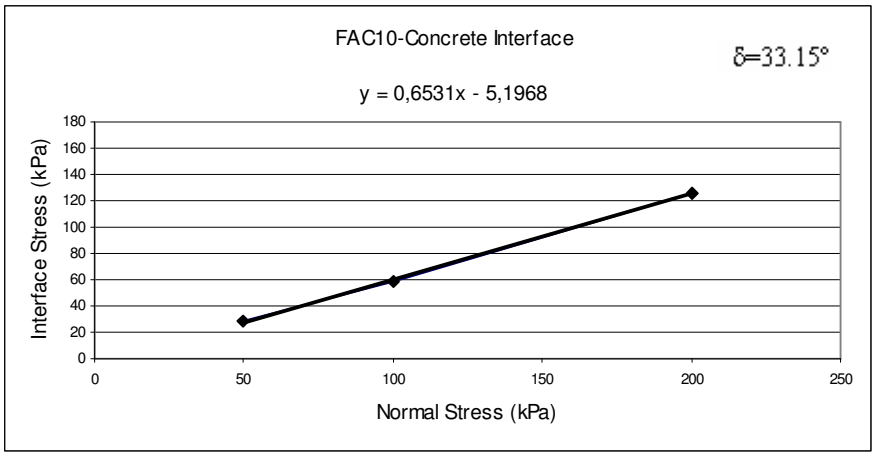

Figure 4.23. The interface friction angle of FAC10 group pellets (δ_{FAc10})

The FAC20 group pellets were the strongest aggregates and attained a maximum interface stress of 128.5 kPa under 200 kPa normal stress where the strain level was approximately 5.5%. Under 100 kPa normal stress, the interface stress was 60.8 kPa. For a 50 kPa of normal stress, FAC20 group couldn't exhibit enough performance and the interface stress remained under FA and FAC10 group pellets. Conversely, under 200 kPa normal stress, the interface stress was higher than that of FA and FAC10 group pellets as expected. The horizontal displacement-interface stress curves of FAC20 group pellets under 50, 100 and 200 kPa normal stress are given in Figure 4.24.

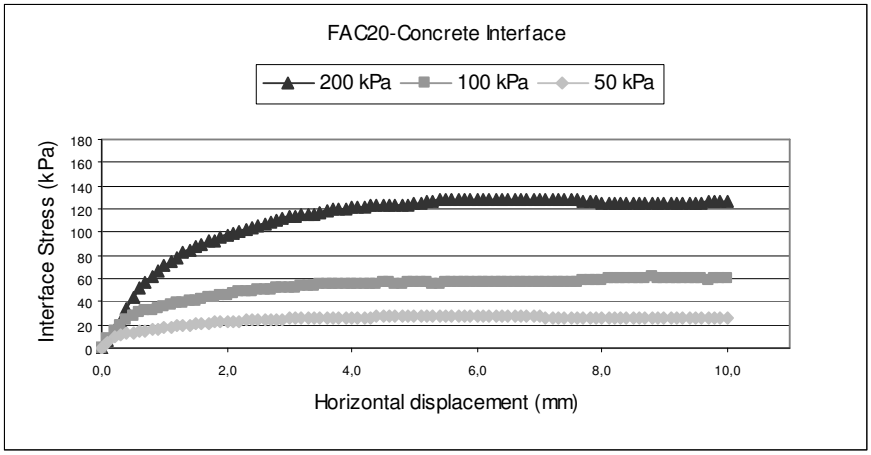

Figure 4.24. The interface stress-horizontal displacement curves of FAC20 group pellets under 50,100 and 200 kPa normal stresses

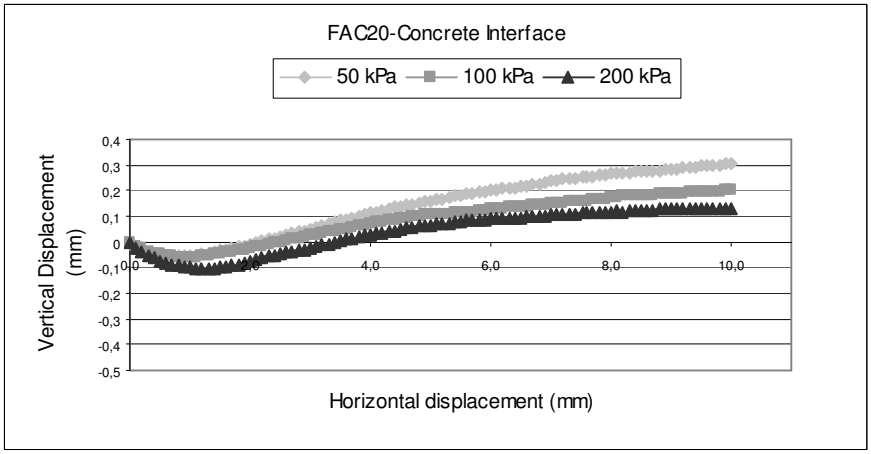

Figure 4.25. The vertical-horizontal displacement curves of FAC20 group pellets under 50,100 and 200 kPa normal stresses

The vertical-horizontal displacement curves of FAC20 group pellets under 50, 100 and 200 kPa normal stress are given in Figure 4.25. The FAC20 group pellets couldn't reach to critical state under 50, 100 and 200 kPa normal stresses, because the dilation angle (α) was not zero at the end of the tests. The contraction increased as the normal stress increased and resulted in a decrease in dilation in the same manner as other groups. Under various normal stresses conditions, FAC20 group pellets exhibited a more dilative behavior with respect to other groups and attain 0.303 mm of vertical displacement even under 200 kPa normal stress which is higher than other groups.

The interface friction angle of FAC20 group pellets between concrete blocks at peak interface stress is represented in Figure 4.26. The interface friction angle for FAC20 group pellets (δ_{FAC20}) was 33.89° which is the highest value obtained in interface tests and very close to the one obtained for FAC10 group pellets.

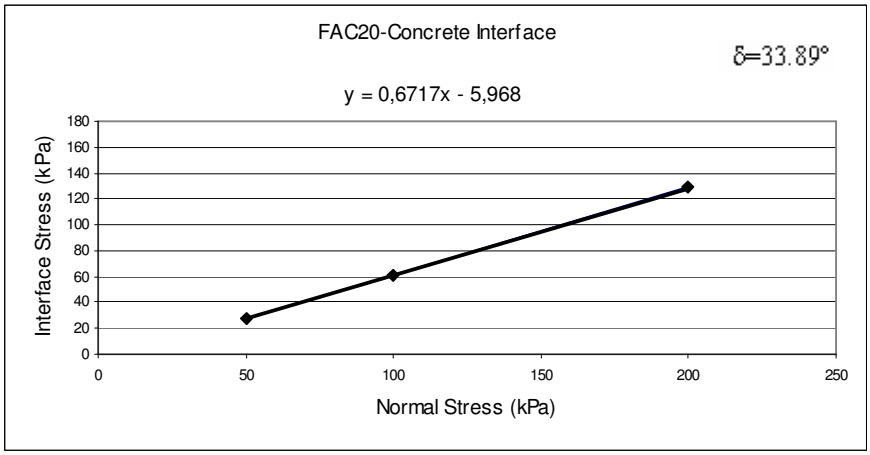

Figure 4.26. The interface friction angle of FAC20 group pellets (δ_{FAc20})

The crushing of pellets was in the same manner of direct shear tests. A slight difference occurred due to the stiff surface of concrete blocks. The crushing of particles increased with the presence of concrete blocks.

The grain size distributions of FA group pellets under 50, 100 and 200 kPa normal stresses for both before and after interface tests are given in Figure 4.27. The crushing of FA group pellets increased with the increase of applied normal load. Under 50 kPa normal

stress the difference of grain size distribution before and after tests was lower relative to 100 and 200 kPa normal stresses. Under 200 kPa normal stress, the difference of grain size distribution before and after interface tests was greater than the ones obtained for 50 and 100 kPa normal stresses. Therefore, the cracked pellets could easily been observed even by naked eye after interface tests performed on FA group pellets under 200 kPa normal stress.

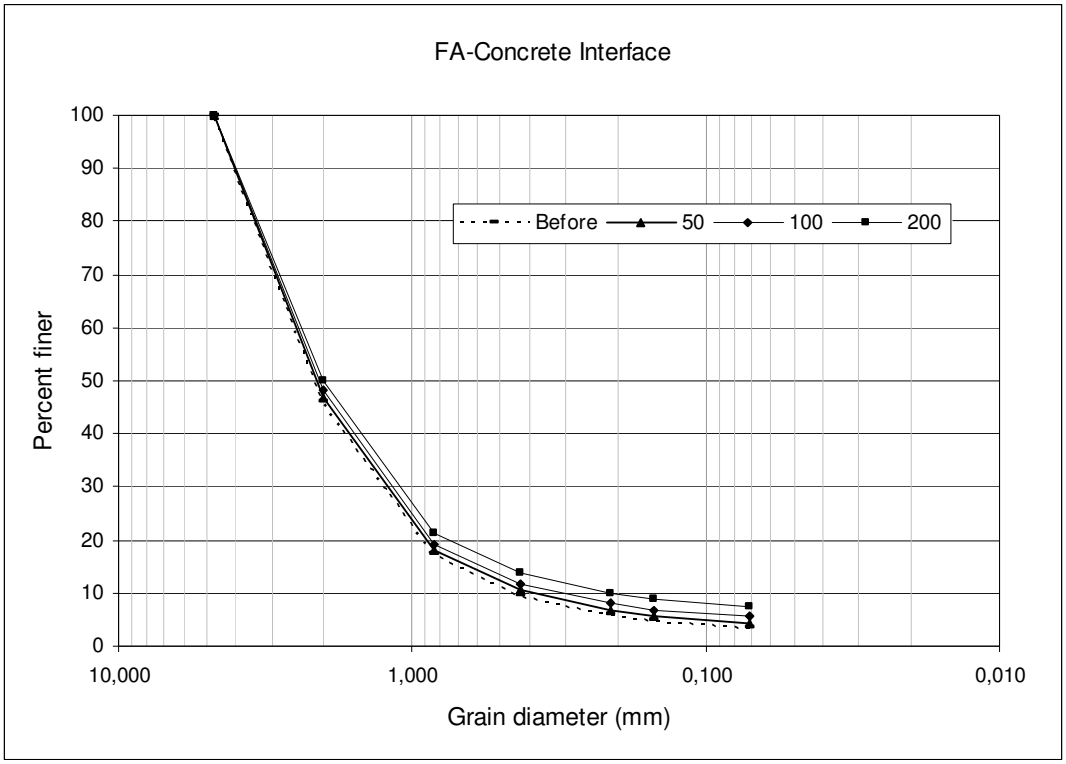

Figure 4.27. The sieve analysis test results of FA group pellets before and after interface tests, under 50 kPa, 100 kPa and 200 kPa normal stresses

The results of sieve analysis tests performed on FAC10 and FAC20 group pellets after tests were also in accordance with the ones obtained in direct shear tests. The FAC10 group pellets were slightly affected by grain crushing under 50 kPa normal stress. The crushing of FAC10 group pellets were noticeable under 100 and 200 kPa normal stresses. The grain size distributions of FAC20 group pellets before and after interface tests showed that FAC20 group pellets slightly or were not affected by grain crushing while FA and FAC10 groups of pellets subjected to particle fracturing. The grain size distribution of FAC10 and FAC20 groups of pellets before and after pellets to concrete interface tests are

given in Figure 4.28. The results of individual sieve analysis tests for all groups of pellets before and after interface tests can be found in appendix B.

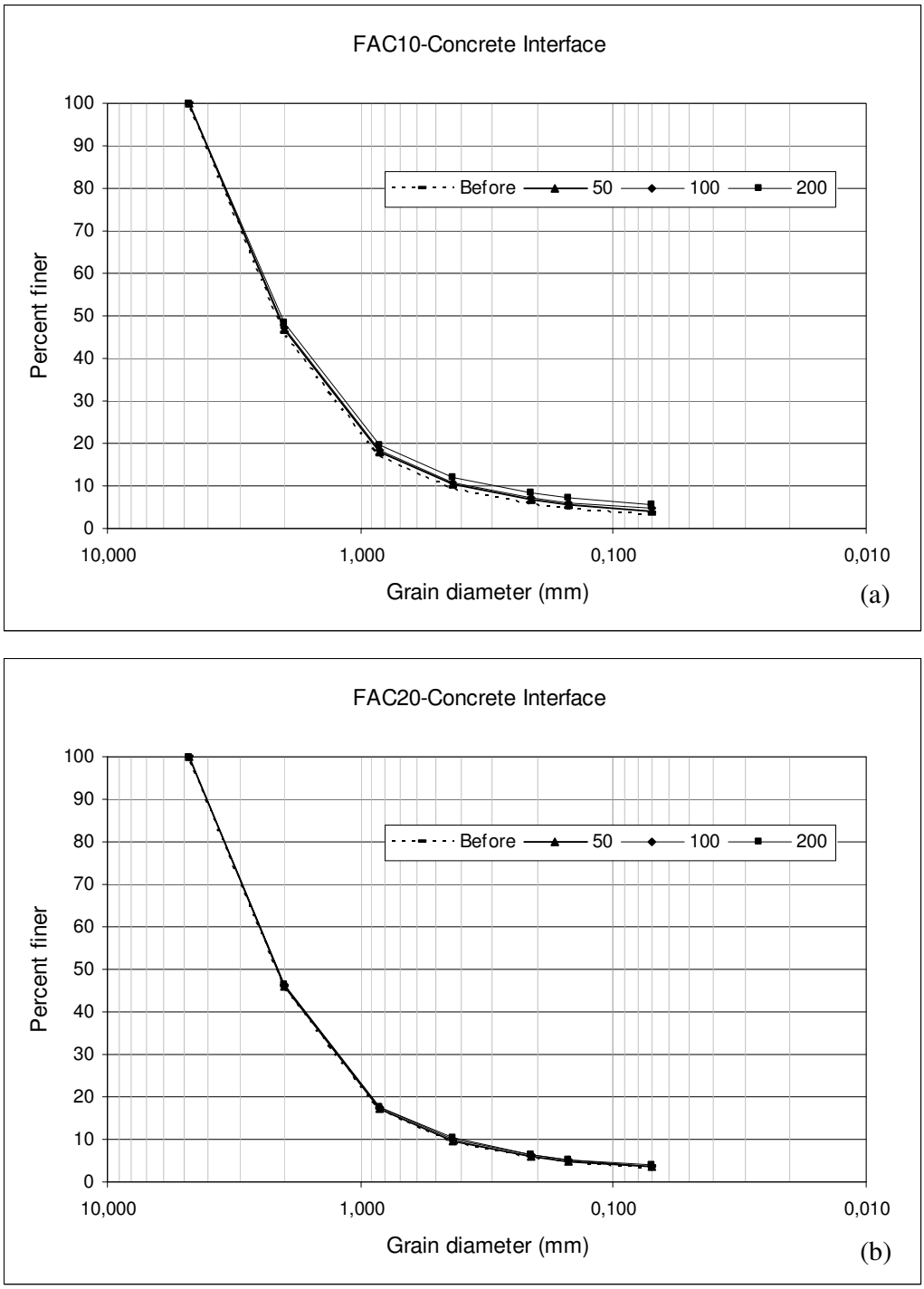

Figure 4.28. The sieve analysis test results of a) FAC10, b) FAC20 group pellets before and after interface tests, under 50 kPa, 100 kPa and 200 kPa normal stresses

4.6. Evaluation of Interface and Direct Shear Tests Results.

The sieve analysis test conducted before and after both shear and interface stress tests showed that under 50 kPa normal stress, grain crushing had only a minor effect on FA, FAC10 and FAC20 group pellets. The FA group pellets initially exhibited a contractive behavior then this was followed by dilation up to 100 kPa normal stress. The effect of grain crushing on the FA group pellets was noticeable under 100 kPa normal stress and when the normal stress attained 200 kPa, the effect of grain crushing was dominant and resulted in a total contractive behavior in FA group pellets during the test. The crushing of particles caused filling the pores between pellets and dilation wasn't observed, consequently the shear and interface stresses dropped suddenly. The results of sieve analysis tests showed that FA group of pellets are the most vulnerable pellets to crushing.

Under 50 kPa normal stress, grain crushing had inconsiderable effect on FAC10 group pellets. But under 100 and 200 kPa normal stresses, the grains were affected by grain crushing which resulted in a decrease in both shear and pellets to concrete interface stresses. The pellets initially showed a contractive behavior then dilation was observed even under 200 kPa normal stress. The grain size distributions of FAC10 group pellets before and after shear and interface stress tests indicate that under 50kPa normal stress the effect of crushing was negligible however, under 100 and 200 kPa normal stresses, the grain crushing resulted in a decrease in both interface and shear stresses.

The most durable group to crushing was FAC20 and was not affected by grain crushing even under 200 kPa normal stress. The results of sieve analysis tests showed that the grain size distribution of FAC20 group pellets before and after tests were nearly the same under 50 and 100 kPa normal stresses. Only a slight difference occurred under 200 kPa normal stress. The addition of cement to the mixture obviously increased the resistance of pellets to crushing.

The microscopic images of randomly selected FA, FAC10 and FAC20 groups of pellets are in Figure 4.29, Figure 4.30 and Figure 4.31 respectively.

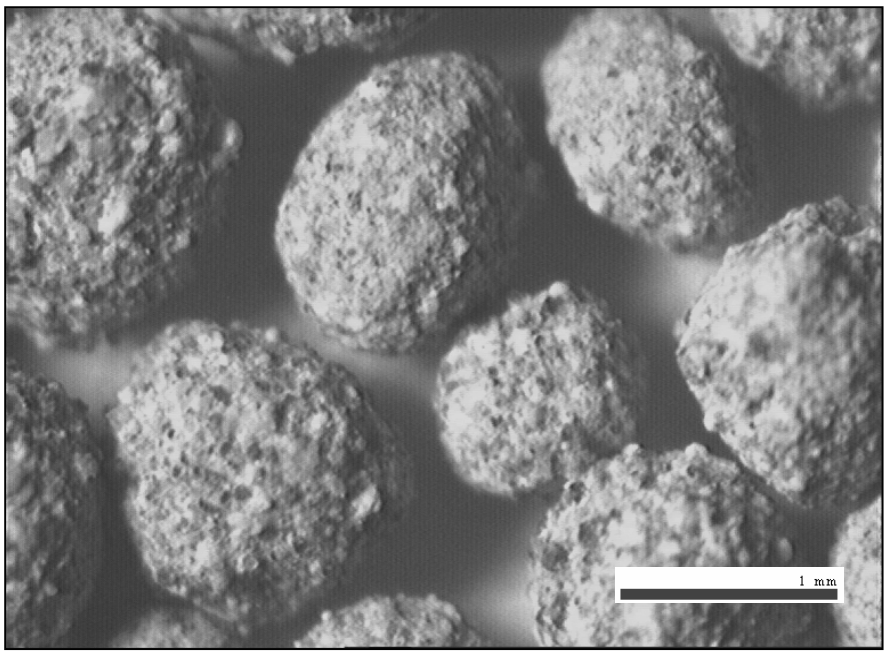

Figure 4.29. The microscopic image of FA group pellets

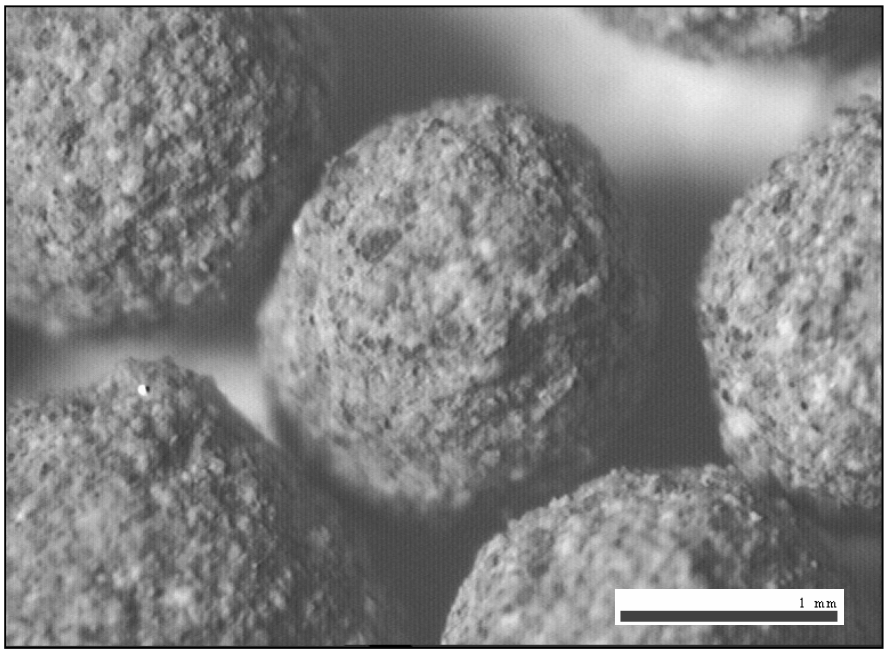

Figure 4.30. The microscopic image of FAC10 group pellets

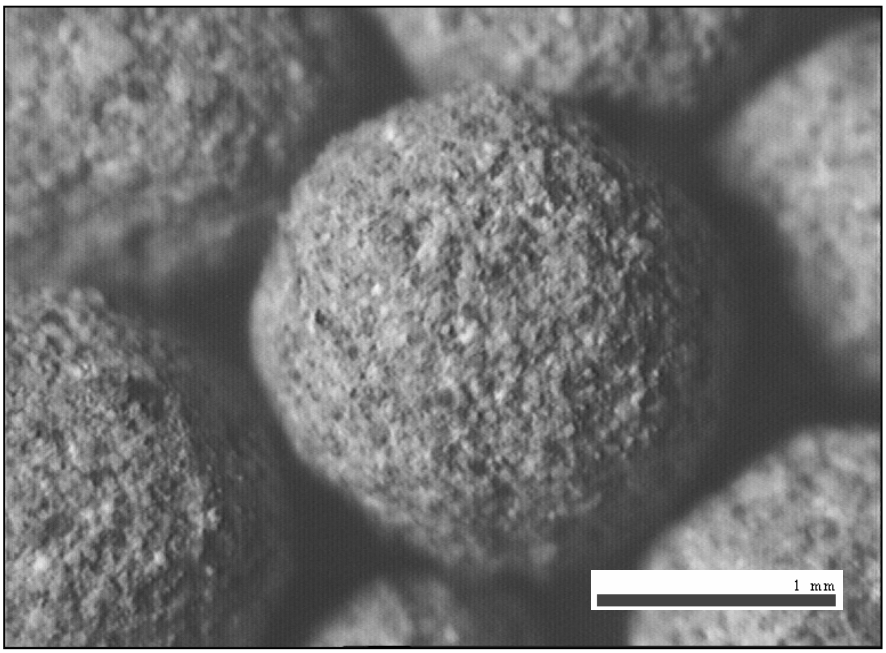

Figure 4.31. The microscopic image of FAC20 group pellets

The shear and interface stresses of FA group pellets under 50 kPa normal stress were 42.94 and 30.45 kPa respectively. In both direct shear tests and interface tests the maximum stress obtained under 50kPa normal stress belongs to FA group pellets. This was followed by FAC10 group pellets which attained a maximum value of 39.86 and 28.42 kPa in shear and interface stress tests. The lowest shear and interface stresses were somehow obtained for FAC20 group pellets under 50 kPa normal stress which were 37.86 and 27.87 kPa respectively.

Figure 4.29 clearly shows that FA group pellets are more angular and have rougher surface with respect to other groups which explains the higher shear and interface resistance of FA group pellets in the tests under 50 kPa normal stress. This phenomenon can be explained by the lower pozzolanic activity of fly ash with respect to cement which prevents the pellets to have more compact structure and spherical shape in pelletization process. The addition of cement resulted in a smoother surface and more spherical shapes of pellets (FAC10 and FAC20) which lead to a decrease in both maximum shear and interface stresses under 50 kPa normal stress.

For both FA, FAC10 and FAC20 groups of pellets, the effect of grain crushing, surface roughness and particle shape were influential on the test results under 100 kPa normal stress. The results in shear and interface stress tests under 100 and 200 kPa must be evaluated in a different manner since the FA group pellets were mostly affected by grain crushing. Under 100 and 200 kPa normal stresses, the advantage of more angular shapes and smoother surfaces of FA group pellets was consequently inadequate to exhibit higher performance than other groups. Thereby, the maximum shear and interface stresses of FA group pellets remained under FAC10 and FAC20 groups of pellets.

The dominant factor was the grain crushing when the normal stress was 200 kPa. The sieve analysis tests showed that FA group pellets crushed under the high normal stress. The FAC10 group pellets were also affected by grain crushing but relatively lower than FA group pellets. The grain size distribution of FAC20 group pellets remained the same or with a negligible difference. Consequently, FAC20 group pellets attained maximum shear and interface stresses of 155.83 and 128.50 kPa respectively which are higher than the ones obtained in both tests for FA and FAC10 groups of pellets. The overall performance of FA, FAC10 and FAC20 groups of pellets in shear and interface stress tests is given in Table 4.4.

Table 4.4. The overall performance of pellets in shear and interface stress tests.

	FA		FAC10		FAC20	
	ϕ	δ	ϕ	δ	ϕ	δ
	30.09°	27.57°	36.55°	33.15°	37.98°	33.89°
Normal Stress (kPa)	Max Shear Stress (kPa)	Max Interface Stress (kPa)	Max Shear Stress (kPa)	Max Interface Stress (kPa)	Max Shear Stress (kPa)	Max Interface Stress (kPa)
50kPa	42.94	30.45	39.08	28.42	37.86	27.87
100kPa	78.23	58.30	79.98	58.67	81.31	60.82
200kPa	131.13	109.11	151.02	125.90	155.83	128.50

The comparison of internal friction and pellets to concrete interface friction tests results of FA group pellets are given in Figure 4.32. The internal friction of FA group pellets was 30.29° which is approximately %10 higher than interface friction.

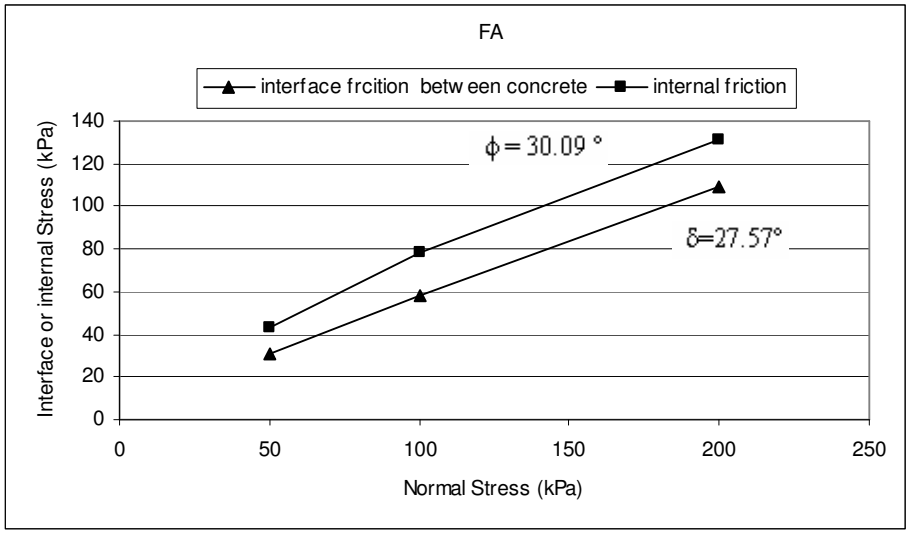

Figure 4.32. Comparison of internal and interface friction angles of FA group pellets

The internal friction angle of FAC10 group pellets was 36.55° which is 10% higher than interface friction in the same manner as FA group pellets. (Figure 4.33)

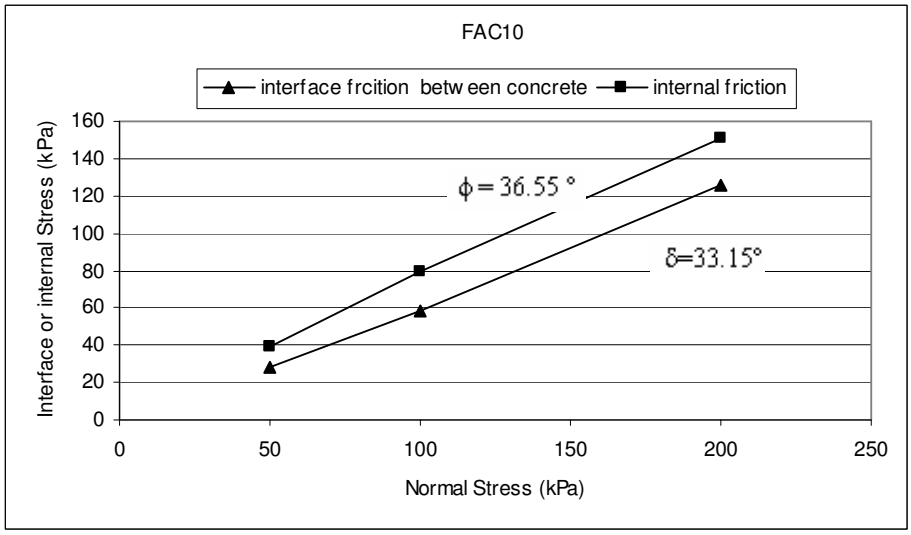

Figure 4.33. Comparison of internal and interface friction angles of FAC10 group pellets

The FAC20 group pellets exhibited a higher performance than both FA and FAC10 group pellets however the internal and interface friction angles were about similar with the

ones in FAC10 group. The internal friction angle of FAC20 group pellets was 37.98° which is approximately 11% higher than interface friction between concrete blocks. The comparison of internal friction and pellets to concrete interface friction of FAC20 group pellets are given in Figure 4.34.

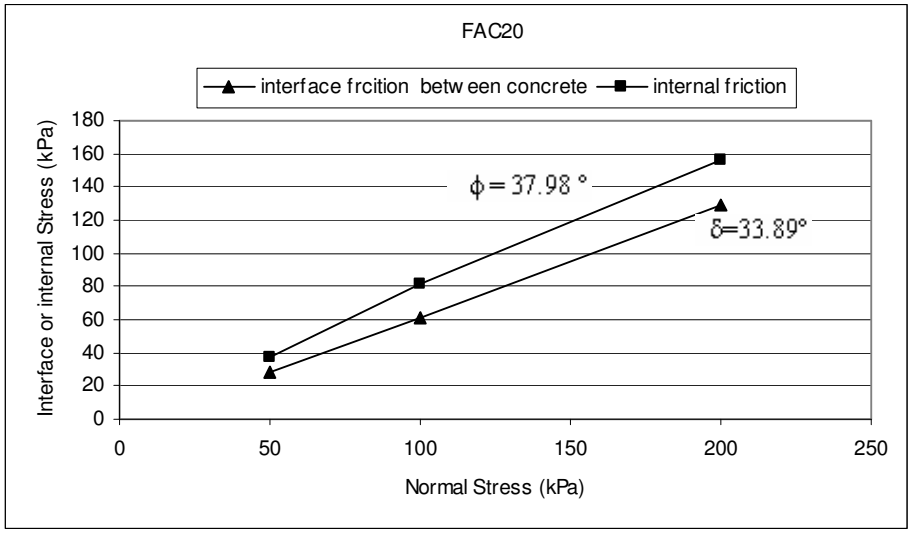

Figure 4.34. Comparison of internal and interface friction angles of FAC20 group pellets

4.7. The Relationship between Surface Roughness of Concrete Blocks and Interface Test Results

The surface plots and three dimensional surface roughness parameters ($\overline{R}_{n3d}$) of C1, C2, C3 and C4 which were obtained with the developed software are given in Figure 4.36. The elevations (light and dark colors) caused by pellets on the surface of C4 can be easily recognized.

The light colors indicate that there is an elevation on the surface and conversely, the dark colors represent the cavities. Essentially, *Rn* formula can be interpreted as; if the amount of transition zones from light to dark or dark to light increases, there will be an increase in the surface roughness parameter of the material.

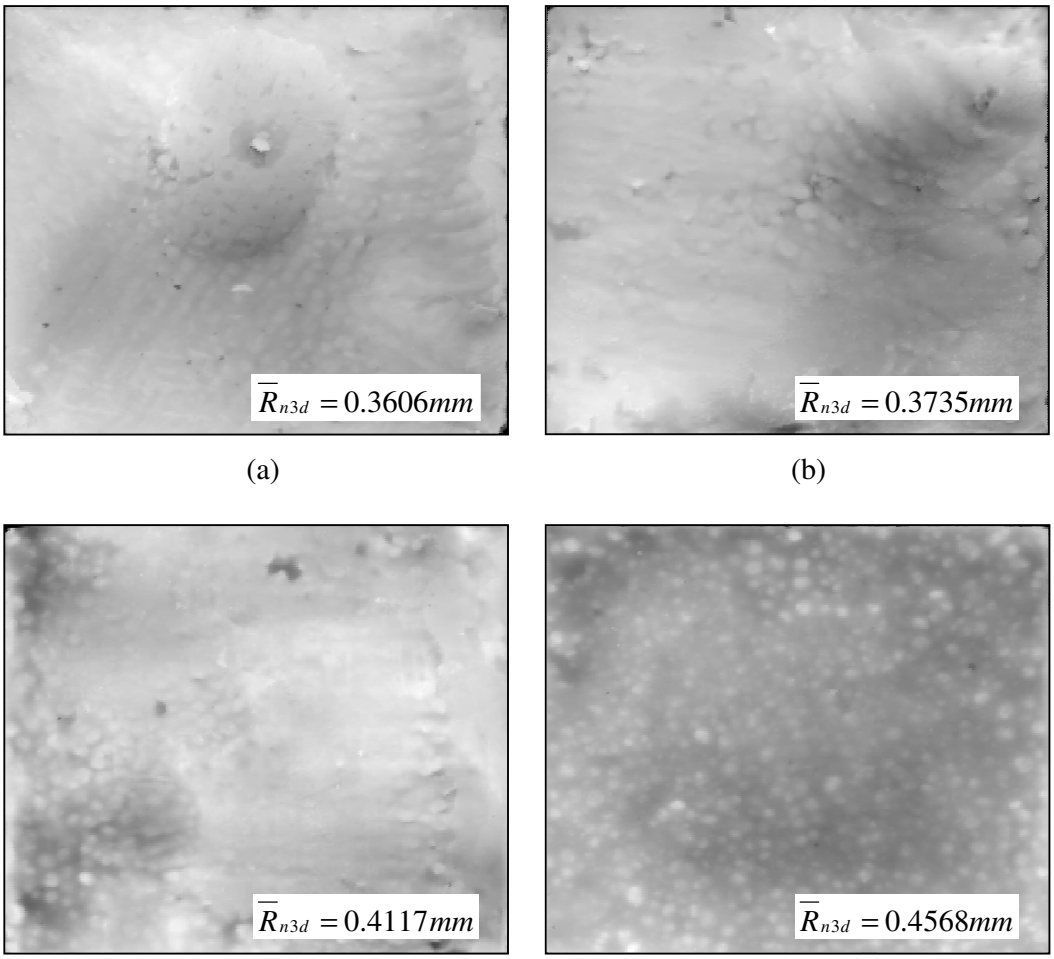

Figure 4.35. The surface plots of a) C1 b) C2 c) C3 and d) C4

According to three dimensional analyses, C4 had the roughest surface which could easily be recognized with the naked eye. This was followed by C3 block with an average value of $\overline{R}_{n3d}$ and consequently, C1 and C2 had the lowest surface roughness values due to their surfaces which are relatively smoother than other blocks.

The interface stress-horizontal displacement and vertical-horizontal displacement curves of C1, C2, C3 and C4 blocks are represented in Figure 4.36 and Figure 4.37 respectively.

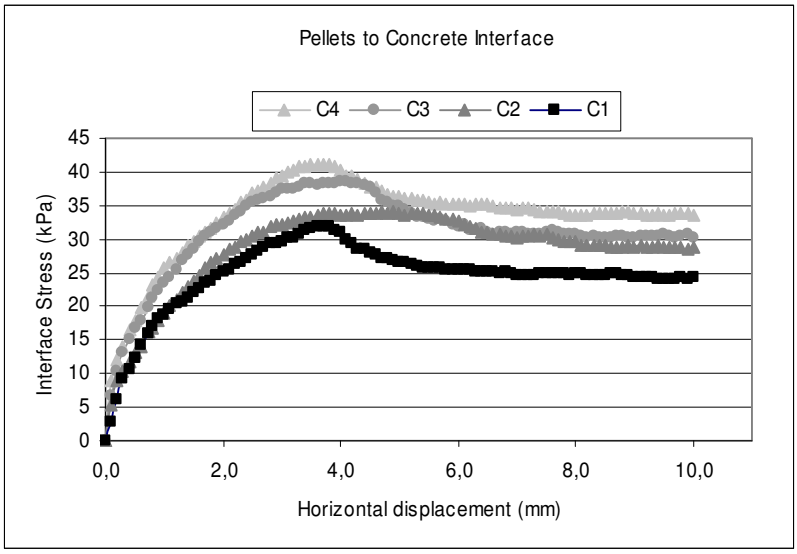

Figure 4.36. The interface stress-horizontal displacement curves of C1, C2, C3 and C4 under 50 kPa normal stress

The maximum interface stress obtained in the tests was 43.17 kPa which belongs to the C4 block. This was followed by C3, C2 and C1 respectively. The C1 block attained a maximum interface stress of 31.87 kPa which was lower than other blocks. The grain size distributions before and after tests showed that there was no particle crushing during the tests as expected.

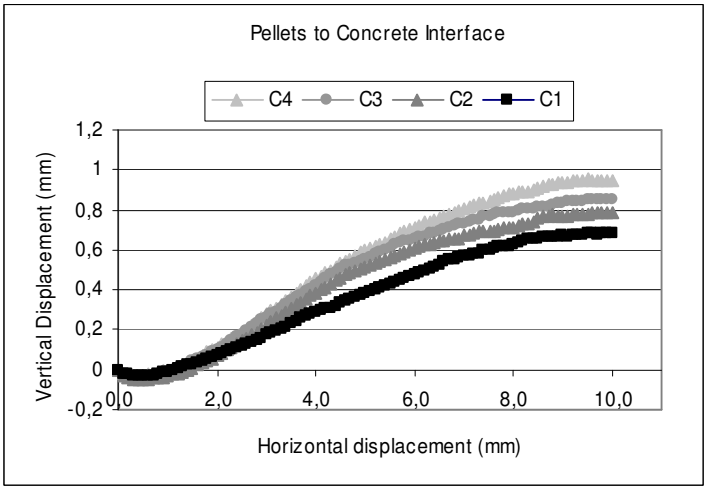

Figure 4.37. The vertical-horizontal displacement curves of C1, C2, C3 and C4 under 50 kPa normal stress.

The vertical to horizontal displacement curves indicate that the surface roughness of concrete blocks affected the dilative behavior of pellets. The concrete block C1 with the smoothest surface had the lowest volume change whereas the C3 block with the roughest surface reached nearly 1 mm of vertical displacement which was the highest volume change in all pellets to concrete interface tests.

The effect of surface roughness on the maximum interface stress of pellets to concrete interface is summarized in Table 4.5

Table 4.5. The relationship between $\overline{R}_{n3d}$ and maximum interface stress

Concrete Block	$\overline{R}_{n3d}$ (mm)	Maximum Interface Stress(kPa)
C1	0.3606	31.87
C2	0.3735	34.02
C3	0.4117	38.49
C4	0.4568	41.17

The results of interface tests performed under 50 kPa normal stress showed that the maximum interface stresses of pellets to concrete interface and the dilative behavior of pellets is highly related with $\overline{R}_{n3d}$. The interface stresses increases with the increase of surface roughness and also the tendency of pellets to exhibit a dilative behavior increases with $\overline{R}_{n3d}$.

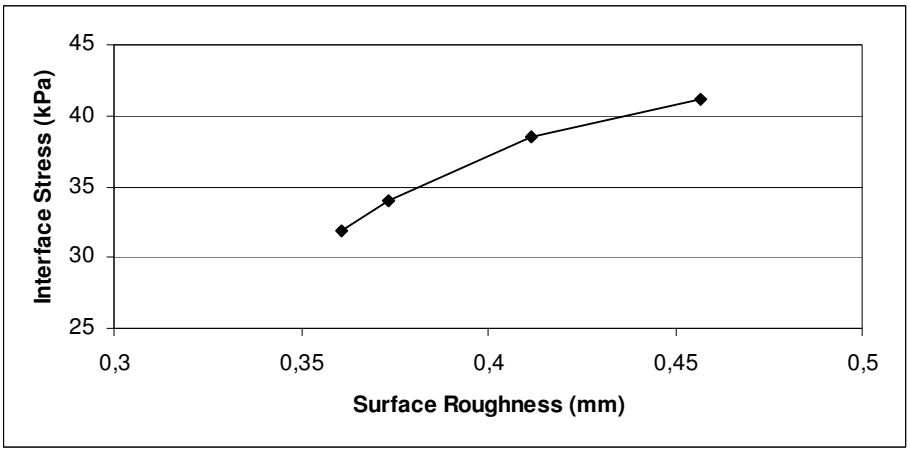

Figure 4.38. The relationship between surface roughness and interface stress.

Figure 4.38 represents the relationship between surface roughness of the concrete and the interface stresses obtained in interface tests. The curve indicates that as the surface roughness increases the acceleration of interface stress decreases.

The results obtained by three dimensional approach were compared with two dimensional approach in order to understand the contribution of the third dimension on the interface stresses. Two dimensional roughness parameters ($\overline{R}_{n1}$, $\overline{R}_{n2}$ and $\overline{R}_{n3}$) were obtained from the sections which divide the profile into four equal pieces. The representation of the two dimensional surface roughness parameters is given in Figure 4.39.

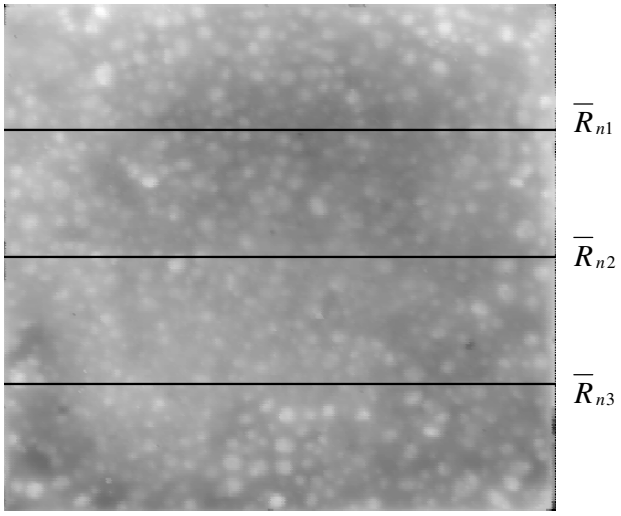

Figure 4.39. Representation of two dimensional surface roughness parameter

The comparison of three dimensional surface roughness parameters ($\overline{R}_{n3d}$) and the two dimensional surface parameters of concrete blocks C1, C2, C3 and C4 are given in Table 4.6. Additionally the two dimensional surface roughness parameter ($\overline{R}_{n2d}$) which is the average of $\overline{R}_{n1}$, $\overline{R}_{n2}$ and $\overline{R}_{n3}$ is represented in Table 4.6. The results showed that the three dimensional surface roughness parameters of C1, C3 and C4 concrete blocks are higher than those obtained by two dimensional approach except C2 concrete block.

Table 4.6. The relationship between $\overline{R}_{n3d}$ and $\overline{R}_{n2d}$

Concrete Block	$\overline{R}_{n1}$ (mm)	$\overline{R}_{n2}$ (mm)	$\overline{R}_{n3}$ (mm)	$\overline{R}_{n2d}$ (mm)	$\overline{R}_{n3d}$ (mm)	$\overline{R}_{n3d} / \overline{R}_{n2d}$
C1	0.3265	0.3588	0.3154	0.3336	0.3606	1.08
C2	0.3500	0.4529	0.3485	0.3838	0.3735	0.97
C3	0.3463	0.3824	0.3824	0.3703	0.4117	1.11
C4	0.4632	0.4404	0.4537	0.4525	0.4568	1.01

Although the maximum interface stress obtained by using C3 block was higher than the one obtained by using C2 block, the surface roughness parameter of C2 block calculated by two dimensional approach was higher than the one obtained for C3 block.

4.8. Compressive Strengths of Lightweight Concrete Specimens

The 5x5 cm lightweight concrete cube specimens consist of only FA group fly ash aggregates were subjected to compression after curing period of 7 and 28 days. The results of compressive strength tests indicate that the compressive strength of concrete which consists of only fly ash aggregates is dominated by the crushing strength of pellets within the concrete. The compressive strengths and unit weights of lightweight concrete specimens for both 7 and 28days are given in Table 4.7.

Table 4.7. Compressive strengths and unit weights of lightweight concrete specimens

Curing Period	Weight (gr)	γ (kN/m^3)	Compressive Strength (MPa)
7 Days	237.93	19.03	29.78
28 Days	242.79	19.42	33.50

Structural lightweight concrete mixtures can be designed to achieve similar strengths as normal weight concrete. The compressive strengths of specimens were greater than 17 Mpa which is the acceptable limit for concrete strength in structural applications.

The unit weight of concrete produced using lightweight aggregates was considerably less than the weight of concrete using normal materials. The results showed that the densities of air dried concrete specimens were lower than 2000 kg/m^3 so the

concrete specimens can be classified as lightweight concrete. The unit weights of concrete specimens for 7 and 28 days were 19.03 and 19.42 kN/m^3 respectively. The primary use of lightweight concrete is to reduce the dead load of a concrete structure which then allows the structural designer to reduce the size of load bearing elements.

The 2% increase in unit weight of lightweight concrete specimens between 7 and 28 days can be explained by the filling of pores in aggregates within the concrete. The porosity of only fly ash lightweight aggregates provides a source of water for internal curing of the concrete that provides continued enhancement of concrete strength and durability.

4. CONCLUSION

The interface behavior between granular materials and concrete was investigated in order to understand the influence of physical and mechanical properties of granular soils on the interface behavior. Following conclusions and recommendations are made to define the experience gained in this research.

The results of interface tests showed that the interface performance is highly related with crushing strength, shape and surface characteristics of granular materials, and also the surface roughness of concrete blocks.

Under low normal stress (50kPa), the dominant mechanism was the surface and the shape of particles which increased the interlocking of aggregates and resulted in a higher maximum shear and interface stress. The vertical-horizontal displacement curves indicated that all groups of aggregates initially contracted and this was followed by dilation except in FA group aggregates under 200 kPa normal stress. Microscopic images of the aggregates clearly showed that FA group has the advantage of rougher surface and angular particles relative to the other groups under low normal stress. Thus, the maximum interface and internal stresses obtained under 50kPa normal stress belong to FA group aggregates.

Under average normal stress (100kPa), surface roughness, shapes of particles and additionally the crushing of particles affected the behavior. Microscopic images showed that FAC10 and FAC20 group aggregates have smoother surfaces and round particles in comparison with FA group aggregates. FAC10 and FAC20 group aggregates exhibited higher performance than FA group aggregates because of their resistance to crushing under normal stress.

As the normal stress increased to 200kPa, the dominant mechanism turned into the crushing of particles. The FA group pellets subjected to crushing and exhibited a total contractive behavior. The most durable group to crushing was FAC20. Consequently, both maximum internal and interface stresses obtained in tests under 200kPa normal stress

belong to FAC20 group aggregates.

The results showed that under low normal stress, aggregates couldn't reach to critical state due to the limitations of direct shear box. It is possible to conduct interface tests on different test devices including cylindrical shear device in which the granular material can reach to critical state because of the unlimited displacement capacity of the device.

The contact efficiencies are calculated by dividing the interface friction angles (δ), by internal friction angles (ϕ) of the aggregates. Although the friction angle at peak shear stress for dilating soils is not a fundamental soil parameter, the comparison of internal and interface friction angles at peak shear stresses obtained in tests showed that the contact efficiencies between FA, FAC10, FAC20 and concrete were 0.92, 0.91, 0.89 respectively. It can be concluded that, surface roughness and angularity of aggregates increase the contact efficiency. Since, FA group aggregates had rougher surfaces and angular shapes; the contact efficiency between granular and concrete was higher than other groups.

The results of interface tests indicate that there is a considerable relationship between surface roughness parameter ($R_{n3d)}$ and the maximum interface stress between granular materials and concrete. The roughness parameter of C4 block was approximately 27% higher than C1 block and the test results showed that the maximum stress obtained in C4 to aggregates interface test is 24% higher than the one obtained in C1 to aggregates interface test. The comparison of three dimensional two dimensional approaches showed that three dimensional surface roughness parameter gives more reliable results. This phenomenon must be further investigated by performing tests on different construction materials such as steel, geotextile, etc. and the results should be compared.

As a conclusion, the effects of grain crushing, particle shape and the surface roughness of both aggregates and concrete play an important role in the interface behavior between granular soils and concrete. Thus, in geotechnical applications, the behavior within the working conditions should be carefully studied and further attention must me paid.

APPENDIX A: THE CRUSHING STRENGTHS OF INDIVIDUAL PELLETS

The 7, 14 and 28 days average crushing strength of FA group pellets are 11.83, 49.88 and 201.62N/cm^2 respectively. FAC10 group pellets attained an average crushing strength of 52.81kPa at 7 days and this was followed by 126.72 and 278.15 N/cm^2 on 14th and 28th days respectively. The FAC20 group pellets were stronger relative to other groups. The average crushing strength of FAC20 group pellets on 7th, 14th and 28th days were 107.40, 254.20 and 341.29 N/cm^2 respectively. The 7, 14 and 28 days individual crushing strengths of FA, FAC10 and FAC20 groups pellets are given in Table A.1 to Table A.9.

Table A.1. 7 days crushing strengths of FA group pellets

No	Class	F	LRC	F(N)	d_1	d_2	d_3	$d_{average}$(cm)	Area(cm^2)	σ (N/cm^2)
1	FA	10	0,00138	13,800	1,36	1,35	1,33	1,35	1,42	9,69
2	FA	11	0,00138	15,180	1,33	1,36	1,35	1,35	1,42	10,66
3	FA	7	0,00138	9,660	1,15	1,08	1,10	1,11	0,97	9,98
4	FA	8	0,00138	11,040	1,15	1,13	1,16	1,15	1,03	10,69
5	FA	11	0,00138	15,180	1,32	1,33	1,33	1,33	1,38	10,98
6	FA	12	0,00138	16,560	1,35	1,29	1,32	1,32	1,37	12,10
7	FA	10	0,00138	13,800	1,19	1,21	1,20	1,20	1,13	12,20
8	FA	11	0,00138	15,180	1,26	1,27	1,27	1,27	1,26	12,05
9	FA	10	0,00138	13,800	1,21	1,20	1,23	1,21	1,16	11,94
10	FA	11	0,00138	15,180	1,24	1,24	1,23	1,24	1,20	12,64
11	FA	12	0,00138	16,560	1,27	1,29	1,33	1,30	1,32	12,54
12	FA	11	0,00138	15,180	1,22	1,23	1,26	1,24	1,20	12,64
13	FA	12	0,00138	16,560	1,30	1,29	1,26	1,28	1,29	12,80
14	FA	14	0,00138	19,320	1,33	1,39	1,41	1,38	1,49	12,98
15	FA	15	0,00138	20,700	1,41	1,38	1,39	1,39	1,52	13,58

Table A.2. 7 days crushing strengths of FAC10 group pellets

No	Class	F	LRC	F(N)	d_1	d_2	d_3	$d_{average}$(cm)	Area(cm^2)	σ (N/cm^2)
1	FC10	32	0,00138	44,160	1,05	1,21	1,09	1,12	0,98	45,09
2	FC10	35	0,00138	48,300	1,15	1,19	1,16	1,17	1,07	45,18
3	FC10	44	0,00138	60,720	1,32	1,27	1,30	1,30	1,32	45,98
4	FC10	42	0,00138	57,960	1,25	1,26	1,25	1,25	1,23	46,98
5	FC10	40	0,00138	55,200	1,18	1,19	1,23	1,20	1,13	48,81
6	FC10	39	0,00138	53,820	1,21	1,22	1,09	1,17	1,08	49,77
7	FC10	55	0,00138	75,900	1,36	1,41	1,38	1,38	1,50	50,50
8	FC10	45	0,00138	62,100	1,22	1,25	1,23	1,23	1,19	51,98
9	FC10	44	0,00138	60,720	1,20	1,20	1,22	1,21	1,14	53,10
10	FC10	54	0,00138	74,520	1,30	1,37	1,34	1,34	1,40	53,11
11	FC10	52	0,00138	71,760	1,29	1,30	1,23	1,27	1,27	56,35
12	FC10	45	0,00138	62,100	1,18	1,16	1,12	1,15	1,04	59,44
13	FC10	40	0,00138	55,200	1,05	1,09	1,11	1,08	0,92	59,89
14	FC10	62	0,00138	85,560	1,31	1,35	1,29	1,32	1,36	62,84
15	FC10	57	0,00138	78,660	1,28	1,21	1,29	1,26	1,25	63,08

Table A.3. 7 days crushing strengths of FAC20 group pellets

No	Class	F	LRC	F(N)	d_1	d_2	d_3	$d_{average}$(cm)	Area(cm^2)	σ (N/cm^2)
1	FC20	78	0,00138	107,640	1,18	1,25	1,31	1,25	1,22	88,18
2	FC20	80	0,00138	110,400	1,19	1,19	1,21	1,20	1,12	98,16
3	FC20	85	0,00138	117,300	1,22	1,25	1,20	1,22	1,18	99,80
4	FC20	88	0,00138	121,440	1,15	1,29	1,24	1,23	1,18	102,76
5	FC20	101	0,00138	139,380	1,33	1,31	1,30	1,31	1,35	102,89
6	FC20	92	0,00138	126,960	1,31	1,21	1,19	1,24	1,20	105,70
7	FC20	90	0,00138	124,200	1,25	1,20	1,21	1,22	1,17	106,25
8	FC20	95	0,00138	131,100	1,25	1,21	1,28	1,25	1,22	107,40
9	FC20	85	0,00138	117,300	1,11	1,17	1,25	1,18	1,09	107,87
10	FC20	82	0,00138	113,160	1,16	1,08	1,20	1,15	1,03	109,58
11	FC20	98	0,00138	135,240	1,29	1,18	1,29	1,25	1,23	109,62
12	FC20	89	0,00138	122,820	1,15	1,12	1,28	1,18	1,10	111,68
13	FC20	92	0,00138	126,960	1,25	1,15	1,15	1,18	1,10	115,44
14	FC20	93	0,00138	128,340	1,15	1,09	1,23	1,16	1,05	122,14
15	FC20	93	0,00138	128,340	1,12	1,18	1,15	1,15	1,04	123,56

Table A.4. 14 days crushing strengths of FA group pellets

No	Class	F	LRC	F(N)	d_1	d_2	d_3	$d_{average}$(cm)	Area(cm^2)	σ (N/cm^2)
1	F	32	0,00138	44,160	1,21	1,28	1,25	1,25	1,22	36,18
2	F	49	0,00138	67,620	1,39	1,40	1,35	1,38	1,50	45,21
3	F	45	0,00138	62,100	1,32	1,33	1,36	1,34	1,40	44,25
4	F	45	0,00138	62,100	1,30	1,28	1,33	1,30	1,33	46,55
5	F	35	0,00138	48,300	1,09	1,20	1,15	1,15	1,03	46,77
6	F	44	0,00138	61,410	1,32	1,26	1,28	1,29	1,30	47,23
7	F	51	0,00138	70,380	1,33	1,33	1,34	1,33	1,40	50,41
8	F	51	0,00138	70,380	1,15	1,17	1,80	1,37	1,48	47,51
9	F	49	0,00138	67,620	1,31	1,36	1,35	1,34	1,41	47,95
10	F	47	0,00138	64,860	1,25	1,31	1,28	1,28	1,29	50,40
11	F	41	0,00138	56,580	1,15	1,25	1,21	1,20	1,14	49,75
12	F	55	0,00138	75,900	1,35	1,28	1,28	1,30	1,33	56,89
13	F	52	0,00138	71,760	1,26	1,27	1,27	1,27	1,26	56,95
14	F	54	0,00138	74,520	1,25	1,32	1,29	1,29	1,30	57,31
15	F	62	0,00138	85,560	1,36	1,25	1,28	1,30	1,32	64,79

Table A.5. 14 days crushing strengths of FAC10 group pellets

No	Class	F	LRC	F(N)	d_1	d_2	d_3	$d_{average}$(cm)	Area(cm^2)	σ (N/cm^2)
1	FC10	82	0,00138	113,160	1,23	1,18	1,19	1,20	1,13	100,06
2	FC10	77	0,00138	106,260	1,18	1,15	1,12	1,15	1,04	102,30
3	FC10	91	0,00138	125,580	1,21	1,23	1,18	1,21	1,14	109,81
4	FC10	115	0,00138	158,700	1,28	1,28	1,39	1,32	1,36	116,56
5	FC10	62	0,00138	85,560	0,92	1,01	0,93	0,95	0,71	119,86
6	FC10	75	0,00138	103,500	1,01	1,05	1,01	1,02	0,82	125,84
7	FC10	126	0,00138	173,880	1,33	1,32	1,30	1,32	1,36	127,71
8	FC10	98	0,00138	135,240	1,15	1,14	1,15	1,15	1,03	130,96
9	FC10	103	0,00138	142,140	1,16	1,16	1,19	1,17	1,08	132,21
10	FC10	122	0,00138	168,360	1,28	1,30	1,24	1,27	1,27	132,21
11	FC10	134	0,00138	184,920	1,29	1,31	1,35	1,32	1,36	135,81
12	FC10	120	0,00138	165,600	1,21	1,24	1,26	1,24	1,20	137,87
13	FC10	150	0,00138	207,000	1,35	1,39	1,36	1,37	1,47	141,11
14	FC10	140	0,00138	193,200	1,30	1,35	1,28	1,31	1,35	143,34
15	FC10	141	0,00138	194,580	1,27	1,30	1,35	1,31	1,34	145,10

Table A.6. 14 days crushing strengths of FAC20 group pellets

No	Class	F	LRC	F(N)	d_1	d_2	d_3	$d_{average}$(cm)	Area(cm^2)	σ (N/cm^2)
1	FC20	165	0,00138	227,700	1,12	1,09	1,13	1,11	0,97	233,90
2	FC20	231	0,00138	318,780	1,33	1,31	1,29	1,31	1,35	236,51
3	FC20	219	0,00138	302,220	1,28	1,25	1,29	1,27	1,27	237,33
4	FC20	238	0,00138	328,440	1,35	1,31	1,32	1,33	1,38	237,60
5	FC20	170	0,00138	234,600	1,10	1,11	1,09	1,10	0,95	246,86
6	FC20	201	0,00138	277,380	1,22	1,19	1,17	1,19	1,12	248,01
7	FC20	201	0,00138	277,380	1,18	1,18	1,15	1,17	1,08	258,00
8	FC20	165	0,00138	227,700	1,07	1,05	1,05	1,06	0,88	259,66
9	FC20	195	0,00138	269,100	1,16	1,13	1,15	1,15	1,03	260,59
10	FC20	165	0,00138	227,700	1,05	1,04	1,05	1,05	0,86	264,64
11	FC20	136	0,00138	187,680	0,92	0,95	0,98	0,95	0,71	264,78
12	FC20	231	0,00138	318,780	1,21	1,24	1,26	1,24	1,20	265,40
13	FC20	132	0,00138	182,160	0,93	0,93	0,94	0,93	0,68	266,25
14	FC20	242	0,00138	333,960	1,27	1,26	1,26	1,26	1,25	266,42
15	FC20	235	0,00138	324,300	1,23	1,22	1,28	1,24	1,21	267,10

Table A.7. 28 days crushing strengths of FA group pellets

No	Class	F	LRC	F(N)	d_1	d_2	d_3	$d_{average}$(cm)	Area(cm^2)	σ (N/cm^2)
1	F	125,0	0,00138	172,500	1,10	1,09	1,10	1,10	0,95	181,52
2	F	190,0	0,00138	262,200	1,31	1,36	1,34	1,34	1,41	185,92
3	F	155,0	0,00138	213,900	1,20	1,21	1,17	1,19	1,11	192,32
4	F	188,0	0,00138	259,440	1,31	1,31	1,32	1,31	1,35	192,49
5	F	205,0	0,00138	282,900	1,34	1,34	1,36	1,35	1,43	197,64
6	F	182,0	0,00138	251,160	1,28	1,27	1,26	1,27	1,27	198,27
7	F	215,0	0,00138	296,700	1,38	1,38	1,38	1,38	1,50	198,37
8	F	150,0	0,00138	207,000	1,13	1,16	1,15	1,15	1,04	199,29
9	F	190,0	0,00138	262,200	1,29	1,29	1,29	1,29	1,31	200,61
10	F	170,0	0,00138	234,600	1,19	1,22	1,22	1,21	1,15	204,02
11	F	165,0	0,00138	227,700	1,19	1,18	1,21	1,19	1,11	204,73
12	F	205,0	0,00138	282,900	1,33	1,30	1,34	1,32	1,37	206,73
13	F	140,0	0,00138	193,200	1,06	1,11	1,09	1,09	0,93	207,04
14	F	185,0	0,00138	255,300	1,25	1,21	1,26	1,24	1,21	211,41
15	F	210,0	0,00138	289,800	1,22	1,23	1,23	1,23	1,19	243,89

Table A.8. 28 days crushing strengths of FAC10 group pellets

No	Class	F	LRC	F(N)	d_1	d_2	d_3	$d_{average}$(cm)	Area(cm^2)	σ (N/cm^2)
1	FC10	262,0	0,00138	361,560	1,34	1,33	1,34	1,34	1,41	256,38
2	FC10	271,0	0,00138	373,980	1,34	1,37	1,33	1,35	1,43	261,27
3	FC10	256,0	0,00138	353,280	1,31	1,31	1,32	1,31	1,35	262,11
4	FC10	255,0	0,00138	351,900	1,29	1,33	1,29	1,30	1,33	265,12
5	FC10	249,0	0,00138	343,620	1,29	1,26	1,25	1,27	1,27	271,26
6	FC10	215,0	0,00138	296,700	1,14	1,18	1,21	1,18	1,09	271,31
7	FC10	205,0	0,00138	282,900	1,16	1,15	1,15	1,15	1,04	272,36
8	FC10	273,0	0,00138	376,740	1,33	1,33	1,31	1,32	1,37	275,30
9	FC10	215,0	0,00138	296,700	1,16	1,17	1,14	1,16	1,06	280,74
10	FC10	212,0	0,00138	292,560	1,16	1,13	1,17	1,15	1,04	281,66
11	FC10	205,0	0,00138	282,900	1,11	1,13	1,13	1,12	0,99	287,15
12	FC10	230,0	0,00138	317,400	1,15	1,16	1,22	1,18	1,09	290,24
13	FC10	165,0	0,00138	227,700	0,98	0,99	1,00	0,99	0,77	295,80
14	FC10	270,0	0,00138	372,600	1,25	1,26	1,26	1,26	1,25	298,82
15	FC10	201,0	0,00138	277,380	1,09	1,08	1,08	1,08	0,92	302,79

Table A.9. 28 days crushing strengths of FAC20 group pellets

No	Class	F	LRC	F(N)	d_1	d_2	d_3	$d_{average}$(cm)	Area(cm^2)	σ (N/cm^2)
1	FC20	250,0	0,00138	345,000	1,18	1,19	1,16	1,18	1,09	315,48
2	FC20	318,0	0,00138	438,840	1,33	1,31	1,34	1,33	1,39	315,87
3	FC20	295,0	0,00138	407,100	1,28	1,27	1,30	1,28	1,29	316,37
4	FC20	315,0	0,00138	434,700	1,30	1,31	1,31	1,31	1,35	322,52
5	FC20	260,0	0,00138	358,800	1,17	1,18	1,18	1,18	1,09	328,09
6	FC20	250,0	0,00138	345,000	1,13	1,13	1,18	1,15	1,04	332,15
7	FC20	230,0	0,00138	317,400	1,10	1,09	1,11	1,10	0,95	333,99
8	FC20	215,0	0,00138	296,700	1,05	1,04	1,05	1,05	0,87	342,65
9	FC20	250,0	0,00138	345,000	1,11	1,16	1,11	1,13	1,00	344,01
10	FC20	315,0	0,00138	434,700	1,25	1,28	1,26	1,26	1,25	348,63
11	FC20	300,0	0,00138	414,000	1,20	1,25	1,20	1,22	1,17	354,15
12	FC20	315,0	0,00138	434,700	1,24	1,24	1,26	1,25	1,23	354,23
13	FC20	298,0	0,00138	411,240	1,22	1,21	1,20	1,21	1,15	357,63
14	FC20	350,0	0,00138	483,000	1,32	1,26	1,29	1,29	1,31	369,55
15	FC20	320,0	0,00138	441,600	1,21	1,21	1,21	1,21	1,15	384,03

APPENDIX B: SIEVE ANALYSIS TEST RESULTS OF PELLETS

The grain size distributions of FA, FAC10 and FAC20 groups of pellets before and after direct shear tests are given in Figure B.1, Figure B.2 and Figure B.3 respectively. The results of sieve analysis tests which were performed on FA, FAC10 and FAC20 group pellets before and after pellets to concrete interface tests are represented in Figure B.4, Figure B.5 and Figure B.6.

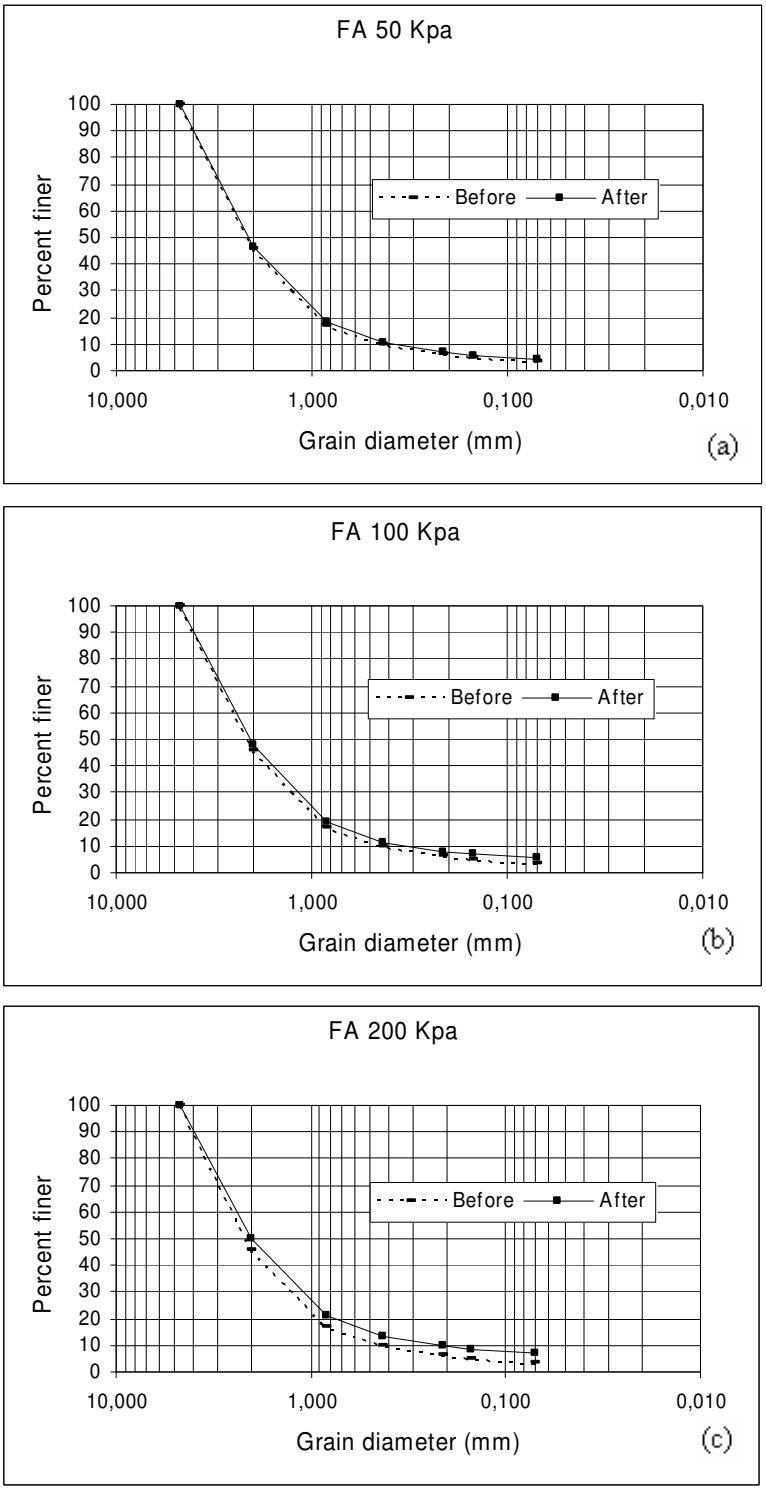

Figure B.1. The sieve analysis tests results of FA group pellets before and after direct shear tests, under a) 50 kPa b) 100 kPa c) 200 kPa normal stresses

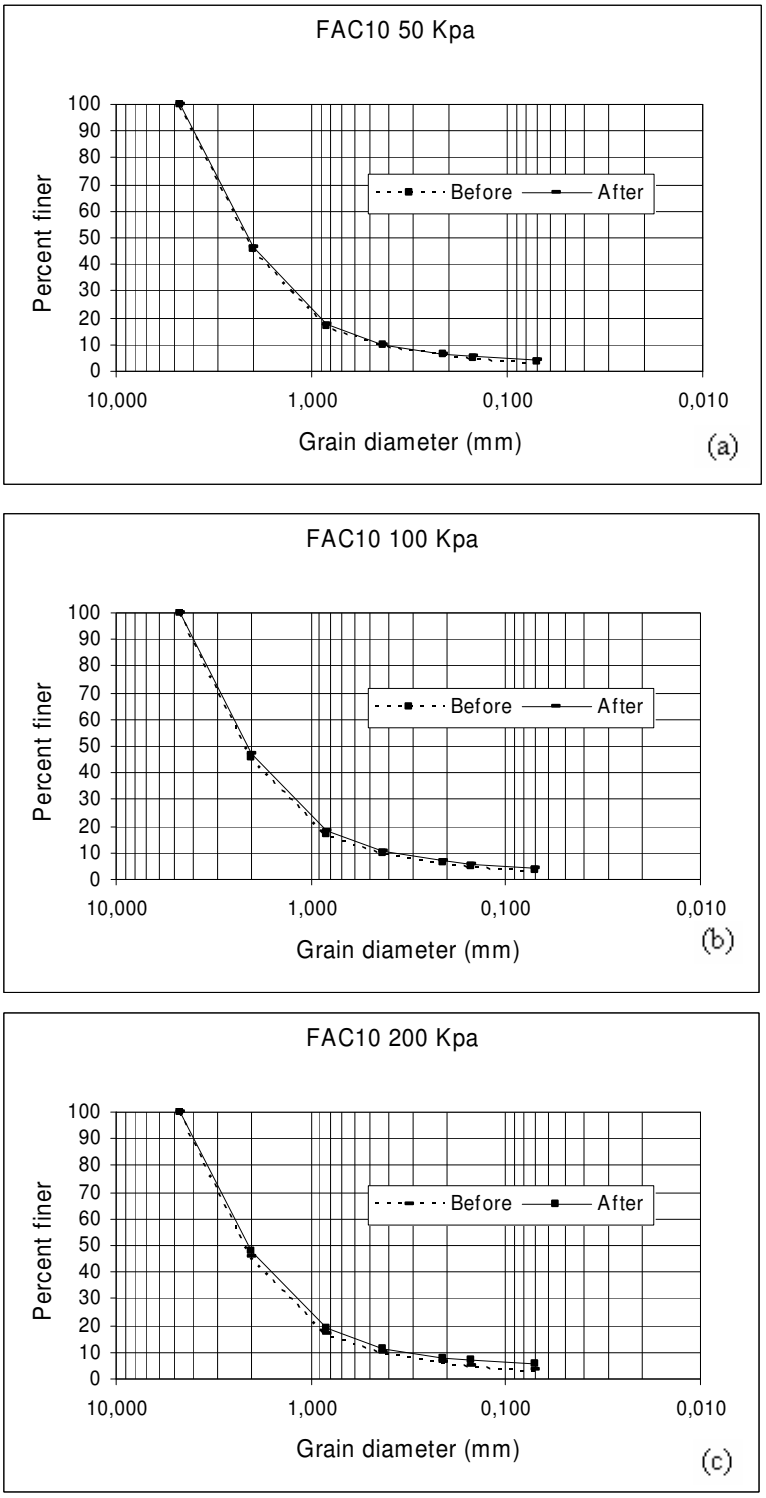

Figure B.2. The sieve analysis tests results of FAC10 group pellets before and after direct shear tests, under a) 50 kPa b) 100 kPa c) 200 kPa normal stresses

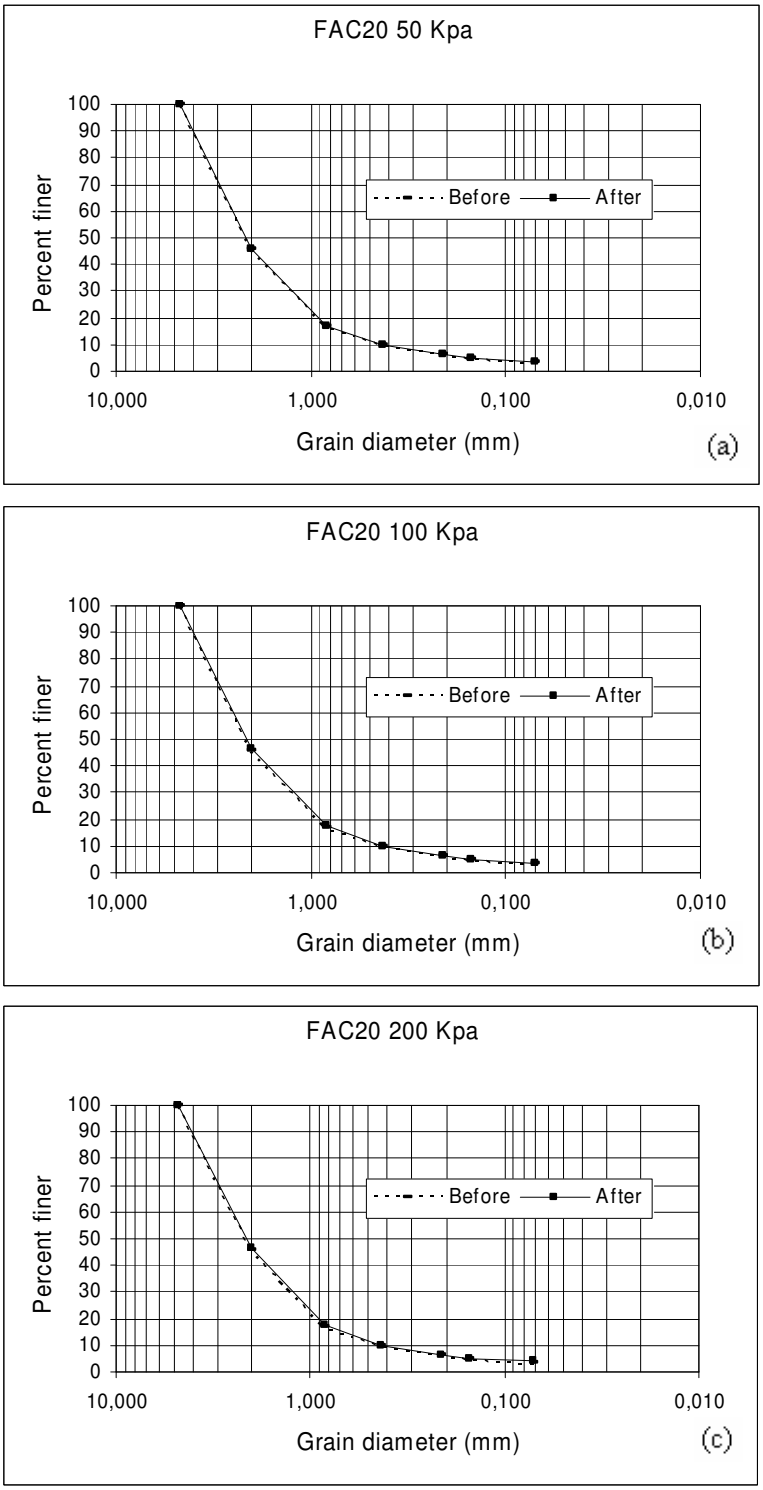

Figure B.3. The sieve analysis tests results of FAC20 group pellets before and after direct shear tests, under a) 50 kPa b) 100 kPa c) 200 kPa normal stresses

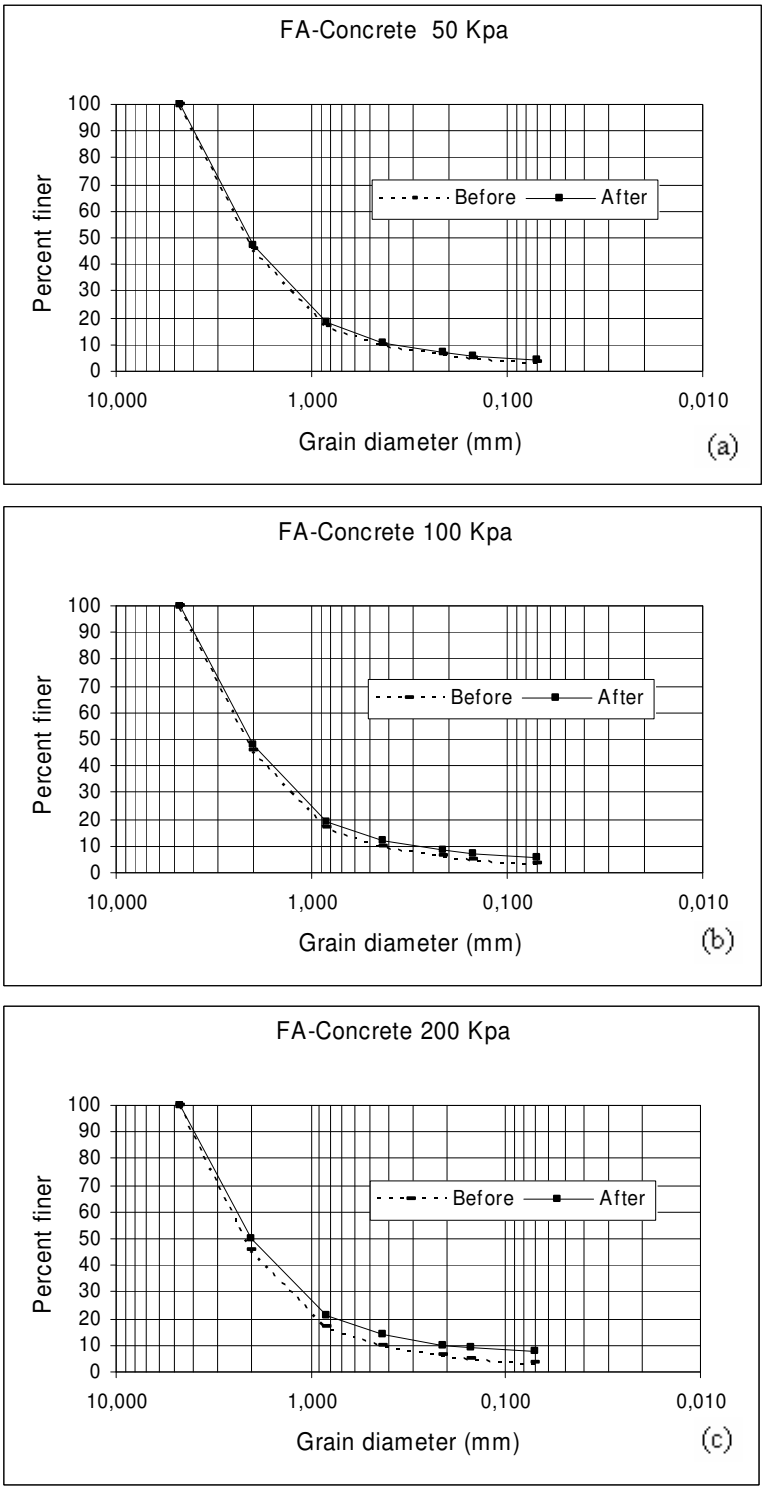

Figure B.4. The sieve analysis tests results of FA group pellets before and after interface tests, under a) 50 kPa b) 100 kPa c) 200 kPa normal stresses

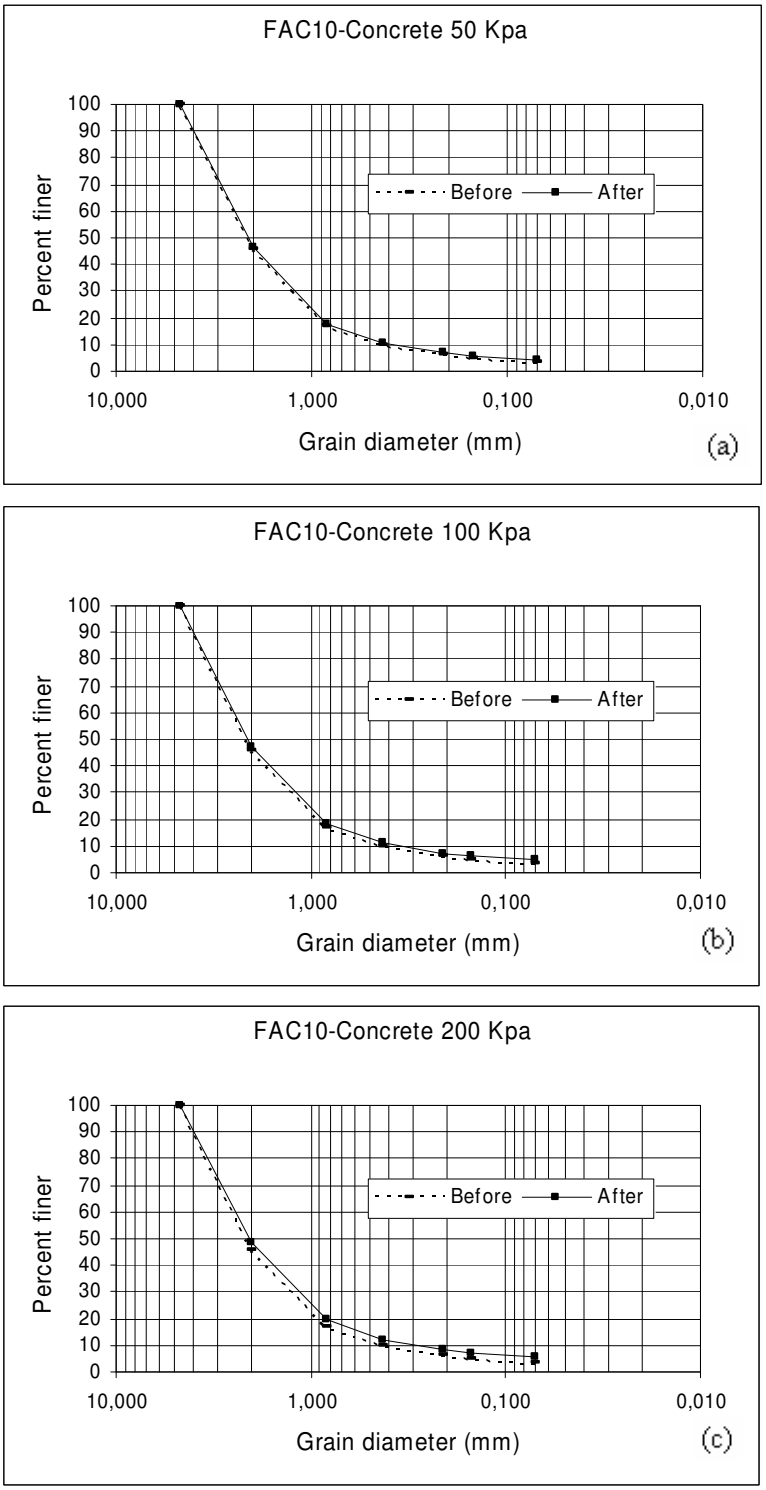

Figure B.5. The sieve analysis tests results of FAC10 group pellets before and after interface tests, under a) 50 kPa b) 100 kPa c) 200 kPa normal stresses

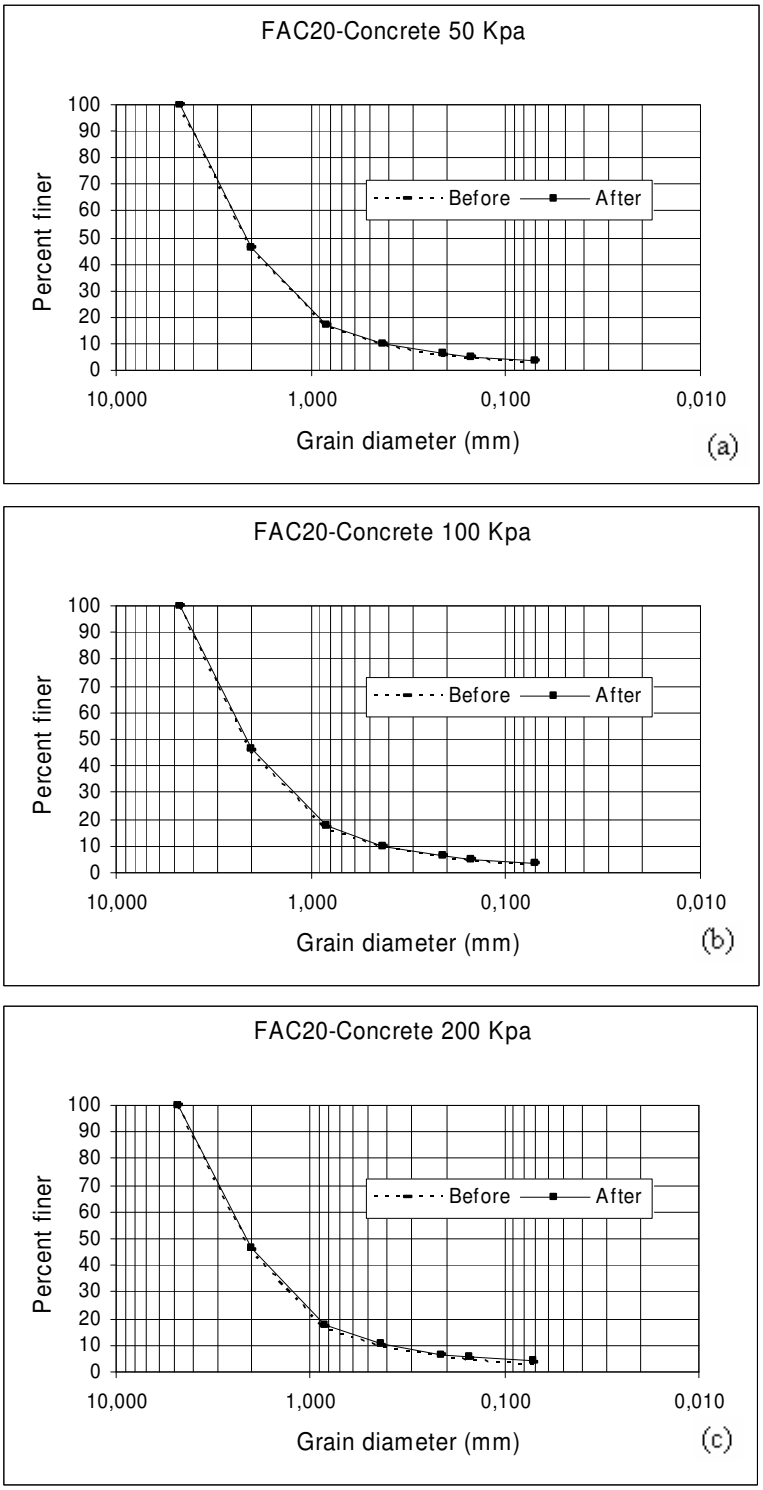

Figure B.6. The sieve analysis tests results of FAC20 group pellets before and after interface tests, under a) 50 kPa b) 100 kPa c) 200 kPa normal stresses

REFERENCES

1. Kézdi, A., *Talajmechanika ("Soil Mechanics", in Hungarian)*, Budapest, Tankonyukiado, 1959.

2. Potyondy, J. G., "Skin friction between various soils and construction materials", *Géotechnique,* Vol. 11, No. 4, pp. 339-353, 1961.

3. Masson, S. and J. Martinez, "Micromechanical Analysis of the Shear Behavior of a Granular Material", *Journal of Engineering Mechanics*, Vol. 127, No. 10, pp. 1007-1016, October 2001.

4. Fukumoto, T., "Particle Breakage Characteristics of Granular Materials", *Soil and Foundations*, Vol. 32, No. 1, pp. 26-40, March 1992.

5. Yukio, N., K. Yoshinori and M. Hidekazu, "Properties of Compression and Single Particle Crushing for Crushable Soil", *Proc. of Sym. on Engineering problem on crushable ground*, Kagoshima, pp. 15-20, 1999.

6. Brumund, W. F. and G. A. Leonards, "Experimental Study of Static and Dynamic Friction between Sand and Typical Construction Materials", *Journal of Testing and Evaluation, JTEVA*, Vol. 1, No. 2, pp. 162-165.

7. Peterson, M. S., F. H. Kulhawy, L. R. Nucci, and B. A. Wasil, "Stress-deformation Behavior of Soil-Concrete Interfaces", *Contact Report B-49 to Niagara Mohawk Power Corporation*, Syracuse, NY, 1976.

8. Acar, Y. B., H. T. Durgunoglu and M. T. Tumay, "Interface Properties of Sand", *Journal of the Soil Mechanics and Foundations Division, ASCE*, Vol. 108, No. 4, pp. 648-654, 1982.

9. Desai, C. S., M. M. Zaman, J. G. Lightner and H. J. Siriwarde, "Thin-layer Elements for Interfaces and Joints", *International Journal for Numerical and Analytical Methods in Geomechanics*, Vol. 8, No. 1, pp. 19-43, 1984.

10. Fakharian, K. and E. Evgin, "An Automated apparatus for Threedimensional Monotonic and Cyclic Testing for Interfaces", *Geotechnical Testing Journal*, Vol. 19, No. 1, pp. 22-31, 1996.

11. Kishida, H. and M. Uesugi, "Tests of the Interface Between Sand and Steel in the Simple Shear Apparatus", *Géotechnique,* Vol. 37, No. 1, pp. 45-52, 1987.

12. Fakharian, K. and E. Evgin, "Simple Shear versus Direct Shear Tests on Interfaces during Cyclic Loading", *Proceedings Third International Conference on Recent Advances in Geotechnical Earthquake Engineering and Soil Dynamics*, S. Prakash, University of Missouri at Rolla, April 1995.

13. Evgin, E. and K. Fakharian, "Effect of Stress Paths on the Behavior of Sand-Steel Interfaces", *Canadian Geotechnical Journal*, Vol. 33, No. 6, pp. 853-865, 1996.

14. Bowles, J. E., *Engineering Properties of Soils and Their Measurement*, McGraw-Hill, Singapore, 1998.

15. Uesugi, M. and H. Kishida, "Frictional Resistance at Yield between Dry Sand and Mild Steel", *Soils and Foundations*, Vol. 26, No. 4, pp. 139-149, 1986a.

16. Uesugi, M. and H. Kishida, "Influential Factors of Friction between Steel and Dry Sands", *Soils and Foundations*, Vol. 26, No. 2, pp. 33-46, 1986b.

17. Shallenberger, W. C. and G. M. Filz, "Interface Strength Determination Using a Large Displacement Shear Box", *Proceedings of the Second International Congress of Environmental Geotechnics*, Osaka, Japan , November 1996.

18. Huck, P. J. and S. K. Saxena, "Response of Soil-Concrete Interface at High Pressure", *Proceedings of the Tenth International Conference on Soil Mechanics and Foundation Engineering, Stockholm*, 1981.

19. Yoshimi, Y. and H. Kishida, "A Ring Torsion Apparatus for Evaluating Friction between Soil and Metal Surfaces", *Geotechnical Testing Journal*, Vol. 4, No. 4, pp. 145-152, 1981.

20. Stark, T. D., T. A. Williamson and H. T. Eid, "HDPE Geomembrane/Geotextile Interface Shear Strength", *Journal of Geotechnical Engineering*, Vol. 122, No. 3, pp. 197-203, 1996.

21. Akkol, O., Z., *A New Test Device and Method: Geotextile-Soil Interface Cylindrical Test (GICT)*, Ph.D. Thesis, Boğaziçi University, 1997.

22. Goodman, R. E., R. L. Taylor and T. L. Brekke, " A Model for the Mechanics of Jointed Rock", *Journal of Soil Mechanics and Foundations Division, ASCE*, Vol. 94, No. 3, pp. 637-659, 1968.

23. Clough, G. W. and J. M. Duncan, "Finite Element Analyses of Retaining Wall Behavior", *Journal of Soil Mechanics and Foundations Division, ASCE*, Vol. 97, No. 12, pp. 1657-1673, 1971.

24. Morrison, C. S., *The Development of a Modular Finite Element Program for Analyses of Soil-Structure Interaction*, Doctoral Dissertation, Virginia Polytechnic Institute and State University, Blacksburg, 1995.

25. Desai, C.S., E. C. Drumm and M. M. Zaman, "Cyclic Testing and Modeling of Interfaces", *Journal of Geotechnical Engineering, ASCE*, Vol. 111, No. 6, pp. 793-815, 1985.

26. Lee, S. W., *Influence of Surface Topography on Interface Strength and Counter face Soil Structure*, Ph.D. Thesis, Georgia Institute of Technology, Atlanta, Georgia, USA, 1998.

27. Frost, J.D., J. T. DeJong and M. Recalde, "Shear Failure Behavior of Granular-Continuum Interfaces", *Engineering Fracture Mechanics*, Vol. 69, No. 17, pp. 2029-2048, November 2002.

28. Subba Rao, K. S., M. M. Allam and R. G. Robinson, "Internal Friction between Sands and Solid Surfaces", *Journal of Geotechnical Engineering*, Vol. 131, pp. 75-82, 1998.

29. Chu, L. and Y. Jian-Hua, "Comparison of Interface Shear Strength of Soil Nails Measured by Both Direct Shear Box Tests and Pullout Tests", *Journal of Geotechnical and Geoenvironmental Engineering*, Vol. 1313, No. 9, pp. 1097-1107, September 2005.

30. Shahrour, I. and F. Rezaine, "An Elastoplastic Constitutive Relation for the Soil-Structure Interface under Cyclic Loading", *Comput. Geotech*, Vol. 21. No. 1, pp. 21-39, 1997.

31. Liu, L., S. E., L. and I. Hoe, "Constitutive Modeling of Soil-Structure Interface Thorough the Concept of Critical State Soil Mechanics", *Mechanics Research Communications*, Vol. 33, No. 4, pp. 515-531, July-August 2006.

32. Oda, M. and K. Iwashita, *Mechanics of Granular Materials*, A.A Balkema, Rotterdam, Netherlands, Brookfield, VT, USA, 1999.

33. Daouadji, A., P. Hicher and A. Rahma, "An Elastoplastic Model for Granular Materials Taking into Account Grain Breakage", *Eur. J. Mech. A/Solids*, Vol. 20. pp. 113-137, January 2001.

34. Bishop, A. W., "The Measurement of Pore Pressure Coefficient in Practice", *Geotechnique*, Vol. 4, pp. 148-152, 1954.

35. Taylor, D. W., *Fundamentals of Soil Mechanics*, John Wiley&Sons, New York, 1948.

36. Oda M. and H. Kazama, "Micro-structure of Shear Bands and its Relation to the Mechanism of Dilatancy and Failure of Granular Soils", *Geotechnique*, Vol. 48, No. 4, pp. 465-481, November 1998

37. Arslan H., *The Effect of Grain Crushing on the Behavior of Granular Materials*, M.S. Thesis, Boğaziçi University, 2003.

38. Lade, P. V., J. A. Yamamuro and P. A. Bopp, "Significance of Particle Crushing", *Journal of Geotechnical Engineering*, Vol. 122, No. 4, April 1996.

39. Döven, A., G., *Lighweight fly ash aggregate production using cold bonding agglomeration process*, Ph.D. Thesis, Boğaziçi University, 1998.

40. Bijen, J., "Fly Ash Aggregates", *American Concrete Institute* SP 79-26, 1986.

41. Vuppala, M.K., D. M. Parikh, and H. R. Bhagat, "Application of Powder-Layering Technology and Film Coating for Manufacture of Sustained-Release pellets Using a Rotary Fluid Bed Processor", *Drug Dev. Ind. Pharm*. Vol. 23, pp. 687-694, 1997.

42. Sastry K. V., *Pelletization of Fine Coals*, Final Report, U.S. Department of Energy Technology Center, 1995.

43. Baykal, G., A. G. Döven, "Utilization of Fly Ash Pelletization Process; - Theory, Application Areas and Research Results", *Resources, Conservation and Recycling* Elsevier Publications, 2000.

44. Head, K. H., *Manual of Soil Laboratory Testing*, Kobham, Surrey, November 1981.